CalVal Jason-3

Jason-3 validation of GDR-F data over ocean

Nomenclature : SALP-RP-MA-EA-23480-CLS

Issue : 1.2

Date : December 1, 2021

CLS - 8-10 Rue Hermès - Parc Technologique du Canal - 31520 Ramonville St-Agne - FRANCE
Telephone 33 5 61 39 47 00 / Fax 33 5 61 75 10 14

Chronology Issues:		
Issue:	Date:	Reason for change:
1.0	2021-06-30	Creation
1.1	2021-09-29	taking into account CNES review
1.2	2021-11-30	Update on Jason-3 to Jason-2 comparisons

People involved in this issue :				
	AUTHORS	**COMPANY**	**DATE**	**INITIALS**
Written by:	H. Roinard J. Coquelin	CLS ALTEN for CLS		
Checked by:	S. Rouge	CLS		
Approved by:	J-F. Legeais François Bignalet-Cazalet	CLS CNES		
Application authorised by:				

Index Sheet :	
Context: Altimetry, CalVal, Jason-3, Poseidon	
Keywords: satellite altimetry, performances, calibration, validation	
Hyperlink:	

Distribution:		
Company	Means of distribution	Names
CLS/DOS	electronic copy	vrosmorduc@groupcls.com
CNES	electronic copy	thierry.guinle@cnes.fr nicolas.picot@cnes.fr francois.bignalet-cazalet@cnes.fr gerald.dibarboure@cnes.fr aqgp_rs@cnes.fr dominique.chermain@cnes.fr delphine.vergnoux@cnes.fr

List of tables and figures

List of Tables

1 Models and standards adopted for Jason-3 product version “D” and “F” . . . 6
2 *Missing passes from 2016 to 2020* . . . 9
3 *Previous (GDR-D) and new (GDR-F) surface classification* . . . 10
4 *thresholds editing rates, from from 2016 to 2020 (cycles 001 to 177)* . . . 15
5 *GDR-D versus GDR-F SSH components for performances at crossover points analysis* . . . 18
6 POE-E and POE-F orbit standard . . . 29
7 AMR radiometer evolution in GDR-F . . . 30
8 Altimeter difference between GDR-D and GDR-F . . . 36
9 *Previous (GDR-D) and new (GDR-F) rain flag values* . . . 49
10 Contributions in sea surface height anomaly global bias . . . 52
11 Waveform classification definition . . . 59
12 *Thresholds editing rates MLE4 vs Adaptive, from 2016 to 2020 (cycles 001 to 177)* . . . 61

List of Figures

1 *Number of data available in 1Hz products for GDR-F and GDR-D (**left**). Number of available points difference : GDR-F - GDR-D (**right**).* . . . 8
2 *Map of missing data differences over cycles 001 to 177. **Blue** : Missing data in GDR-F (available in GDR-D). **Red** : Missing data in GDR-D (available in GDR-F).* . . . 9
3 *Cyclic mean of number of ocean data available for GDR-F and GDR-D (**left**). Data available difference over ocean : GDR-F - GDR-D (**right**)* . . . 10
4 *Surface type / classification over one cycle in GDR-D (**left**) and GDR-F (**right**)* . . . 11
5 *Number of identified ocean point in GDR-F that are not ocean in GDR-D (**left**). GDR-D surface_type values for ocean additional GDR-F points (**right**)* . . . 11
6 *Percentage of valid measurement for GDR-D and GDR-F with no surface type selection on (**left**), and with selection over ocean on (**right**). Note that GDR-D surface_type (resp. GDR-F surface_classification) is used to select ocean points on GDR-D (resp. GDR-F) analysis.* . . . 12
7 *Cyclic number of measurements that are valid in one case and not in the other until cycle 177 (**top**). Map of valid GDR-D / invalid GDR-F points (**left**) and map of valid GDR-F / invalid GDR-D points (**right**). All the other records have the same valid/invalid status on both GDR-D and GDR-F datasets.* . . . 13
8 *Map of the number of valid points difference in percentage (**left**). Blue boxes indicate that there are more valid measurements in GDR-D. Red boxes indicate that there are more valid measurements in GDR-F. Monitoring in function of distance to coast (**right**). Both figures are computed over one year of data.* . . . 13
9 *Number of rejected measurement per cycle on land + ice criterion, for GDR-D and GDR-F. Map of the number of ice points difference in percentage (computed over one year of data with GDR-F surface_classification for both solutions). Blue boxes indicate that there are more ice flagged measurements in GDR-D. Red boxes indicate that there are more ice flagged measurements in GDR-F.* . . . 14
10 *Percentage of valid measurement difference between GDR-D and GDR-F (**green**) or GDR-F with ionospheric correction raw (**black**) at global (**left**) and over ocean (**right**).* . . . 16

11 *Differences in percentage of valid measurements for SLA with non-filtered ionospheric solution for both GDR-d and GDR-F (**right**), or with filtred solution for GDR-F (**left**). Maps (**top**) and with regard to distance to coast (**bottom**)* . . . 17

12 *Cyclic mean of SSH differences at crossovers for GDR-F and GDR-D (selection on |latitude| < 50, oceanic variability < 20cm and bathymetry < -1000m) (**top**). Mean of SSH differences at crossovers map average over the whole period for GDR-D (**bottom left**) and GDR-F (**bottom right**)* . . . 19

13 *Difference (GDR-F - GDR-D) of variance at SSH differences at crossover. Difference per cycle (with selection on |latitude| < 50, oceanic variability < 20cm and bathymetry < -1000m) (**left**) and map in percentage (**right**)* . . . 20

14 *Difference (GDR-F - GDR-D) of variance at SSH differences at crossover in case of non filtered ionospheric correction for both GDR-D and GDR-F SSH. Difference per cycle (with selection on |latitude| < 50, oceanic variability < 20cm and bathymetry < -1000m) (**left**) and map in percentage (**right**)* . . . 20

15 *Cyclic monitoring of pseudo time tag bias for Jason-3 and Jason-2* . . . 21

16 *Periodogram of pseudo time tag bias* . . . 22

17 *Standard deviation of sea level anomaly (over ocean + Caspian Sea) difference over GDR-F and GDR-D datasets* . . . 22

18 *SLA variance difference between GDR-F and GDR-D (top left: GDR-F with filtered ionospheric correction. top right: GDR-F with raw ionospheric correction).* . . . 23

19 *SLA variance difference between GDR-F and GDR-D with regard to GDR-D level of variance (**left**: GDR-F with filtered ionospheric correction. **right**: GDR-F with raw ionospheric correction.* . . . 23

20 *Cyclic count of measurements with time difference between GDR-F and GDR-D > $1\mu s$* . . . 25

21 *Points with difference in datation between GDR-D and GDR-F for cycle 2, 40, 71, 113, 115 and 160* . . . 25

22 *Difference between POE-F and POE-E : Mean (**left**) and standard deviation (**right**). Difference between POE-F and POE-E (**bottom**)* . . . 29

23 *Difference of variance between POE-F and POE-E* . . . 30

24 *Brightness temperatures: mean per day (selection on SLA_MLE4 valid points only).* . . . 31

25 *Radiometer minus model wet tropospheric corrections (selection on SLA_MLE4 valid points only).* 31

26 *Difference of along-track SLA variance (without Caspian sea) using wet tropospheric correction GDR-F or GDR-D* . . . 32

27 *Difference of along-track SLA variance and mean fonction of distance to coast* . . . 32

28 *atmos_corr_sig0_ku (selection on SLA_MLE4 valid points only).* . . . 33

29 *water vapor content from radiometer difference in kg/m^2 (**top**) and atmosphere cloud liquid water from radiometer difference in in kg/m^2 (**bottom**) (selection on SLA_MLE4 valid points only).* . . . 34

30 *water vapor content from radiometer difference in kg/m^2, Computed over 2016 (**left**) and 2019 (**right**) (selection on SLA_MLE4 valid points only).* . . . 35

31 *atmosphere cloud liquid water from radiometer difference in in kg/m^2, Computed over 2016 (**left**) and 2019 (**right**) (selection on SLA_MLE4 valid points only).* . . . 35

32 *Daily mean of square_off_nadir_angle_wf_ku GDR-F minus GDR-D (selection on SLA_MLE4 valid points only).* . . . 36

33 *Daily mean of swh_ku GDR-F minus GDR-D (selection on SLA_MLE4 valid points only).* . . . 37

34 *Daily mean (**left**) and map averaging (**right**) of sig0_ku GDR-F minus GDR-D (selection on SLA_MLE4 valid points only).* . . . 37

35 *Histograms of altimeter and model wind speed (**top**), daily mean (**left**) and map averaging (**right**) of wind_speed_alt GDR-F minus GDR-D (selection on SLA_MLE4 valid points only).* . . . 38

36 *GDR-F and GDR-D histograms of sea_state_bias_ku* ***(top)****, daily mean* ***(left)*** *and map averaging* ***(right)*** *of sea_state_bias_ku GDR-F minus GDR-D (selection on SLA_MLE4 valid points only).* . . 39
37 *Difference of GDR-F and GDR-D SLA variance using non filtered ionospheric correction in both cases* ***(top left)****. Cyclic monitoring (without Caspian sea)* ***(top right)****. Variance difference at crossovers* ***(bottom)*** . . . 39
38 *Difference of GDR-F and GDR-D SLA variance using filtered ionospheric correction in case of GDR-F and non filtered solution in case of GDR-D* ***(left)****. Cyclic monitoring (without Caspian sea)* ***(right)****. Variance difference at crossovers* ***(bottom)****, note that a seection is done on $|latitude| < 50$, bathymetryi-1000m and on shallow waters on the difference at crossover monitoring (bottom right).* . . . 41
39 *Daily monitoring of GDR-F minus GDR-D GOT or FES ocean tide mean difference* ***(top)****. Mean difference of SSH at crossover between global tide models FES2014b and GOT4.8* ***(bottom)*** . . . 42
40 *Difference of SSH differences at crossovers and along-track SLA variance (without Caspian sea) between global tide models FES2014b and GOT4.8* . . . 43
41 *ocean_tide_non_equil GDR-F minus GDR-D difference (selection on SLA_MLE4 valid points only).* 43
42 *Variance and mean difference of SSH at crossover between GDR-F without internal tide and GDR-F with internal tide* . . . 44
43 *Difference of SLA variance (without Caspian sea) between GDR-F without internal tide and GDR-F with internal tide* . . . 45
44 *GDR-F and GDR-D histograms of pole_tide over the whole mission period* ***(top)****. GDR-F munis GDR-D pole_tide difference* ***(bottom)*** *(selection on SLA_MLE4 valid points only).* . . . 46
45 *Difference of SLA variance (without Caspian sea) between GDR-F without pole tide models Wahr (1985) and Desai (2015)* . . . 46
46 *GDR-F minus GDR-D MSS difference* ***(left)****. Difference of SLA variance (without Caspian sea) between MSS CNES/CLS11 and MSS CNES/CLS15* ***(right)*** . . . 47
47 *mean_topography over 1 cycle (selection on SLA_MLE4 valid points only): GDR-F* ***(left)*** *and GDR-F minus GDR-D difference* ***(right)****.* . . . 47
48 *geoid over 1 cycle (selection on SLA_MLE4 valid points only* ***(top)*** *or all along-track global monitoring* ***(bottom)****): GDR-F* ***(left)*** *and GDR-F minus GDR-D difference* ***(right)****.* . . . 48
49 *bathymetry over 1 cycle (selection on SLA_MLE4 valid points only* ***(top)*** *or all along-track global monitoring* ***(bottom)****): GDR-F* ***(left)*** *and GDR-F minus GDR-D difference* ***(right)****.* . . . 49
50 *Global rain flag for GDR-D (****left****) and GDR-F (****right****) over cycle 175.* . . . 50
51 *Rain flag activated for GDR-D (****left****) and GDR-F (****right****) over cycle 175.* . . . 50
52 *Rain flag for GDR-F for activated flag in GDR-D.* . . . 51
53 *GDR-F minus GDR-D : Sea surface height anomaly (left) and mean sea surface (right) over common valid points* . . . 53
54 *GDR-F minus GDR-D : orbit minus range difference (****top left****) and GDR-D minus GDR-F : sum of range corrections differences (****top right****), sea state bias (****bottom left****) and pole tide (****bottom right****) contributions.* . . . 54
55 *Cyclic mean of along-track SLA, without Caspian sea. Periodogram of SLA difference (GDR-F - GDR-D)* . . . 55
56 *Mean per cycle of SLA without correction (****left****) and SLA (****right****) of residuals (= interpolated over theorical ground track) SLA along-track. For $GDR-D$ comparisons (****top****) or $GDR-F/GDR-F_like$* ***(bottom)*** . . . 56
57 *SLA difference (Jason3 - Jason2) between cycle 25 to 58* . . . 56
58 *GMSL difference GDR-F - GDR-D of reference SLAs* . . . 57
59 *Waveform classification* . . . 59
60 *Pourcentage of valid point for GDR-F MLE4 and GDR-F Adaptive* . . . 60

61 *Number of measurements that are valid for GDR-F MLE4 and invalid for GDR-F Adaptive (top left, and bottom blue). Number of measurements that are invalid for GDR-F MLE4 and valid for GDR-F Adaptive (top right and bottom red)* 60
62 *Standard deviation of range fonction of SWH for **MLE4** and **Adaptive*** 62
63 *SWH spectrum 20hz for cycle 174* 62
64 *Histogram (**top left**) of SWH for GDR-F MLE4 and GDR-F Adaptive retracking and adaptive minus mle4 swh difference (**top right**) over cycle 073. swh differences wrt altimeter or era5 model over the whole period (**bottom**)* 63
65 *Mean of SSH difference at crossover points (selection on common valid points, $|latitude| < 50$, oceanic variability < 20cm and bathymetry < -1000m): cyclic monitoring (**top**), and map averaging (**bottom**) for GDR-D (**left**) or GDR-F (**right**).* 64
66 *Difference of SSH at crossover points : Variance difference (left) (selection on common valid points, $|latitude| < 50$, oceanic variability < 20cm and bathymetry < -1000m), pourcentage of error reduction (right)* 64
67 *Along track SLA variance difference between GDR-F adaptive and GDR-F MLE4 (caspian sea not included). Cyclic monitoring (**top left**), in function of distance to coast (**top right**). Map of absolute difference of variance (**bottom left**) and percentage relative to MLE4 level of variance (**bottom right**)* 65
68 *SLA spectrum 20hz for cycle 174* 66
69 *Difference of cyclic mean of Sea Level Anomaly (GDR-F adaptive - GDR-F MLE4)* 66
70 *SLA, range, ssb and ionospheric correction differences between adaptive and MLE4 over one cycle* 67
71 *GMSL difference GDR-F adaptive - mle4 SLAs over the whole period **(left)** or excluding cycles 057 to 085 **(right)*** 67
72 *Mean wave direction **left** and period **right** for one Jason-3 GDR-F cycle* 69
73 *Difference of editing point between SSB and SSB 3D (MLE4 retracking)* 70
74 *SSH difference at crossover for ssb_3d and ssb (with iono GIM). Note that figures are computed over a common valid points dataset.* 70
75 *SSH at crossover for ssb_3d and ssb (with iono GIM): difference of variance (ssb_3d - ssb) and pourcentage of error-reduction (ssb_3d - ssb). Note that figures are computed over a common valid points dataset.* 71
76 *SLA for ssb_3d and ssb (with iono GIM). Difference of variance (SSB_3D - SSB_2D) on cycllic monitoring (**left**) or geobox averaging (**right**)* 71
77 *GMSL difference GDR-F mle4 SLA with ssb - SLA with ssb_3d* 72
78 *Difference of editing point between SSB and SSB 3D (adaptive retracking)* 72
79 *SSH (adaptive retracking) difference at crossover for ssb_3d and ssb (with iono GIM). Note that figures are computed over a common valid points dataset.* 73
80 *SSH (adaptive retracking) difference at crossover for ssb_3d and ssb (with iono GIM): difference of variance (ssb_3d - ssb) and pourcentage of error-reduction (ssb_3d - ssb). Note that figures are computed over a common valid points dataset.* 73
81 *SLA for ssb_3d and ssb. Difference of variance (SSB_3D - SSB_2D) on cycllic monitoring (**left**) or geobox averaging (**right**)* 74
82 *GMSL difference GDR-F adaptive SLA with ssb - SLA with ssb_3d* 74

List of items to be defined or to be confirmed

Applicable documents / reference documents

Contents

1. Introduction **1**

2. Data used and processing **2**
2.1. **Data used** . . . 2
2.2. **GDR Standards** . . . 2
2.3. **Jason-2 data used for comparison** . . . 7

3. Data coverage and validity of measurements **8**
3.1. **Missing measurements** . . . 8
3.2. **Edited measurements** . . . 12
3.2.1. Overview . . . 12
3.2.2. Rejection on land and ice detection . . . 14
3.2.3. Rejection on threholds criteria . . . 14
3.2.4. Details on ionospheric correction filtering impact . . . 16

4. Quality overview and performances **18**
4.1. **Sea Surface Height at crossover points** . . . 18
4.1.1. Performance at crossover between GDR-F and GDR-D . . . 18
4.1.2. Estimation of the pseudo datation bias . . . 21
4.2. **Along-track performance of Sea Level Anomaly** . . . 22

5. Details of the changes in GDR-F standard **24**
5.1. **Datation difference** . . . 24
5.2. **GDR-F Precise Orbit Ephemeris POE-F** . . . 26
5.3. **Radiometer parameters** . . . 30
5.3.1. Brightness temperatures . . . 30
5.3.2. Radiometer minus model wet tropospheric corrections difference . . . 31
5.3.3. Atmospheric attenuation . . . 33
5.3.4. Atmosphere cloud liquid water and water vapor content . . . 34
5.4. **Altimeter parameters and corrections derived from the altimeter** . . . 36
5.4.1. Mispointing . . . 36
5.4.2. SWH . . . 37
5.4.3. Sigma0 . . . 37
5.4.4. Wind-speed . . . 37
5.4.5. Sea State Bias and dual-frequency ionospheric correction . . . 38
5.5. **Others corrections involved into SSH computation** . . . 42
5.5.1. Global tide models . . . 42
5.5.2. Internal tide . . . 44
5.5.3. Pole tide correction . . . 45
5.5.4. Mean Sea Surface . . . 46
5.6. **Other ancilliary data** . . . 47
5.6.1. Mean Dynamic Topography . . . 47
5.6.2. Geoid . . . 47
5.6.3. Bathymetry . . . 48
5.6.4. Surface type . . . 49
5.6.5. Rain flag . . . 49

6. Global and Regional Mean Sea Level long term monitoring **52**
6.1. **Sea Level Anomalies along-track analysis** . . . 52
6.1.1. Difference between Jason-3 GDR-F and GDR-D . . . 52
6.1.2. Difference between Jason-3 and Jason-2 . . . 55
6.2. **Reprocessing impact on Global Mean Sea Level trends** . . . 57

7. Analysis of the new retracker solution : the adaptive retracker **58**
7.1. **Waveforms classification** . . . 58
7.2. **Point to point validation process (editing)** . . . 60
7.3. **Focus on altimeter parameters** . . . 62
7.4. **Performances** . . . 63
7.4.1. Performances at crossovers . . . 63
7.4.2. Performances of along-track SLA . . . 64
7.5. **SLA and GMSL** . . . 66
7.6. **Conclusions** . . . 68

8. Analysis of the new sea state bias solution : add of mean wave period information **69**
8.1. **Mean wave period and direction** . . . 69
8.2. **Results on MLE4 retracking** . . . 69
8.3. **Results on adaptive retracking** . . . 72

9. Conclusion **75**

10. References **77**

1. Introduction

This document presents the synthesis report concerning validation activities of Jason-3 GDR-F provided in 2021 under SALP contract supported by CNES.

Since the launch of the Jason-3 satellite on 17th of January 2016, the GDR (Geophysical Data Record) data were distributed in D version. Jason-3 GDR products have been computed in version D until cycle 177. Jason-3 data have been reprocessed during 2021 with new GDR-F standard to improved data performance. From cycle 178 onwards (December 7 2020), the operational version of the Jason-3 GDR products have only been computed in version F.

This present global report deals with the complete reprocessed period of the Jason-3 mission, thanks to comparison with previous Jason-3 GDR-D standard (cycle 0 to 177), as well as comparison with Jason-2. It also contains the impact of the reprocessing on the mean sea level trend.

This report is split into 7 main sections after this introduction describing the keys of the reprocessing campaign:

- first, the **data used** are presented, with a status of the geophysical content of the fields that have changed between GDR-D and GDR-F.
- the **data coverage** and measurement validity issues are then presented.
- a global validity overview of the **performance improvement** is synthetized.
- the **impact of the reprocessing on the main altimeter, radiometer parameters and new geophysical models** is presented.
- the impact of the reprocessing on **Mean Sea Level** is detailed on the global and regional drift.

The two final chapters deal with new available variables:

- first, the analysis of the **differences between the MLE4 and Adaptive** retracking data
- and finally, the analysis of the **new sea state bias solution**.

Jason-3 GDR-F product contain MLE3, MLE4 and adaptive retraking algorithm outputs. Except on the dedicated adaptive retracking analysis chapter, only the data from MLE4 retracking algorithm are analysed.

2. Data used and processing

2.1. Data used

This document deals with the global impact of Jason-3 altimeter mission reprocessing (cycle 001 to 177) covering the period from 12th of february 2016 to 17th december 2020. Jason3 GDR products have been computed in version D until cycle 177. Data were available in version F since cycle 171 and along the way. From cycle 178 onwards, the operational version of the Jason-3 GDR products have only been computed in version F.

The operational version of IGDR have passed October 29 2020 from standard D to standard F (cycle 174).

In this document, some comparisons are realized with L2P product (more information about L2P in dedicated handbook [19]).

2.2. GDR Standards

Table 1 gives the content of L2 data used in this report, for the previous version ("D") and for the new version ("F").

Model	Product Version "D"	Product Version "F"
Reference Ellipsoid	TOPEX/Poseidon	WGS84
Orbit	DORIS and/or SLR and/or GPS tracking data (Orbit standard "POE-E" until cycle 094), DORIS and/or GPS tracking data (Orbit standard "POE-F" from cycle 095 onwards)).	DORIS and/or GPS tracking data (Orbit standard "POE-F").
Altimeter Instrument Corrections	Two sets : • one set consistent with MLE4 retracking • one set consistent with MLE3 retracking	Identical to version "D" No set needed for adaptive retracking
Jason-3 Advanced Microwave Radiometer (AMR) Parameters	Using calibration parameters derived from long term calibration tool developed and operated by NASA/JPL	Using **new calibration parameters** derived from long term calibration tool developed and operated by NASA/JPL

<table>
<tr><th>Model</th><th>Product Version “D”</th><th>Product Version “F”</th></tr>
<tr><td>Altimeter Retracking</td><td><u>“Ocean MLE4” retracking :</u>
MLE4 fit from 2nd order Brown analytical model : MLE4 simultaneously retrieves the 4 parameters that can be inverted from the altimeter waveforms :
• Epoch (tracker range offset : altimeter range)
• Composite Sigma : SWH
• Amplitude : Sigma0
• Square of mispointing angle (Ku band only, a null value is used in of the C band retracking algorithm)
<u>“Ocean MLE3” retracking :</u>
MLE3 fit from 1st order Brown analytical model : MLE3 simultaneously retrieves the 3 parameters (Epoch, composite Sigma and Amplitude, see ocean MLE4 retracking) that can be inverted from the altimeter waveforms.

<u>“Ice” retracking :</u>
Geometrical analysis of the altimeter waveforms, which retrieves Epoch and Amplitude (see ocean MLE4 retracking)</td><td><u>“Ocean MLE4” retracking :</u>
Identical to version “D”

<u>“Ocean MLE3” retracking :</u>
Identical to version “D”

<u>“Ice” retracking :</u>
Identical to version “D”

<u>“Adaptive” retracking :</u>
Adaptive retracking fit from Brown numerical model taking the real on-board PTR. Adaptive simultaneous retrieves the 4 parameters that can be inverted from the altimeter waveforms :
• Epoch (tracker range offset : altimeter range)
• Composite Sigma : SWH
• Amplitude : Sigma0
• Gamma</td></tr>
</table>

Model	Product Version "D"	Product Version "F"
Sea State Bias	Two empirical models: • MLE4 version derived from 1 year of MLE4 Jason-2 altimeter data with version "D" geophysical models • MLE3 version derived from 1 year of MLE3 Jason-2 altimeter data with version "D" geophysical models	• MLE3 version derived from 1 year of MLE3 Jason-2 altimeter data with version "D" geophysical models • CLS empirical solution fitted on one year of Jason-3 GDR-F data. Two solutions for each retracking (MLE4 and adaptive): – 2D model from SWH and altimeter wind-speed (standard version) – 3D model from SWH, altimeter wind-speed and t02 mean wave period from model (improved version)
Altimeter wind speed model	Derived from Jason-1 data	Following Gourrion's approach (Gourrion, 2020), based on Collard's model computed from Jason-1 (Collard, 2005)
Wind speed from model	ECMWF model	Identical to version "D"
Ionopheric correction	From Ku/C range difference	Two solutions: • From Ku/C range difference correction • From Ku/C range difference filtered correction
Ionopheric model correction	Based on Global Ionophere TEC Maps from JPL	Identical to version "D"
Wet Troposphere Range Correction from Model	From ECMWF model.	From ECMWF model. 2 solutions : integration from sea surface level or using altimetry range
Dry Troposphere Range Correction	From ECMWF atmospheric pressures and model for S1 and S2 atmospheric tides.	From ECMWF atmospheric pressures and model for S1 and S2 atmospheric tides. 2 solutions : integration from sea surface level or using altimetry range

Model	Product Version “D”	Product Version “F”
Inverse Barometer Correction	Computed from ECMWF atmospheric pressures after removing S1 and S2 atmospheric tides	Identical to version “D”
Non-tidal high-frequency dealiasing correction	Mog2D high resolution ocean model. Ocean model forced by ECMWF atmospheric pressures after removing S1 and S2 atmospheric tides	not available
Dynamical Atmospheric Correction	not available	Mog2D high resolution ocean model + inverse barometer. Ocean model forced by ECMWF wind field and atmospheric pressures after removing S1 and S2 atmospheric tides
Tide solution 1	GOT4.8 + S1 ocean tide. S1 load tide ignored	GOT4.10c
Tide solution 2	FES2004 + S1 and M4 oceans tides. S1 and M4 load tide ignored	FES2014b (non-equilibrium long-period ocean tide model not included)
Internal tide model	not available	HRET_v8.1, Zaron (2019)
Equilibrium long-period ocean tide model	From Cartwright and Taylor tidal potential	Identical to GDR-D
Non-equilibrium long-period ocean tide model	Mm, Mf, Mtm and Msqm from FES2004	Mm, Mf, Mtm, Msqm, Sa and Ssa from FES2014b
Solid earth tide model	From Cartwright and Taylor tidal potential	Identical to version “D”
Pole tide model	Equilibrium model	From Desai (2015) and MPL (2017)
Mean Sea Surface	MSS_CNES-CLS11 (7 years reference)	2 solutions: MSS_CNES-CLS15 and MSS_DTU_2018
Mean Dynamic Topography	MDT_CNES-CLS09	MDT_CNES-CLS18
Geoid	EGM96	EGM2008
Bathymetry Model	DTM2000.1	ACE2 (from EAPRS Laboratory)
Rain flag	Derived from comparisons to threshold of the radiometer-derived integrated liquid water content and of the difference between the measured and the expected Ku-band backscatter coefficient	Identical method to version “D”, using an updated table of the difference between the measured and the expected Ku-band backscatter coefficient

Model	Product Version “D”	Product Version “F”
Ice flag	Derived from comparison of the model wet tropospheric correction to a dual-frequency wet tropospheric correction retrieved from radiometer brightness temperatures, with a default value issued from climatology table	Identical to version “D”

Table 1 – Models and standards adopted for Jason-3 product version “D” and “F”

2.3. Jason-2 data used for comparison

Between Febuary 12 2016 to October 2 2016 (cycle 000 to 023 for Jason-3), the tandem flight phase is specially suited for intercomparison between Jason-3 and Jason-2, as both satellite were only 80 seconds apart on the same ground track. Jason-2 mission ended on October 1 2019.

In this current report, Jason-2 GDR-D standard was used to compare to Jason-3 reprocessed data. Several corrections for Jason-2 are updated to have as much as possible homogeneous data between Jason-2 and Jason-3 GDR-F (only range, wet tropospheric correction, DAC and solid earth tide are from GDR-D). These corrections are:

- Orbit standard POE-F
- Sea state bias (Tran, 2018 for Jason-2 and 2020 for Jason-3).
- Ionopheric filtered correction from Jason-2 range GDR-D and updated SSB (2018)
- Dry tropospheric correction (ECMWF zero altitude)
- Ocean tide FES14b (non equilibrium long-period ocean tide model included)
- Internal tide (HRET_v8.1, Zaron, 2019)
- Pole tide (Desai 2015 and MPL 2017)
- Mean sea surface (CNES-CLS 2015)

3. Data coverage and validity of measurements

This part consists in analysing the availability of data for level 2 products before and after the reprocessing exercise. Futhermore the edited (invalidated) measurements are monitored.

3.1. Missing measurements

The reprocessed GDR-F data are globally as available as GDR-D (see figure 1) with less than 10 points difference per cycle (except for cycle 000 to 003, cycle 057 and cycle 173, details below). Each event of missing data in GDR-D is detailed on the cyclic validation reports [2] and the main events are summarized in table 2.

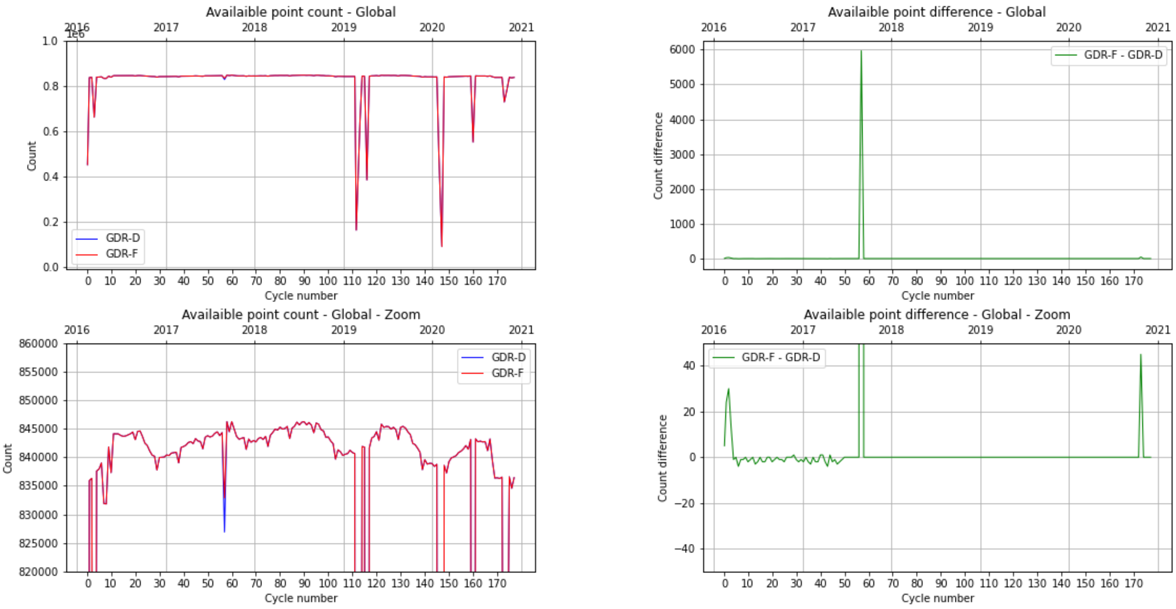

*Figure 1 – Number of data available in 1Hz products for GDR-F and GDR-D (**left**). Number of available points difference : GDR-F - GDR-D (**right**).*

The main differences in coverage are :

- Between cycle 000 to 003, more missing points in GDR-D (less than 30 points per cycle). Some datation difference between GDR-F and GDR-D before Platform GPS software upload (Cycle 003 - passes 182 to 232) can explain this difference in number of data at 1Hz before and after reprocessing.
- Over cycle 057: additionnal available measurements in GDR-F over passes 152 and 153 (these two passes appear in red on figure 2).
- Over cycle 173: 45 missing points in GDR-D before DORIS incident on october 27 2020 between 13:23:02 and 13:23:44 are available in GDR-F product thanks to a computing procedure update in case of event.

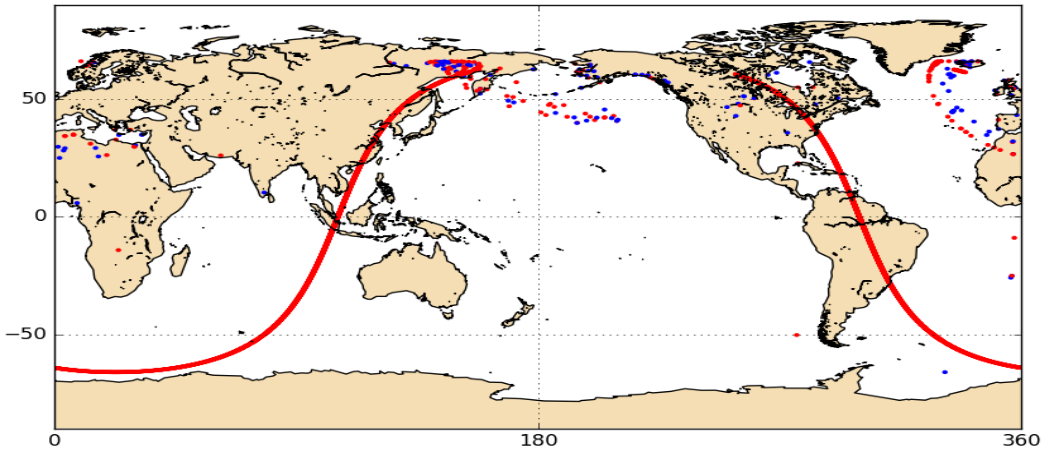

Figure 2 – Map of missing data differences over cycles 001 to 177. ***Blue*** *: Missing data in GDR-F (available in GDR-D).* ***Red*** *: Missing data in GDR-D (available in GDR-F).*

Table 2 gives the main data gaps during mission Jason-3 (until the end of year 2020) and the associated events. More details are available in [3].

Jason-3 cycle	Pass	Event
Cycle 0	Passes 0 to 116	No data in both dataset. Cycle begin at pass 117
Cycle 3	Passes 182 to 232	No data in both dataset. Platform GPS software upload
Cycle 57	Pass 124	No data in both dataset. DEM update
Cycle 57	Passes 152 and 153	No data in GDR-D. Additionnal available measurement in GDR-F
Cycle 112	Passes 50 to 254	No data in both dataset. SHM
Cycle 113	Passes 1 to 60	No data in both dataset. SHM
Cycle 116	Passes 108 to 245	No data in both dataset. SHM
Cycle 146	Passes 154 to 254	No data in both dataset. SHM
Cycle 147	Passes 1 to 32 and 45 to 236	No data in both dataset. SHM
Cycle 160	Passse 101 to 186	No data in both dataset. SHM
Cycle 173	Passse 223 to 254	No data in both dataset. DORIS incident
Cycle 174	Passse 1 to 16	No data in both dataset. DORIS incident
from cycle 178 onwards	All	No GDR-D data. End of production

Table 2 – Missing passes from 2016 to 2020

Data coverage over ocean:
The use of the GDR surface_classification leads to a higher number of ocean points for GDR-F than GDR-D, with near 500 additionnal ocean data per cycle in GDR-F (see figure 3). Previous surface classification has 4 classes and new has 7 (see details in table 3 and figure 4). Both of them use 0 for ocean. However, there are more measurements flag to 0 in new classiffication (GDR-F) than in previous (GDR-D). These additional measurements are mainly near coast and were flagged as land in GDR-D (see figure 5).

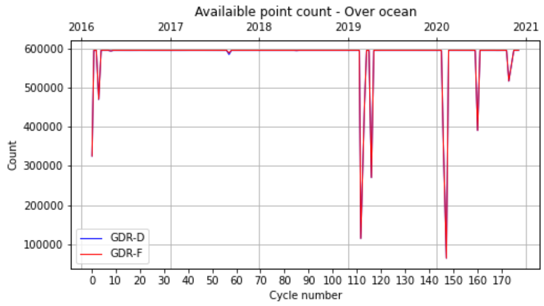

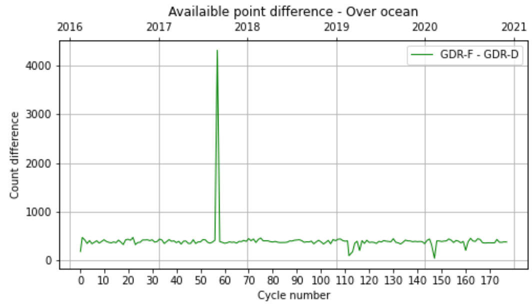

*Figure 3 – Cyclic mean of number of ocean data available for GDR-F and GDR-D (**left**). Data available difference over ocean : GDR-F - GDR-D (**right**)*

	Previous classification (GDR-D)	New classification (GDR-F)
0	ocean	open ocean
1	lake, enclosed sea	land
2	ice	continental water
3	land	aquatic vegetation
4	-	continental ice or snow
5	-	floating ice
6	-	salted basin

Table 3 – Previous (GDR-D) and new (GDR-F) surface classification

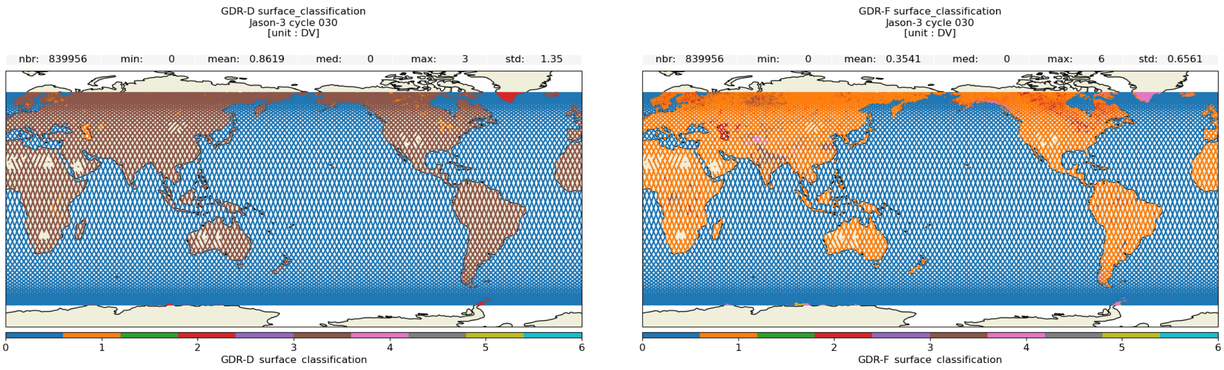

*Figure 4 – Surface type / classification over one cycle in GDR-D (**left**) and GDR-F (**right**)*

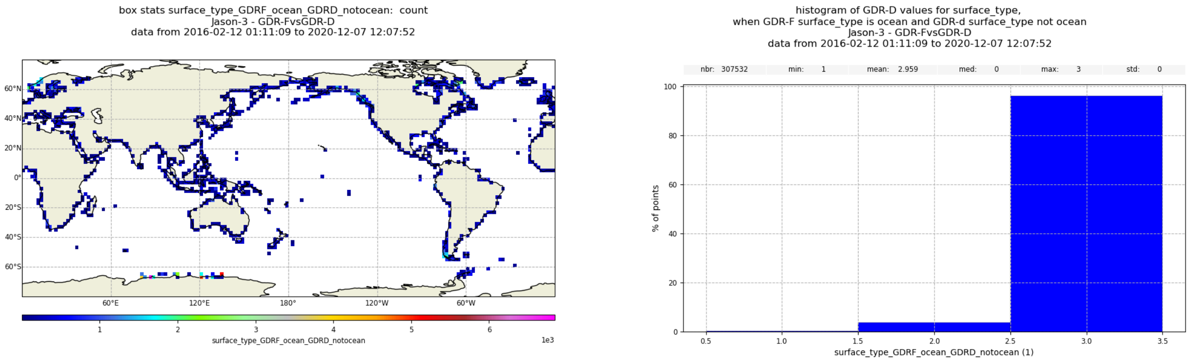

*Figure 5 – Number of identified ocean point in GDR-F that are not ocean in GDR-D (**left**). GDR-D surface_type values for ocean additional GDR-F points (**right**)*

3.2. Edited measurements

3.2.1. Overview

Data editing is necessary to remove altimeter measurements having lower accuracy. Once data over land are excluded, its consists in:

- First, removing the data corrupted by ice.
- Then, threshold criteria are applied on altimeter, radiometer and geophysical parameters as described in the following table 4. Except for the dual frequency ionosphere correction, only Ku-band measurements are used in this editing procedure, as they mainly represent the end user dataset.
- The third step uses cubic splines adjustements to the Sea Surface Height Anomaly (SSH-MSS) to detect remaining spurious measurements.
- The last step consists in removing an entire pass if SSH-MSS mean and standard deviation have higher values than thresholds. This criterion is used to detect problems such as bad orbit quality or time tag problems. Nevertheless for Jason-3 GDR with MLE4 or adaptive retracker, it has never edited data. *(With MLE3 retracking, it happens only for cycle 003 / pass 018, which is very short due to data gap.)*

The percentage of valid data per cycle after editing process for GDR-F and GDR-D product is monitored on figure 6. The rate of rejected data is quite equivalent on GDR-D and GDR-F datasets, GDR-F rate of valid data is globally slightly lower than for GDR-D (difference $< 0.2\%$ over ocean).

Except for cycle 030 (on which there is a peak for both datasets due to radiometer wet tropospheric correction set to defaut value during an AMR anomaly over 34 passes), valid data represent 59 to 67 % of global available data, depending on seasonal ice coverage, for both GDR-F and GDR-D. Over ocean, valid data rate increases between 83 and 93%.

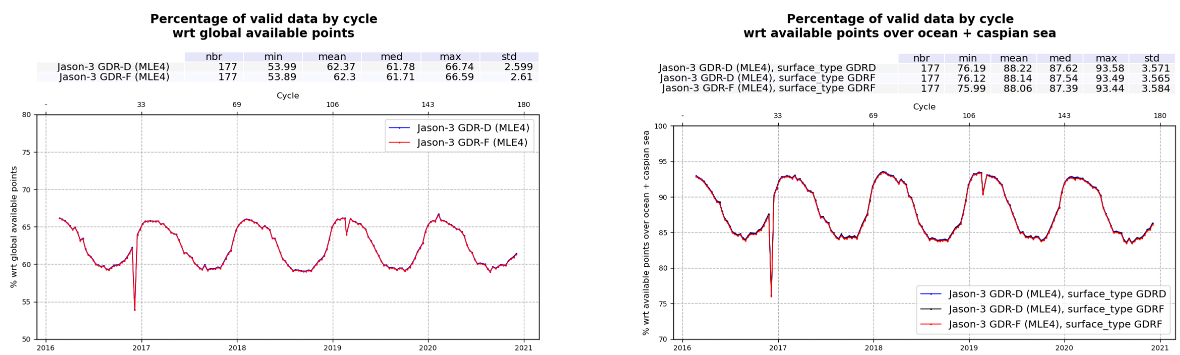

*Figure 6 – Percentage of valid measurement for GDR-D and GDR-F with no surface type selection on **(left)**, and with selection over ocean on **(right)**. Note that GDR-D surface_type (resp. GDR-F surface_classification) is used to select ocean points on GDR-D (resp. GDR-F) analysis.*

If global rates of valid measurements over ocean are quite equivalent between GDR-D and GDR-F, some discrepancies are visible on the spatial distribution of these valid data (figure 7). Globally, measurements are more valid over open ocean on GDR-F dataset than on GDR-D dataset (red points on figure 7 and left of figure 8), but there are more rejected data in GDR-F near ice and coasts (blue points on figure 7 and figure 8), this is mainly due to the ionospheric correction filtering behavior near coasts and ice (see dedicated part 3.2.4.).

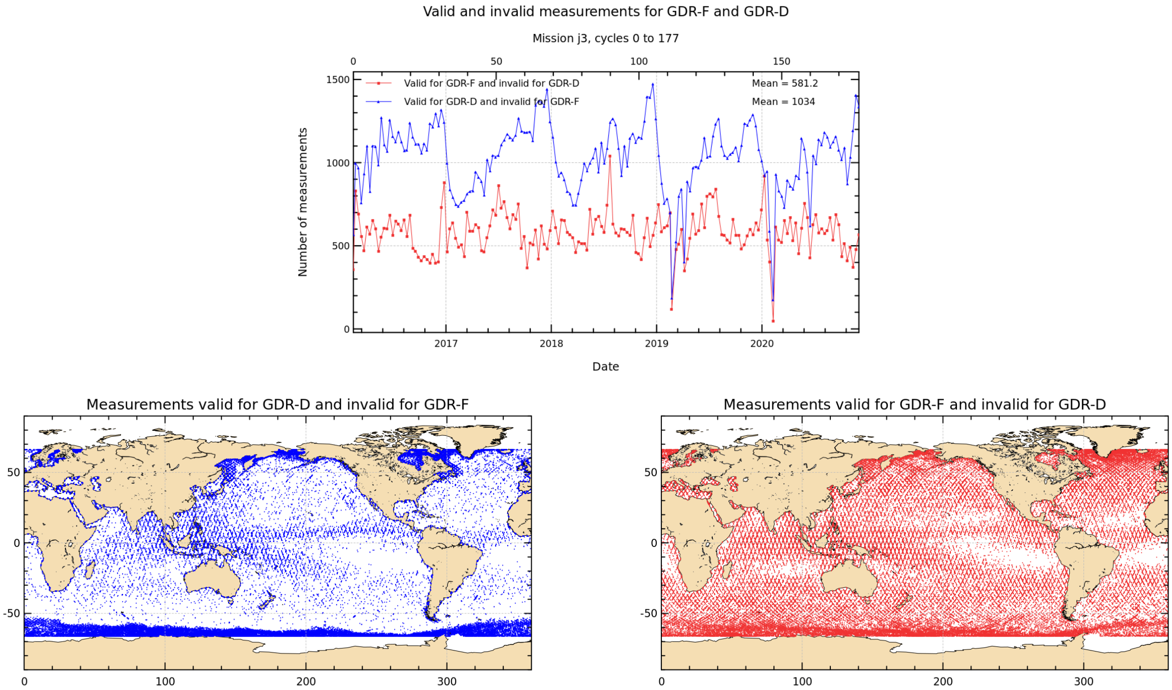

*Figure 7 – Cyclic number of measurements that are valid in one case and not in the other until cycle 177 (**top**). Map of valid GDR-D / invalid GDR-F points (**left**) and map of valid GDR-F / invalid GDR-D points (**right**). All the other records have the same valid/invalid status on both GDR-D and GDR-F datasets.*

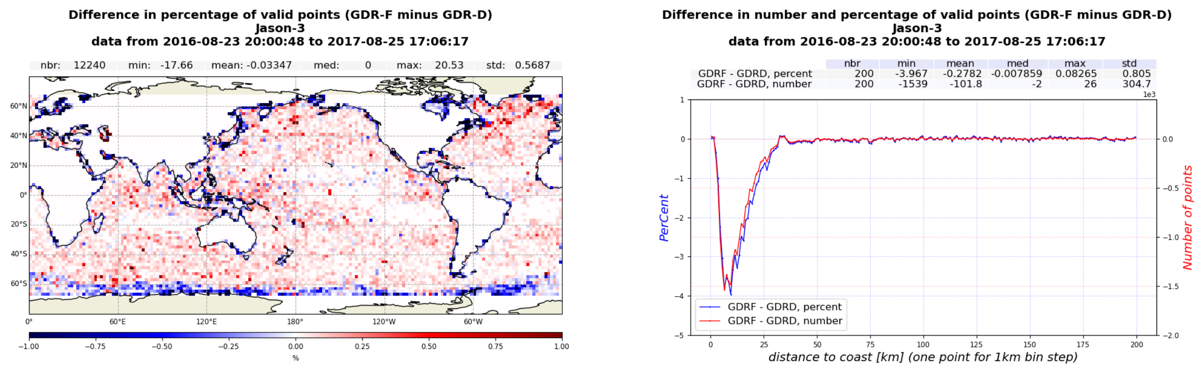

*Figure 8 – Map of the number of valid points difference in percentage (**left**). Blue boxes indicate that there are more valid measurements in GDR-D. Red boxes indicate that there are more valid measurements in GDR-F. Monitoring in function of distance to coast (**right**). Both figures are computed over one year of data.*

3.2.2. Rejection on land and ice detection

The first step of editing process includes the remove of points over land, and ice detection. As concerned land detection, surface classification evolution is described in table 3 and figure 4.

In average, the number of points rejected on land + ice detection on GDR-F is lower than 443 points per cycle compared to GDR-D. On one hand, there are more ocean points in GDR-F surface_classification (see figure 3), and on the other hand, when considering GDR-F surface_classsification, there are more points with altimeter ice flag activated for GDR-F data than GDR-D data (see figure 9).

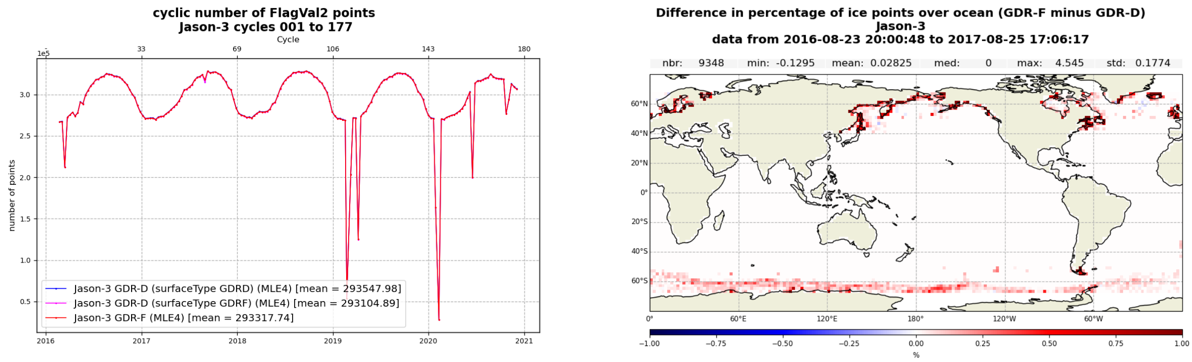

Figure 9 – Number of rejected measurement per cycle on land + ice criterion, for GDR-D and GDR-F. Map of the number of ice points difference in percentage (computed over one year of data with GDR-F surface_classification for both solutions). Blue boxes indicate that there are more ice flagged measurements in GDR-D. Red boxes indicate that there are more ice flagged measurements in GDR-F.

3.2.3. Rejection on threholds criteria

Editing on thresholds criteria is done after remove of land and ice points, so that the change in surface_type / surface_classification described in part 3.1. has an impact on the rate of measurements rejected at this step. In order to avoid any misunderstanding of difference in these rate differences, the evolution of rejected on thresholds number of points is computed on GDR-D data, using the updated to GDR-F version of surface_classification (see 5th column in table 4).

Considering the same ocean surface definition, significant differences in rejected on thresholds rate are only visible on ionospheric correction and sea level anomaly criteria. In both cases these differences are linked to the filtering solution of ionospheric correction (see 3.2.4.): there are slightly less rejected points on ionospheric correction over open ocean, but more rejected points on SLA thresholds due to set to DV points near coasts and ice.

Parameter	Threshold min	Threshold max	GDR-D MLE4	GDR-D MLE4 (surface type 7 classes)	GDR-F MLE4
swh	0	11m	0.57 %	0.64 % ↗	0.64 % ↔
square off nadir angle	-0.2 deg^2	0.64deg^2	0.50 %	0.65 % ↗	0.65 % ↔
sea surface height (orbit - range)	-130 m	100 m	0.74 %	0.82 % ↗	0.82 % ↔
range : number of 20Hz meas.	10	20	1.02 %	1.10 % ↗	1.10 % ↔
range : std of 20Hz meas.	0	0.2 m	1.33 %	1.40 % ↗	1.40 % ↔
sigma0	7 dB	30 dB	0.56 %	0.63 % ↗	0.63 % ↔
sigma0 : number of 20Hz meas.	10	20	1.01 %	1.09 % ↗	1.09 % ↔
sigma0 : std of 20Hz meas.	0	1 dB	2.07 %	2.14 % ↗	2.13 % ↔
wind speed from altimeter	0	30 m/s	1.03 %	1.10 % ↗	1.08 % ↘
sea state bias	-0.5 m	0	0.51 %	0.58 % ↗	0.58 % ↔
ionospheric correction (filtered)	-0.4 m	0.4 m	-	-	0.90 % ↘ (compared to raw iono)
ionospheric correction (raw data)	-0.4 m	0.4 m	0.97 %	1.05 % ↗	1.05 % ↔
radiom. wet tropospheric corr.	-0.5 m	-0.001 m	0.16 %	0.16 % ↔	0.15 % ↔
sea level anomaly	-2 m	+2 m	-	-	1.45 % ↗ (compared to raw iono)
sea level anomaly (iono raw)	-2 m	+2 m	0.90 %	0.97 % ↗	0.96 % ↔
ocean tide (FES)	-5 m	5 m	0.17 %	0.19 % ↗	<0.01 % ↘
ocean tide (GOT)	-5 m	5 m	<0.01 %	0.01 % ↗	<0.01 % ↔
cyclic mean number of edited points by thresholds					
- GDR-D: non filtered iono.			17011	17500	
- GDR-F: filtered iono.					17856
percentage of rejected points by thresholds wrt non ice (ocean + caspian sea)			3.23 %	3.30 % ↗	3.37 % ↗

Table 4 – thresholds editing rates, from from 2016 to 2020 (cycles 001 to 177)

3.2.4. Details on ionospheric correction filtering impact

The main differences in thresholds editing are due to ionospheric correction criterion. Note that in GDR-F, a filtered ionospheric correction is used whereas GDR-D validation status values are obtained using non filtered ionospheric correction. A particular version of GDR-F is presented in this part, using the raw ionospheric correction (non filtered, also available in GDR-F product), like in GDR-D.

Figure 10 and figure 11 highlight that when considering the non filtered solution in both GDR-D and GDR-F, the difference in global number of rejected points is significantly reduced. However, it is important to keep in mind that filtering of ionospheric correction leads to a small loss of valid SLA near coasts and ice in GDR-F but improves SSH estimations performance (see part 4. and part 5.4.5.).

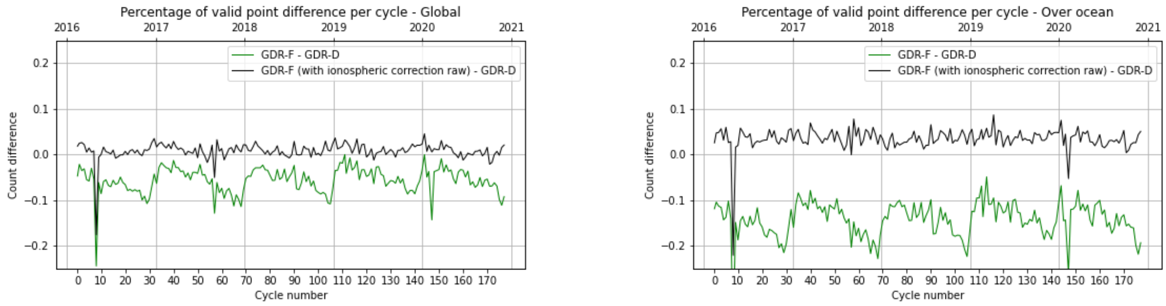

*Figure 10 – Percentage of valid measurement difference between GDR-D and GDR-F (**green**) or GDR-F with ionospheric correction raw (**black**) at global (**left**) and over ocean (**right**).*

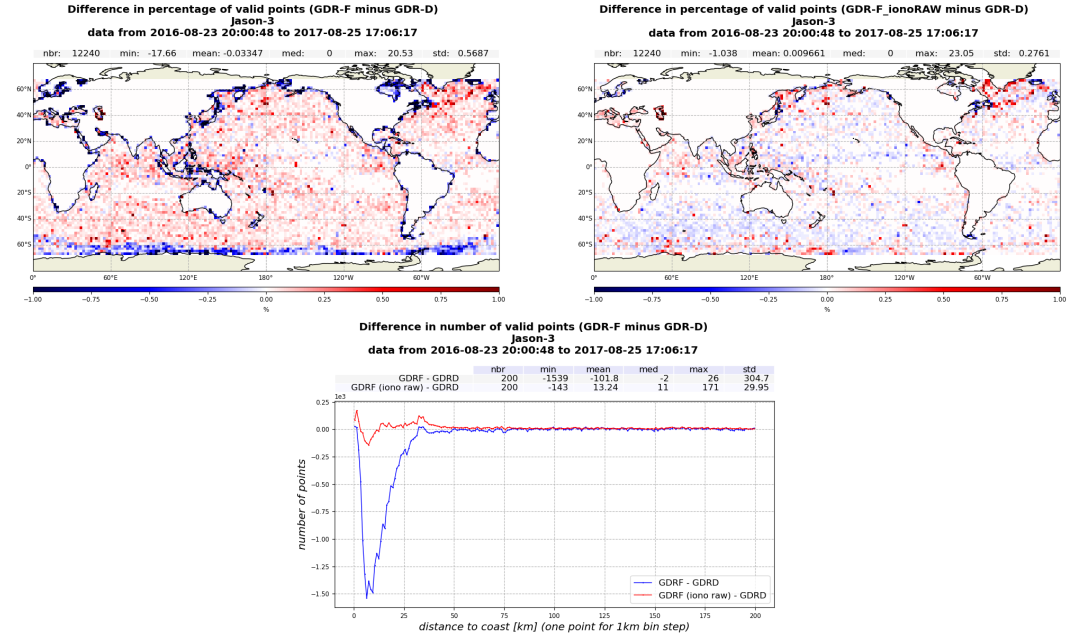

*Figure 11 – Differences in percentage of valid measurements for SLA with non-filtered ionospheric solution for both GDR-d and GDR-F (**right**), or with filtred solution for GDR-F (**left**). Maps (**top**) and with regard to distance to coast (**bottom**)*

4. Quality overview and performances

In this chapter the performances of Jason-3 GDR-F data are analyzed at crossovers and along-track.

4.1. Sea Surface Height at crossover points

Ascending and descending SSH (Sea Surface Height) differences are computed at crossover points. These differences are done for time differences less than 10 days between points from ascending and descending tracks. This allows to minimize the contribution of the oceanic variability (mesoscale). Therefore the variance of the SSH differences at crossover points gives an information of the altimeter system performance.

4.1.1. Performance at crossover between GDR-F and GDR-D

The SSH calculation for Jason-3 are defined below :

$$SSH_{GDR-D} = Orbit_{GDR-D} - AltimeterRange_{GDR-D} - \sum_{i=1}^{n} Correction_{GDR-D_i} \tag{1}$$

with $Orbit_{GDR-D}$ = POE-E until cycle 094 and POE-F from cycle 095 onwards.

$$SSH_{GDR-F} = Orbit_{GDR-F} - AltimeterRange_{GDR-F} - \sum_{i=1}^{n} Correction_{GDR-F_i} \tag{2}$$

	$\sum_{i=1}^{n} Correction_{GDR-D_i}$ equal to the sum of	$\sum_{i=1}^{n} Correction_{GDR-F_i}$ equal to the sum of
Non parametric sea state bias corr.	from GDR-D	from GDR-F
Dual frequency ionospheric corr.	from GDR-D (non filtered)	from GDR-F (filtered)
Radiometer wet tropospheric corr.	from GDR-D	from GDR-F
Dry tropospheric corr.	operational ECMWF	identical to GDR-D
Dynamical atmospheric corr.	operational MOG2D	identical to GDR-D
Ocean tide corr.	GOT4.8 (including loading tide)	FES14B (including loading tide and dynamical waves)
Internal tide corr.	N/A	HRET8.1 (ZARON2019), 4 waves included
Earth tide height	Cartwright and Taylor	identical to GDR-D
Pole tide height	Wahr85 (constant mean pole location)	Desai2015 / MPL2017

Table 5 – GDR-D versus GDR-F SSH components for performances at crossover points analysis

Thanks to POE-F orbit solution, a 120 days signal at crossovers on cyclic mean of SSH differences at crossovers is reduced and its phase changed (top of figure 12). As concerned mean of SSH differences at crossover point averaging over the whole period, geographically correlated patterns are very slightly reduced (see figure 12). This can be link to 120 days signal reduction that is visible on top figure 12.

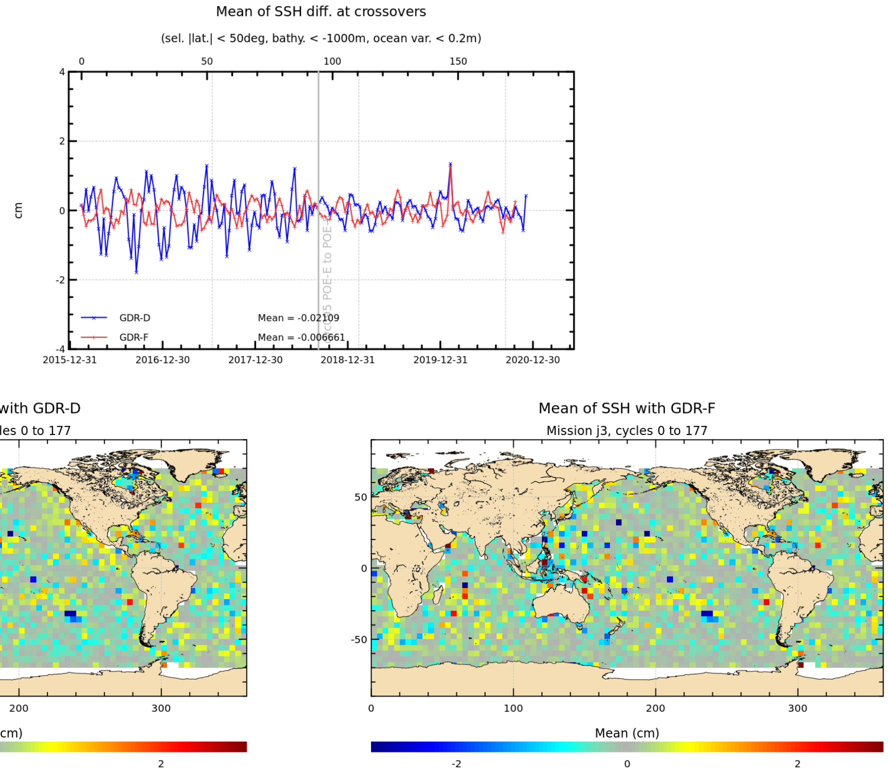

*Figure 12 – Cyclic mean of SSH differences at crossovers for GDR-F and GDR-D (selection on |latitude| < 50, oceanic variability < 20cm and bathymetry < -1000m) (**top**). Mean of SSH differences at crossovers map average over the whole period for GDR-D (**bottom left**) and GDR-F (**bottom right**)*

The global variance reduction from GDR-D to GDR-F, using only corrections that are available in L2 products, is -4.41cm^2 (Figure 13). It is reduced everywhere between 5 and 25%.

The main contributor to this variance reduction of SSH differences between ascending and descending passes is the filtering version of the ionospheric correction (figure 14): computing the same differences with non filtered ionospheric correction solution on GDR-F SSH leads to a variance reduction of -1.25cm^2.

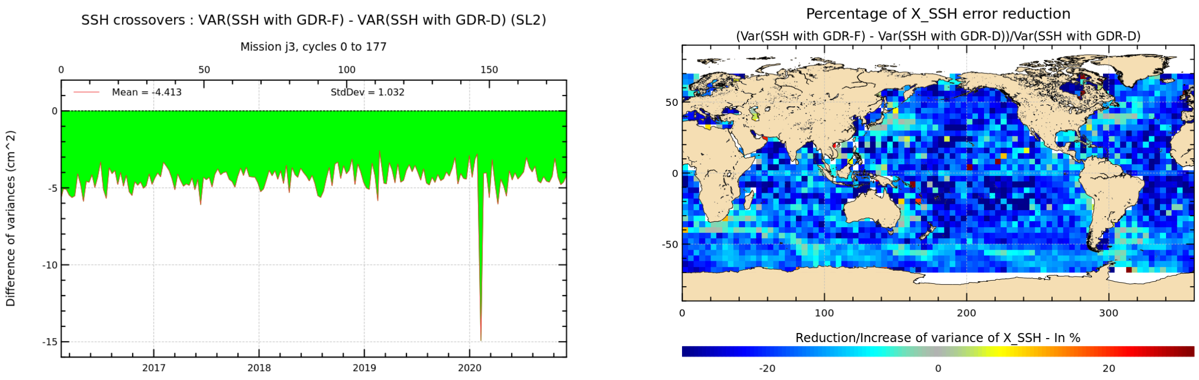

*Figure 13 – Difference (GDR-F - GDR-D) of variance at SSH differences at crossover. Difference per cycle (with selection on |latitude| < 50, oceanic variability < 20cm and bathymetry < -1000m) (**left**) and map in percentage (**right**)*

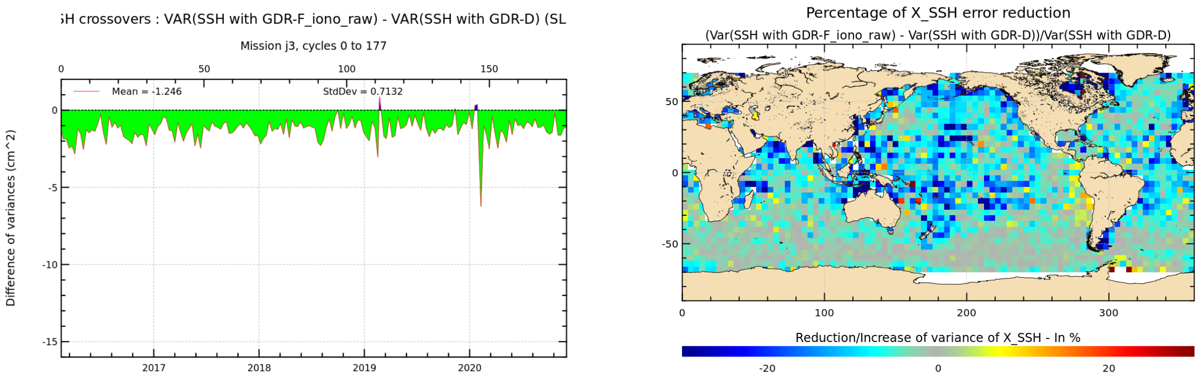

*Figure 14 – Difference (GDR-F - GDR-D) of variance at SSH differences at crossover in case of non filtered ionospheric correction for both GDR-D and GDR-F SSH. Difference per cycle (with selection on |latitude| < 50, oceanic variability < 20cm and bathymetry < -1000m) (**left**) and map in percentage (**right**)*

In conclusion, the different contributors to this improvement of -1.3cm^2 at monomissions crossover points are :

- **ocean tide (-0.48cm^2, figure 40),**
- **internal tide (-0.47cm^2, figure 42),**
- **orbit (-0.21cm^2, figure 23),**
- **sea state bias + ionospheric correction (-0.11cm^2 without filtering of ionospheric correction , figure 37)**

Adding the filtering of the ionospheric correction leads to a total reduction of 4.4cm^2).

4.1.2. Estimation of the pseudo datation bias

The pseudo time tag bias is found by computing at SSH crossovers a regression between SSH and orbital altitude rate ($\dot{H}$), also called satellite radial speed :

$$SSH = \alpha \dot{H} \tag{3}$$

This method allows us to estimate the time tag bias but it absorbs also other errors correlated with $\dot{H}$ as for instance orbit errors. Therefore it is called "pseudo" time tag bias.

The monitoring of this coefficient estimated at each cycle is performed for Jason-3 and Jason-2 in the figure 15: it highlights that pseudo time tag bias is close to zero (mean value lower than 0.06 ms) for both missions. There is no significant impact of reprocessing on pseudo datation bias estimation.

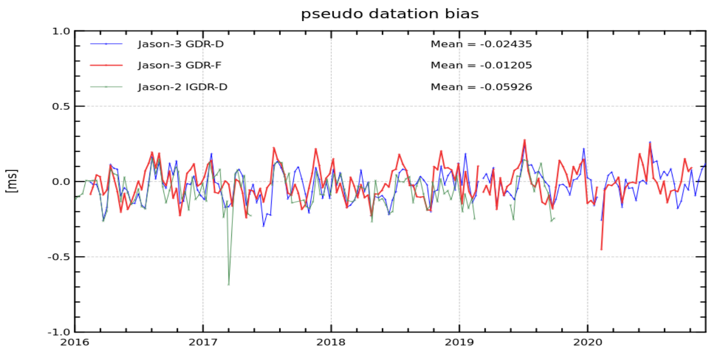

Figure 15 – Cyclic monitoring of pseudo time tag bias for Jason-3 and Jason-2

Figure 16 present periodograms of this pseudo time tag bias. Jason-3 GDR-D and Jason-2 IGDR-D have peak around 58 to 59 days (with a lower amplitude for Jason-3 than Jason-2). The 59 day-signal was analysed in 2014 Jason-2 CalVal report wrt ocean tide solution used in SSH computation [6]. Jason-3 GDR-F significantly reduce this signal compared to GDR-D, this is probably linked to the use of the FES14B solution for ocean tide correction and the update of orbit standard. Nevertheless, a near 174 days signal has a higher amplitude for GDR-F than GDR-D.

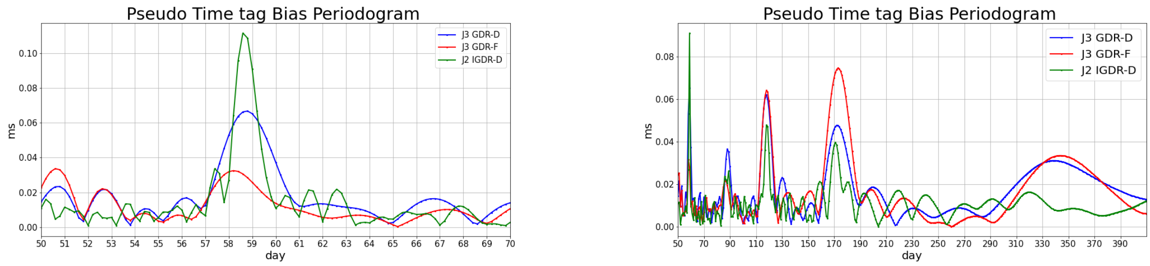

Figure 16 – Periodogram of pseudo time tag bias

4.2. Along-track performance of Sea Level Anomaly

The Sea Level Anomaly corresponds to the Sea Surface Height where the mean sea surface is removed (SLA = SSH - MSS). In the frame of this analysis, only CNES/CLS15 mean sea surface solution has been used for GDR-F dataset (CNES/CLS11 for GDR-D dataset). Along track sea level anomaly standard deviation is lower with GDR-F than GDR-D : -0.8 cm for GDR-F with filtered ionospheric correction and -0.6 cm for GDR-F with ionospheric correction raw (see figure 17).

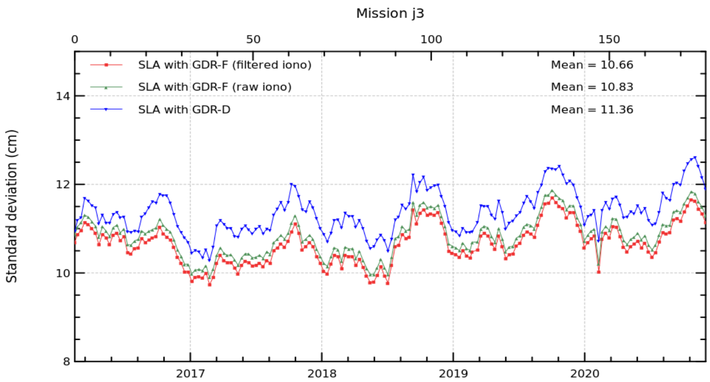

Figure 17 – Standard deviation of sea level anomaly (over ocean + Caspian Sea) difference over GDR-F and GDR-D datasets

The variance of the SLA is lower for GDR-F than GDR-D: -15.5 cm^2 with GDR-F filtered ionospheric correction and -11.8 cm^2 with GDR-F non filtered ionospheric correction. These variance reductions are respectively -12.1 cm^2 and -8.6 cm^2 when excluding the Caspian sea (see figure 18).

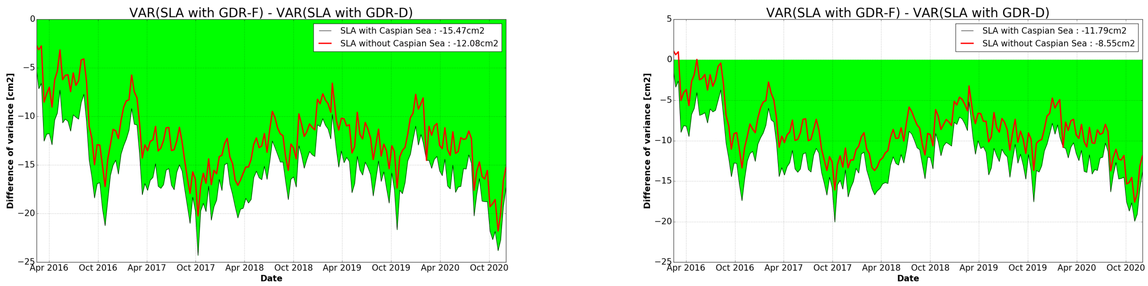

Figure 18 – SLA variance difference between GDR-F and GDR-D (top left: GDR-F with filtered ionospheric correction. top right: GDR-F with raw ionospheric correction).

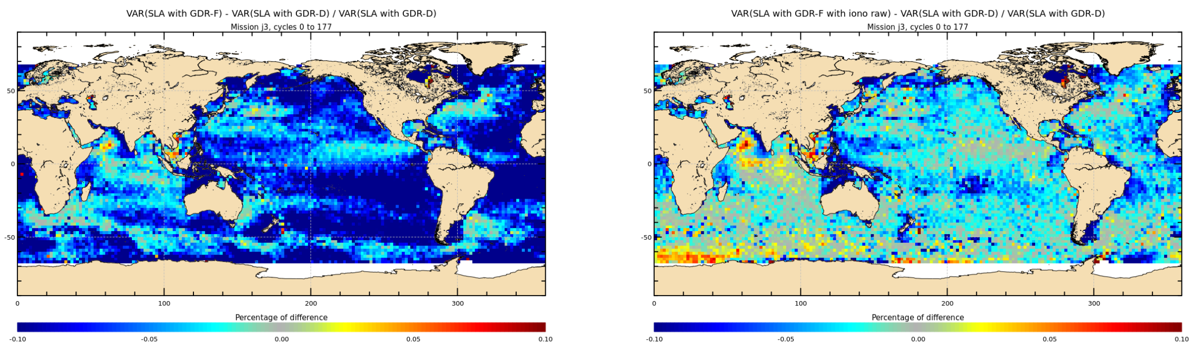

*Figure 19 – SLA variance difference between GDR-F and GDR-D with regard to GDR-D level of variance (**left**: GDR-F with filtered ionospheric correction. **right**: GDR-F with raw ionospheric correction.*

5. Details of the changes in GDR-F standard

In this following chapter the changes of the GDR-F standard (compared to GDR-D) are detailed.

The following points are adressed:

- the datation
- the orbit standard
- the radiometer related parameters
- the altimeter related parameters
- the other corrections.

5.1. Datation difference

Datation can be different between GDR-F and GDR-D. This is due to slight difference in the 20hz measurements that are taken into account to compute one 1hz point. Figure 20 shows the number of measurement where the difference is higher than 1μs.

The global number of point per cycle with datation difference higher than 1μs is near 30 points from cycle 52 onwards except for some cycles. Before cycle 52, this number can reach more than 1600 points. A change of level 1 processing on GDR-D can explain this difference before and after cycle 52. After the update of the L1 library during GDR-D processing mid-2017, the number of points with differences in datation is reduced to less than 30 points per cycle from cycle052 (see figure 20) onwards except for the following cycles :

- cycle 071 (11-21/01/2018), 989 points: one 20hz record was taken into account over pass 22 in GDR-D and is integrated to pass 23 in GDR-F with a result of 0.0509 seconds of difference between datations
- cycle 113 (06-13/03/2019), 4841 points: this datation difference is lower than 1.5μs. All points are between pass 61 and 91, just after SHM event (see table 2)
- cycle 115 (304 points): 0.2 secondes of difference during part of pass 123 in North Pacific
- cycle 160 (182 points): datation difference is lower than 1.5μs. All points are between pass 187 and 254, just after SHM event (see table 2)

Figure 21 present point with difference in datation for each case and exception.

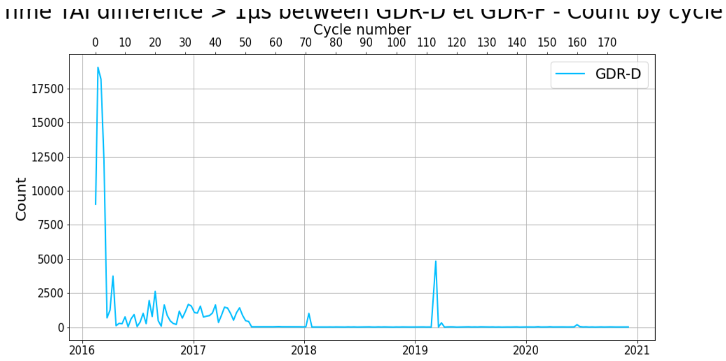

Figure 20 – Cyclic count of measurements with time difference between GDR-F and GDR-D > $1\mu s$

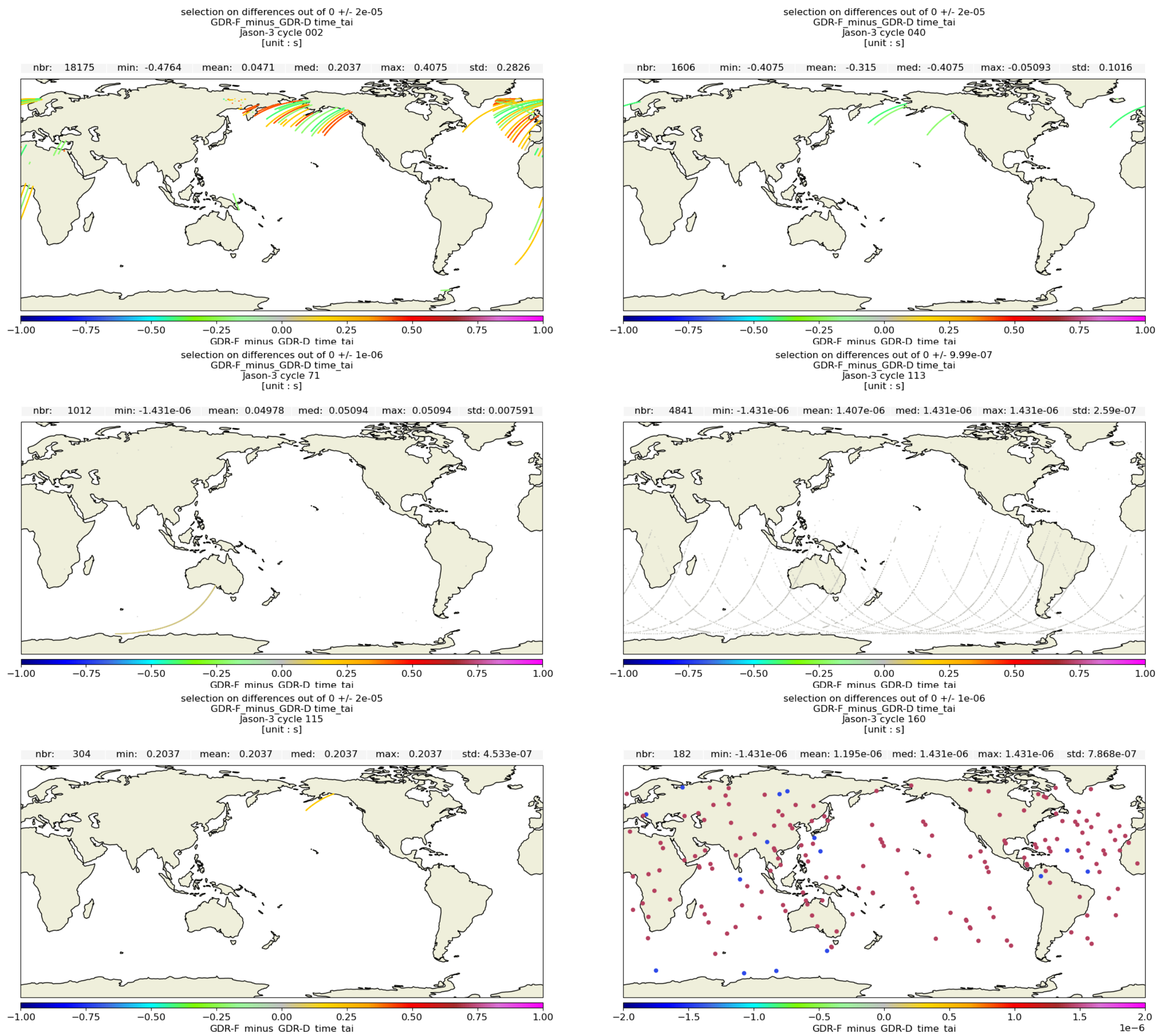

Figure 21 – Points with difference in datation between GDR-D and GDR-F for cycle 2, 40, 71, 113, 115 and 160

5.2. GDR-F Precise Orbit Ephemeris POE-F

GDRD-D orbit solution is POE-E until cycle 094. GDR-F (and GDR-D from cycle 095 onwards) data contain the Precise Orbit Ephemeris standard F (POE-F). Differences between POE-F and previous version POE-E are summarized below.

Parameter	POE-E	POE-F
Gravity model	• EIGEN-GRGS.RL03-v2.MEAN-FIELD • Non-tidal TVG : one annual, one semi-annual, one bias and one drift terms for each year up to **deg/ord 80**; C21/S21 modeled according to IERS2010 conventions • Solid Earth tides : IERS2003 conventions • Ocean tides : **FES2012** • Oceanic/atmospheric gravity : **6hr NCEP pressure fields (70x70) + tides from IERS2010 conventions** • Pole tide : solid earth and ocean from IERS2010 conventions • Thirds bodies : Sun, Moon, Venus, Mars and Jupiter	• EIGEN-GRGS.RL04-v1.MEAN-FIELD • Non-tidal TVG : one annual, one semi-annual, one bias and one drift terms for each year up to **deg/ord 90**; C21/S21 modeled according to IERS2010 conventions • Solid Earth tides : Unchanged • Ocean tides : **FES2014** • Oceanic/atmospheric gravity : **3hr dealiasing products from GFZ AOD1B RL06** • Pole tide : Unchanged • Thirds bodies : Unchanged
Suface forces	• Radiation pressure model : calibrated semi-empirical solar raidation pressure model • Earth radiation : Knocke-Ries albedo and IR satellite model • Atmospheric density model : DTM-13 for Jason satellites and HY-2A. **MSIS-86 for other satellites**	• Radiation pressure model : Unchanged • Earth radiation : Unchanged • Atmospheric density model : DTM-13 for Jason satellites and HY-2A. **MSIS-00 for other satellites**
Estimates dynamical parameters	Stochastic solutions	Unchanged

Parameter	POE-E	POE-F
Satellite reference	• Mass and center of gravity : post-launch values + variations generated by Control Center • Attitude model : For jason satellites, quaternions and solar panel orientation from control center, completed by nominal yaw steering law when necessary. Other satellites nominal attitude law	• Mass and center of gravity : Unchanged • Attitude model : **Refined nominal attitude laws**
Displacement of reference points	• Earth tides : IERS2003 conventions • Ocean loading : **FES2012** • Pole tide : solid earth pole tides and ocean pole tides (DESAI, 2002), **cubic+linear mean pole model from IERS2010** • S1-S2 atmospheric pressure loading, implementation of Ray and Ponte (2003) by Van Dam • Reference GPS constellation : **JPL solution - fully consistent with IGS08**	• Earth tides : Unchanged • Ocean loading : **FES2014** • Pole tide : solid earth pole tides and ocean pole tides (DESAI, 2002), **new linear mean pole model** • S1-S2 atmospheric pressure loading : Unchanged • Reference GPS constellation : **GRG solution - fully consistent with IGS14**
Geocenter variations	• Tidal: Ocean loading and S1-S2 atmospheric pressure loading • Non-tidal: **Seasonal model from J.ies applied to DORIS/SLR stations**	• Tidal: Unchanged • Non-tidal: **Full non-tidal model (semi-annual, annual and inter-annual) derived from DORIS data and the OSTM/Jason-2 satellite, applied to DORIS/SLR stations and GPS satellites**
Terrestrial Refrence Frame	**Extended ITRF2008 (SLRF/ITRF2008, DPOD2008, IGS08)**	**Extended ITRF2014 (SLRF/ITRF2014, DPOD2014, IGS14)**
Earth orientation	Consistent with IERS2010 conventions and **ITRF2008**	Consistent with IERS2010 conventions and **ITRF2014**

Parameter	POE-E	POE-F
Propagation delays	• SLR troposphere correction : Mendes-Pavlis • SLR range correction : **Constant 5.0cm range correction for Envisat, elevation dependent range correction for Jason** • DORIS troposphere correction : **GPT/GMF model** • DORIS beacons phase center correction • GPS PCO/PCV (emitter and receiver) consistent with constellation orbits and clocks **(IGS08 ANTEX), pre-launch GPS receiver phase map** • GPS phase wind-up correction	• SLR troposphere correction : Unchanged • SLR range correction : **Geometrical models for all satellites** • DORIS troposphere correction : **GPT2/VMF1 model** • Unchanged • GPS PCO/PCV (emitter and receiver) consistent with constellation orbits and clocks **(IGS14 ANTEX), in flight adjusted GPS receiver phase map** • GPS phase wind-up correction : unchanged
Estimated measurement parameters	• DORIS : one frequency bias per pass, one troposphere zenith bias per pass • SLR : Reference used to evaluate orbit precision and stability • GPS : **Floating ambiguity** per pass, receiver clock adjusted per epoch	• DORIS : one frequency bias per pass **and drift (for "SAA stations")** per pass, one troposphere zenith bias per pass, **horizontal tropospheric gradients per arc** • SLR : Unchanged • GPS : **fixed ambiguity (when possible)** per pass, receiver clock adjusted per epoch
Tracking Data corrections	Jason-1 DORIS data : Updated South Atlantic Anomaly model (J.-M. Lemoine et al.) applied before and after DORIS instrument change. Doris Time-tagging bias for Envisat and Jason aligned with SLR before and after intrument change.	Unchanged

Parameter	POE-E	POE-F
DORIS weight	**1.5 mm/s (1.5cm over 10sec)**	**Process data down to as low elevation angles as possibles (from 10° to 5° elevation cut-off angle) with a consistent down-weightling law**
SLR weight	15cm. Reference used to evaluate orbit precision and stability	Unchanged
GPS weight	2cm (phase) / 2m (code)	Unchanged

Table 6 – POE-E and POE-F orbit standard

Cyclic mean of the differences between the two orbit solutions is stable in time, with variations under +/-1mm (see top left of figure 22).

The standard deviation of the difference between the two solutions is slightly lower from mid-2017 onwards (top right of figure 22). POE-E and POE-F are differently computed out of yaw fix period, and from mid-2017 onwards, yaw fix periods are longer, so that the impact on the orbit differences is lower.

The map of the differences between the two orbit solutions (bottom figure 22), computed over 85 cycles shows no global bias (mean < 0.01cm). This is coherent with top left of figure 22. Geographically correlated patterns can reach +/-0.6cm, but are not stable in time (not shown here).

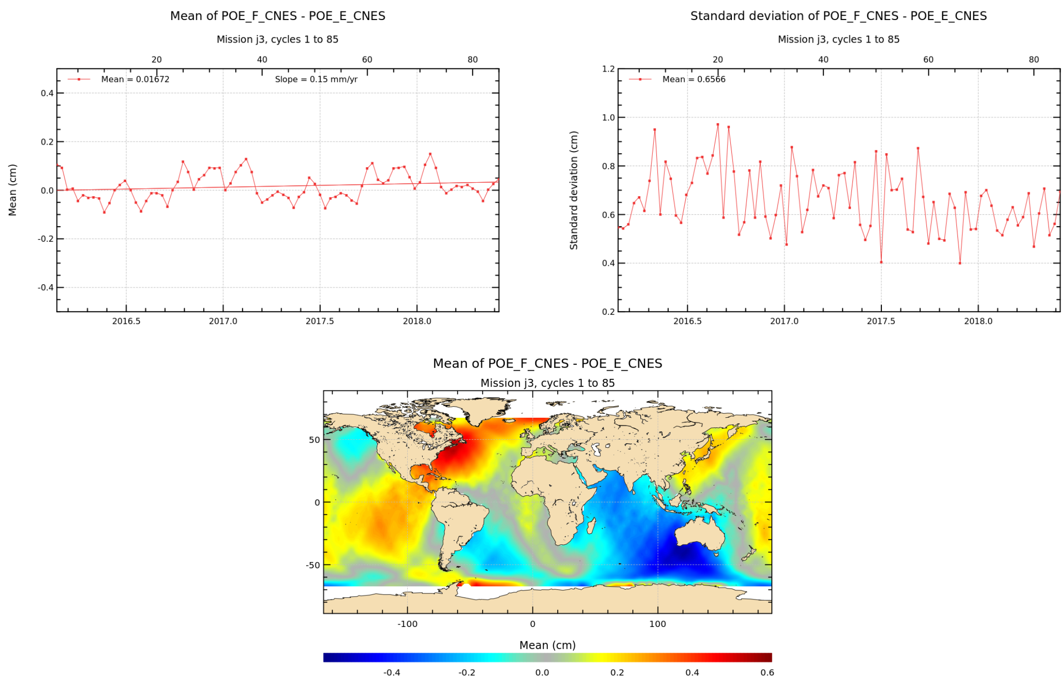

*Figure 22 – Difference between POE-F and POE-E : Mean **(left)** and standard deviation **(right)**. Difference between POE-F and POE-E **(bottom)***

Variance of SSH differences at crossovers are compared using different solutions as a key performance indicator (figure 23). In our case, a global reduction of 0.21 cm^2 using POE-F SSH computation compared to SSH POE-E indicates an improvement.

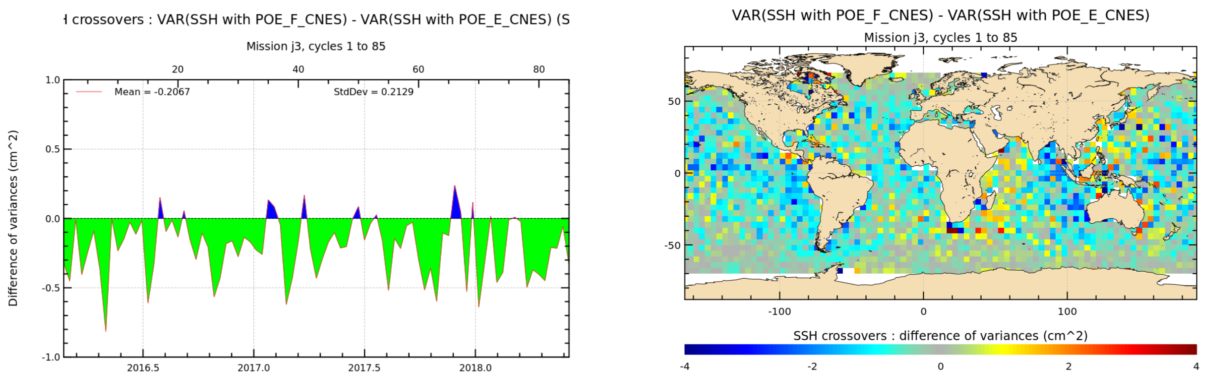

Figure 23 – Difference of variance between POE-F and POE-E

5.3. Radiometer parameters

In this part, a comparaison between GDR-D and GDR-F is realized for radiometer parameters. Main difference in product are detailled in table 7.

Identification	Description
AMR land flag	Fix the anomaly on the AMR land flag
New Radiometer Surface Mask	New AJ3_SUR static file
New reference (J-CS/S6) for antenna temperature coefficient	New AJ3_ANT dynamic file : [Sh Brown 2020] coeff file. Improves the wet tropospheric correction for early JA3 cycles (2.4 mm drift)
Level-1B AMR algo	Update the level-1B AMR algorithm in order to take into account a specific computation of the brightness temperature quality flags (algorithm called AMR-TB_QUAL_01) (change request 10551)

Table 7 – AMR radiometer evolution in GDR-F

5.3.1. Brightness temperatures

Daily monitoring of the mean difference (GDR-F minus GDR-D) of brightness temperatures are really stable after the first mid-year of the mission. In average, these differences are near -1.1K for tb_340, near 0.9K for tb_238 and near 0.4K for tb_187 (see figure 24).

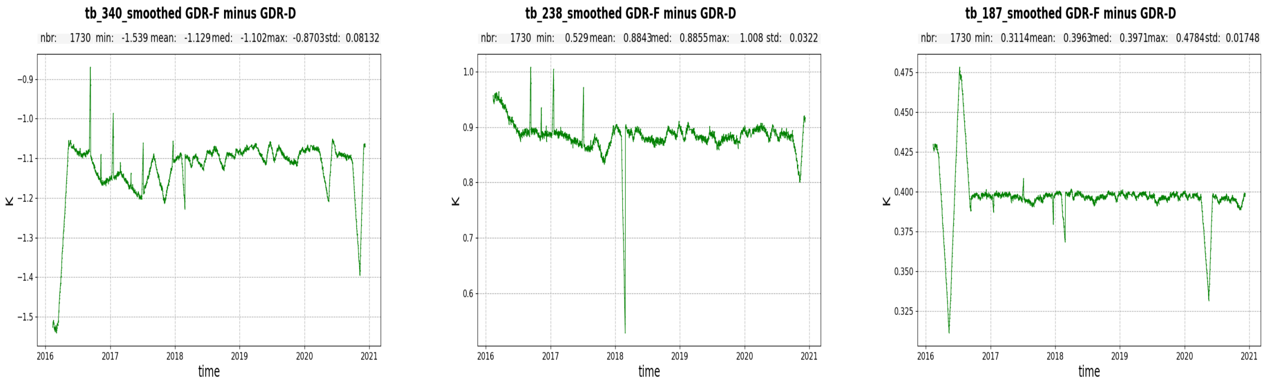

Figure 24 – Brightness temperatures: mean per day (selection on SLA_MLE4 valid points only).

5.3.2. Radiometer minus model wet tropospheric corrections difference

Thanks to new calibration coefficients, radiometer minus model wet tropospheric corrections difference is closer to zero (bottom right of figure 25). Except for early 2016 and mid 2020, mean difference between GDR-D and GDR-F radiometer wet tropospheric correction is quite stable between -6.2 and -6.4 mm with local variation lower than 0.5 cm in average. The impact of the drift correction on the first mission monthes is visible on the top left part of figure 25, with a difference increase from –7.4 to –6.0mm between febuary (beginning) to july 2016 and a difference decrease from – 6.0 to –6.4mm between july and september 2016. Geographical impact of these differences is visible on bottom of figure 25, with no visible impact of the analysis year on these patterns (not shown here).

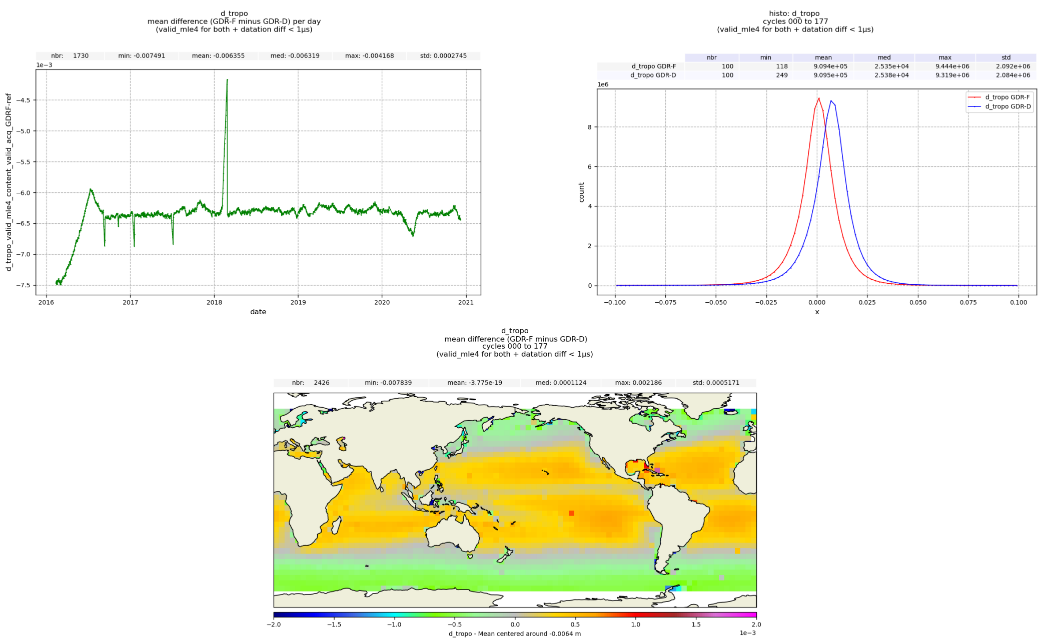

Figure 25 – Radiometer minus model wet tropospheric corrections (selection on SLA_MLE4 valid points only).

There is no significant impact at crossover, but a reduction of -0.08cm^2 in SLA variance (figure 26).

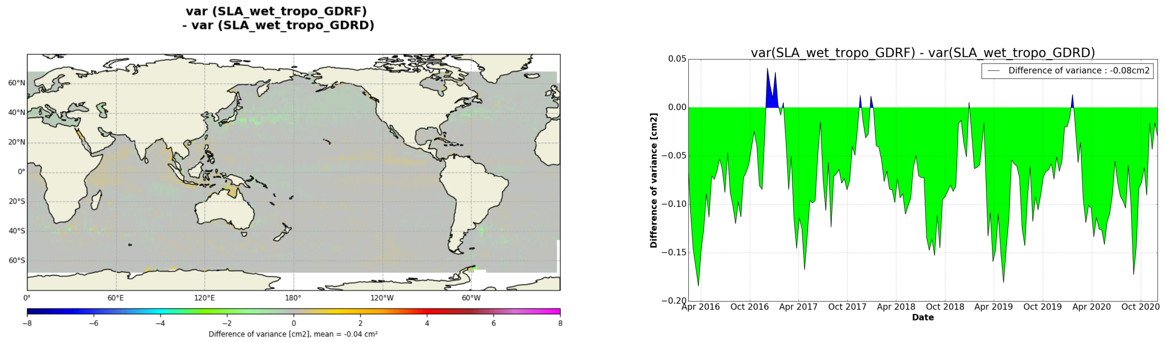

Figure 26 – Difference of along-track SLA variance (without Caspian sea) using wet tropospheric correction GDR-F or GDR-D

A small impact of this radiometer reprocessing is visible near coast (figure 27).

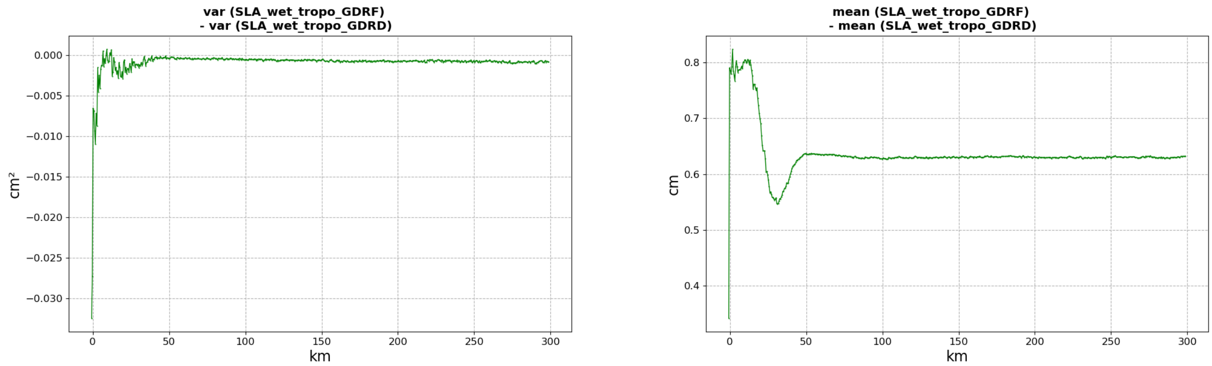

Figure 27 – Difference of along-track SLA variance and mean fonction of distance to coast

5.3.3. Atmospheric attenuation

The atmospheric attenuation applied to sigma0 is derived from radiometer parameters. Atmospheric attenuation is lower for GDR-F than GDR-D. This difference is more important in open sea (see figure 28). The difference between GDR-F and GDR-D atmospheric attenuation is very low(<0.01dB oon ddailly averaging and <0.1 dB localy). Very small differences (around 0.2 to 0.3dB) can be reach near coast.

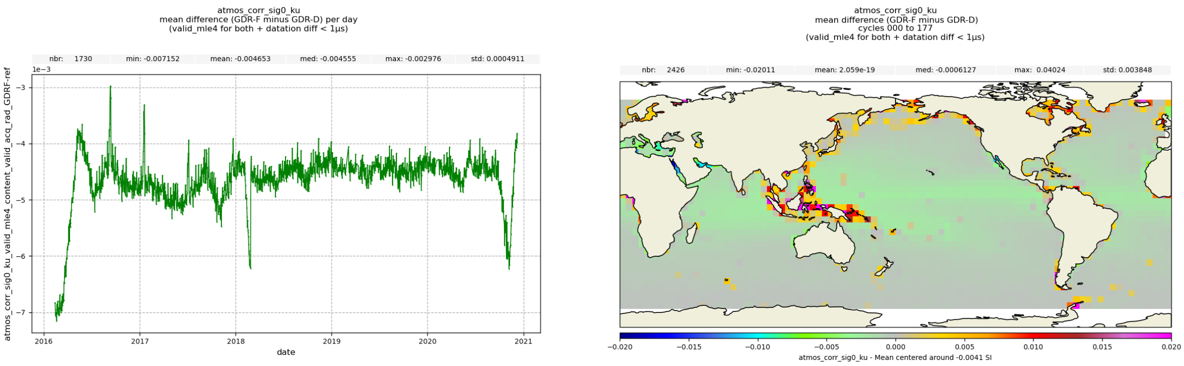

Figure 28 – atmos_corr_sig0_ku (selection on SLA_MLE4 valid points only).

5.3.4. Atmosphere cloud liquid water and water vapor content

Radiometer atmosphere cloud liquid water and water vapor content are slightly modified with reprocessing. It leads to a water vapor content from radiometer difference about 1.03 kg/m^2 in average over the whole reprocessed period and -0.024 kg/m^2 as concerned atmosphere cloud liquid water from radiometer difference (figure 29). Geographically correlated impact depends on the period considered (see figure 30 and figure 31, year 2016 at the top and 2019 at the bottom).

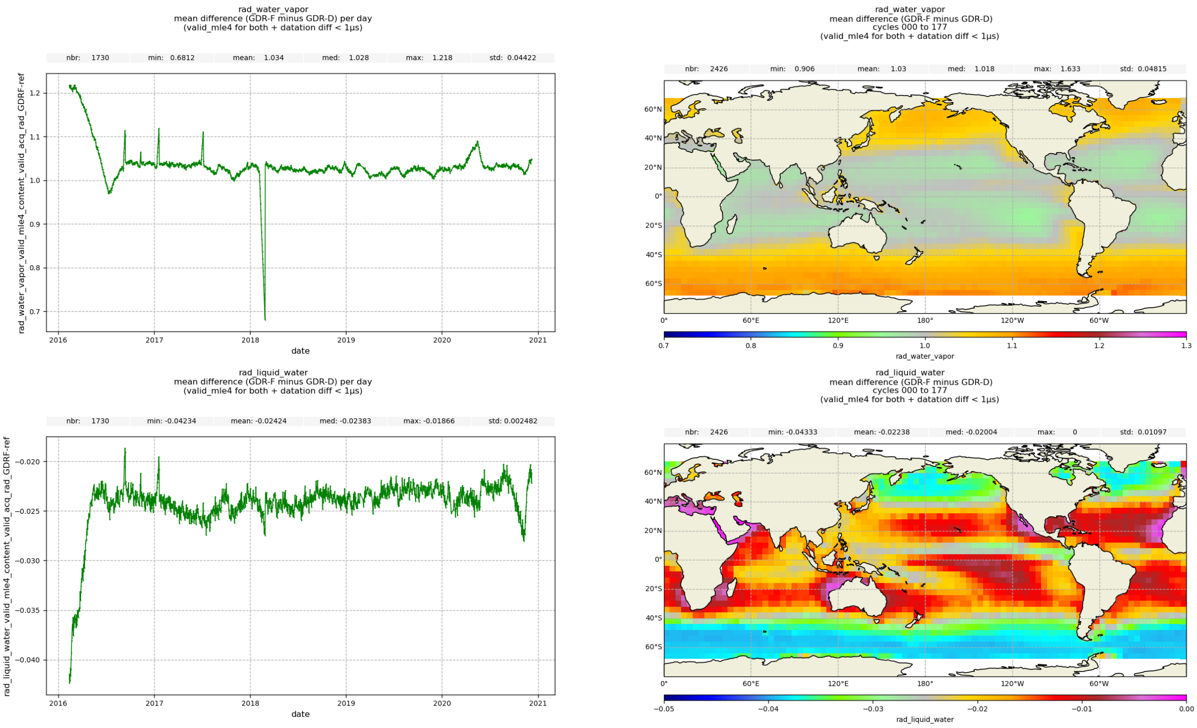

*Figure 29 – water vapor content from radiometer difference in kg/m^2 **(top)** and atmosphere cloud liquid water from radiometer difference in in kg/m^2 **(bottom)** (selection on SLA_MLE4 valid points only).*

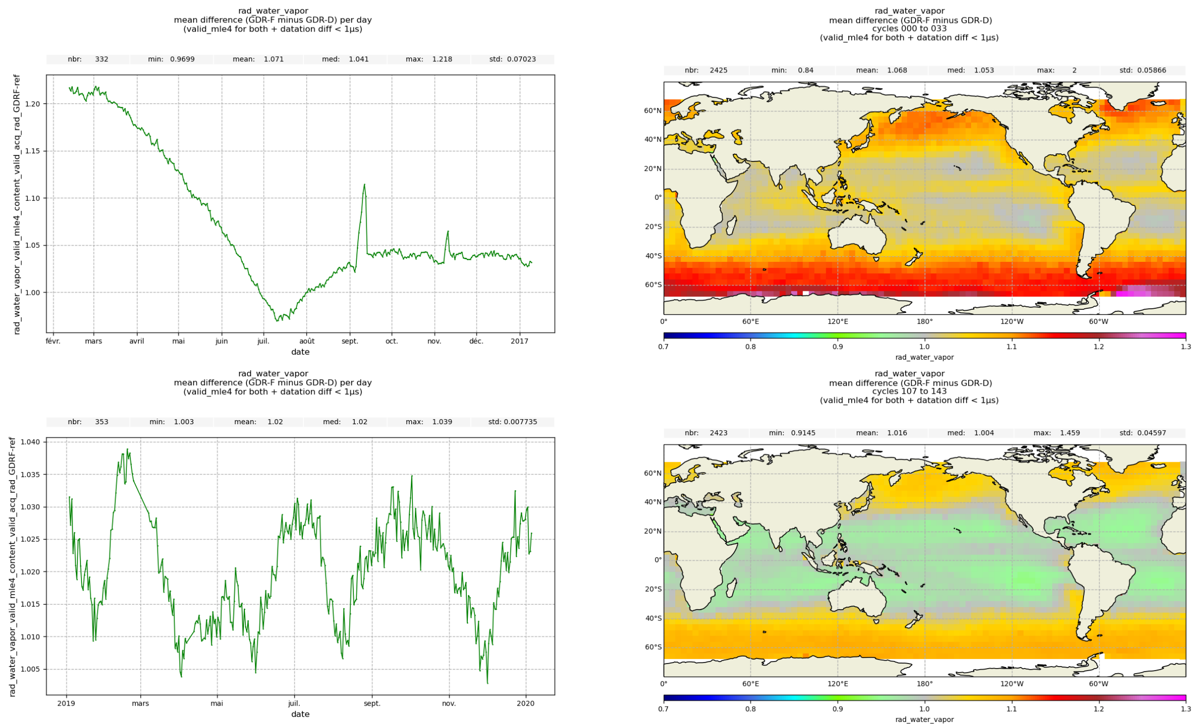

Figure 30 – water vapor content from radiometer difference in kg/m^2, Computed over 2016 ***(left)*** *and 2019* ***(right)*** *(selection on SLA_MLE4 valid points only).*

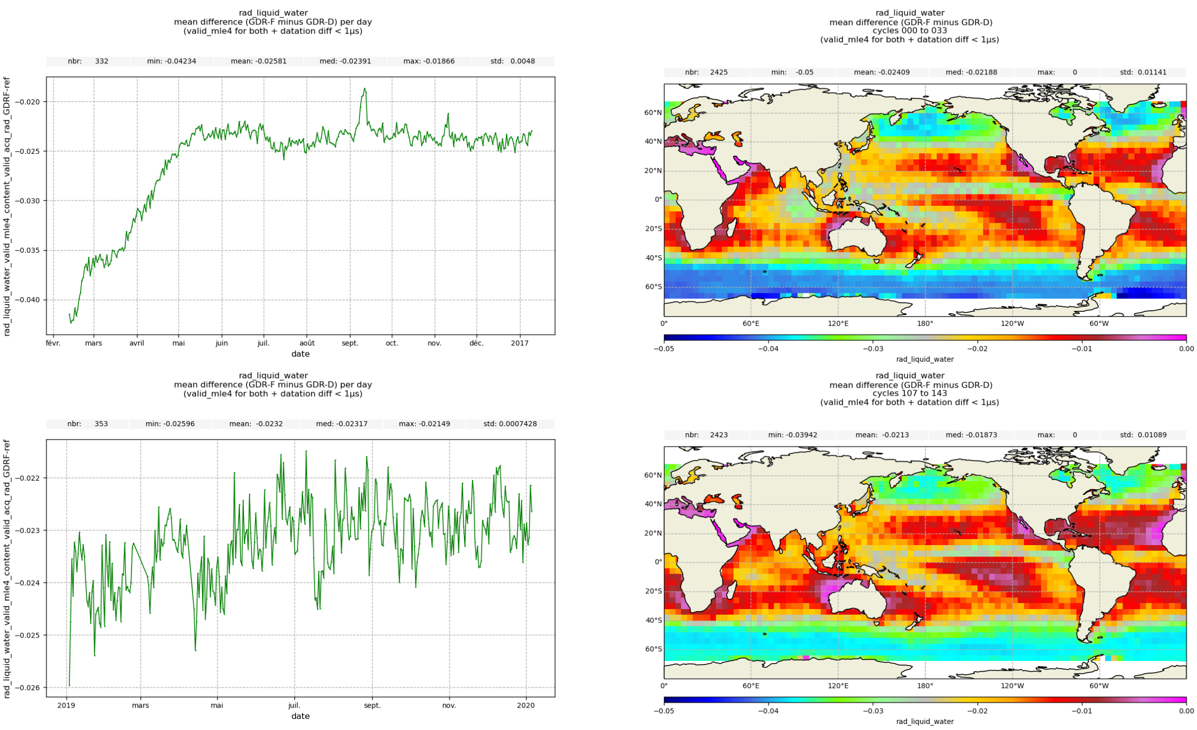

Figure 31 – atmosphere cloud liquid water from radiometer difference in in kg/m^2, Computed over 2016 ***(left)*** *and 2019* ***(right)*** *(selection on SLA_MLE4 valid points only).*

5.4. Altimeter parameters and corrections derived from the altimeter

In this part, a comparaison between GDR-D and GDR-F is realized for altimeter parameters and corrections derived form the altimeter. Main difference in product are detailled in table 8.

Identification	GRD-D	GRD-F
CAL1 Total Power of the PTR	1e-2 precision	1e-4 precision
CAL 2 (LPF) normalization	Normalization by max gate	Normalization by averaging gates
MLE4 Mispointing validity map	Not provided	Provided
Waveform classification	-	Neural network
Adaptive retracking	-	Adaptive retracking
Tracker Range Rate	Not reported in S-IGDRs and S-GDRs	Reported in S-IGDRs and S-GDRs
Waveform	Provide the waveforms non corrected from the LPF filter	Provide the waveforms corrected from the LPF filter
Doppler correction	Applied on ocean retracked ranges	Applied on all retracked ranges

Table 8 – Altimeter difference between GDR-D and GDR-F

5.4.1. Mispointing

There is no significant impact of reprocessing on mispointing from waveforms. Some very small bias can be observed before july 2016 when difference between GDR-D and GDR-F change (figure 32, -0.00024 deg^2 before and 0 after). This is due to LTM difference.

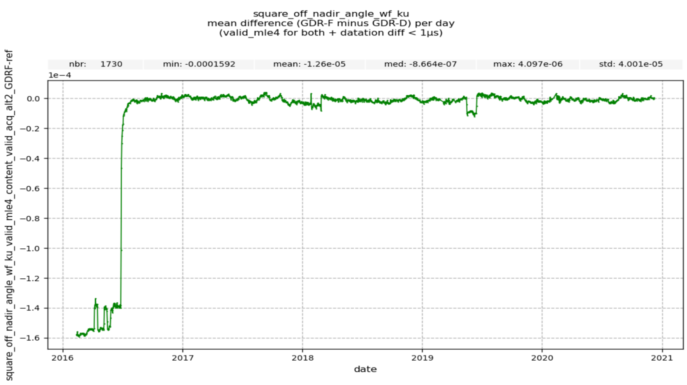

Figure 32 – Daily mean of square_off_nadir_angle_wf_ku GDR-F minus GDR-D (selection on SLA_MLE4 valid points only).

5.4.2. SWH

There is no significant impact of reprocessing on SWH. As in case of mispointing, small differences can only be observed before july 2016 (under 1.4 mm).

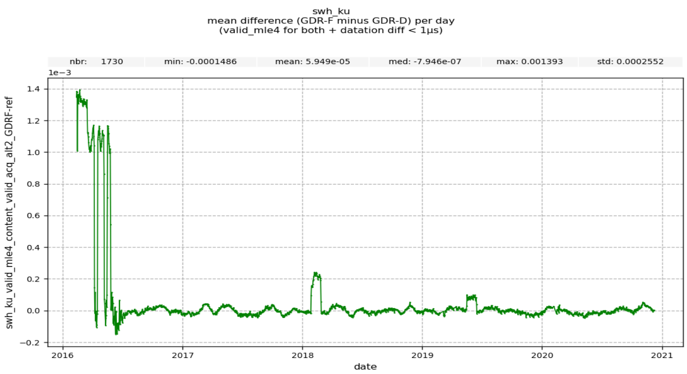

Figure 33 – Daily mean of swh_ku GDR-F minus GDR-D (selection on SLA_MLE4 valid points only).

5.4.3. Sigma0

The GDR-F minus GDR-D difference of backscater coefficient (figure 34) shows a bias of -0.04dB in average, and is stable except before july 2016 when bias is between -0.025 and -0.03 dB. This bias is slightly lower in shallow water.

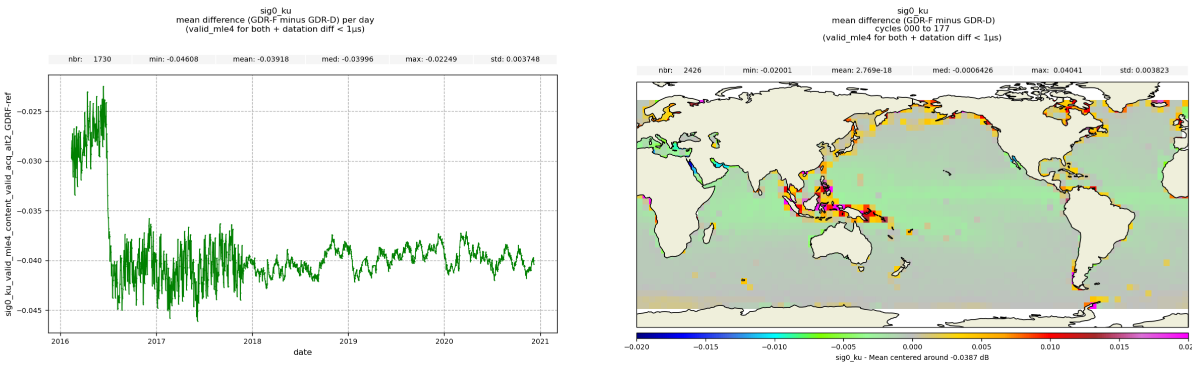

Figure 34 – Daily mean ***(left)*** *and map averaging* ***(right)*** *of sig0_ku GDR-F minus GDR-D (selection on SLA_MLE4 valid points only).*

5.4.4. Wind-speed

A dedicated to Jason-3 GDR-F bias is applied to sigma0 before computing the Collard algorithm. It results in higher wind-speed estimations (+0.32 to +0.38 m/s), closer to ERA-5 statistics (figure 35)

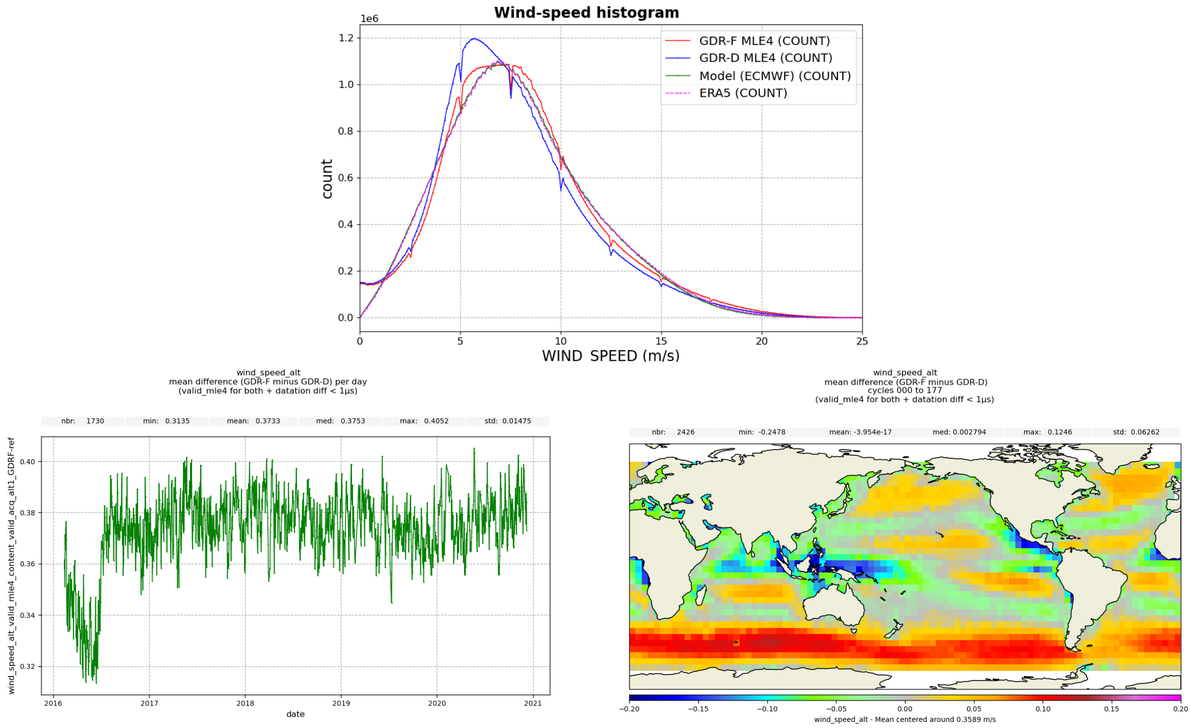

*Figure 35 – Histograms of altimeter and model wind speed **(top)**, daily mean **(left)** and map averaging **(right)** of wind_speed_alt GDR-F minus GDR-D (selection on SLA_MLE4 valid points only).*

5.4.5. Sea State Bias and dual-frequency ionospheric correction

In GDR-D product, Sea State Bias (SSB) was computed with an empirical solution fitted on Jason-2 GDR-C data (Tran 2011). For GDR-F, SSB is computed using one year of 2016/2017 GDR-F dataset (Tran 2020). Difference between GDR-F and GDR-D fluctuates between -2 and -1.8 cm, with some geographically correlated patterns correlated to swh (figure 36). There is no significant impact on mean of ssh differences at crossovers (not shown here). The variance of the SSH difference at crossovers is -0.11cm^2 with non filtered ionospheric correction , and the SLA variance is reduced by 0.75cm^2 (see figure 37).

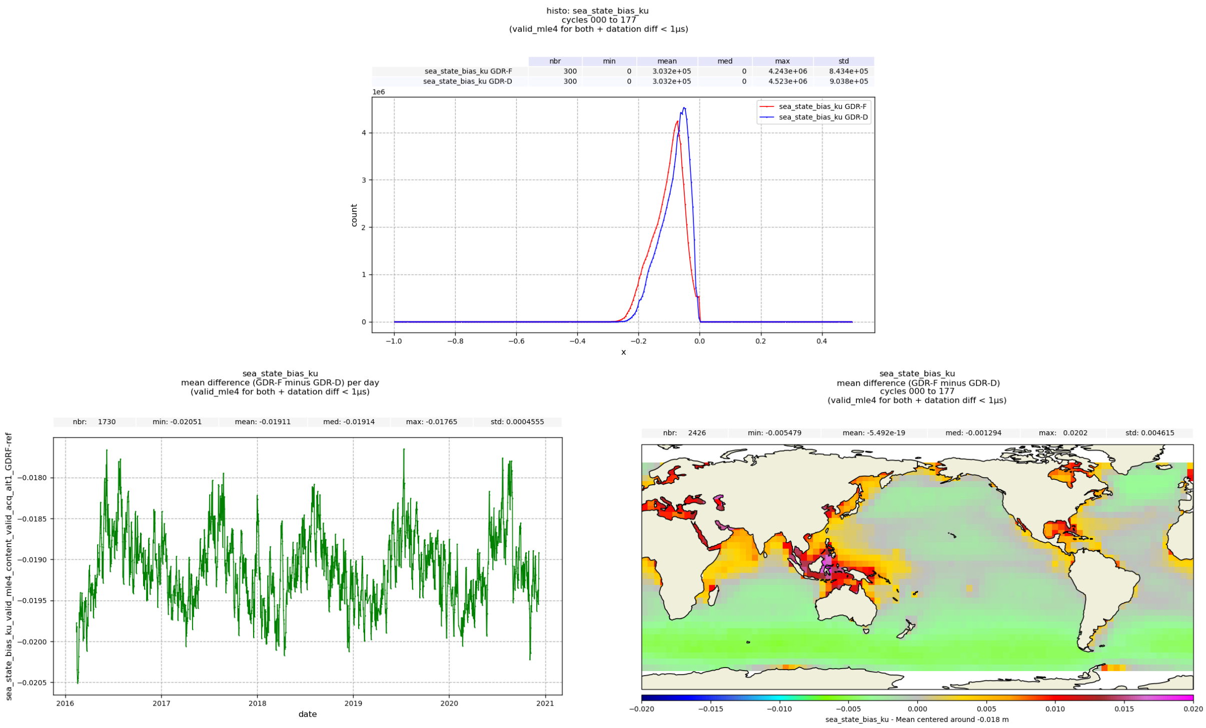

*Figure 36 – GDR-F and GDR-D histograms of sea_state_bias_ku **(top)**, daily mean **(left)** and map averaging **(right)** of sea_state_bias_ku GDR-F minus GDR-D (selection on SLA_MLE4 valid points only).*

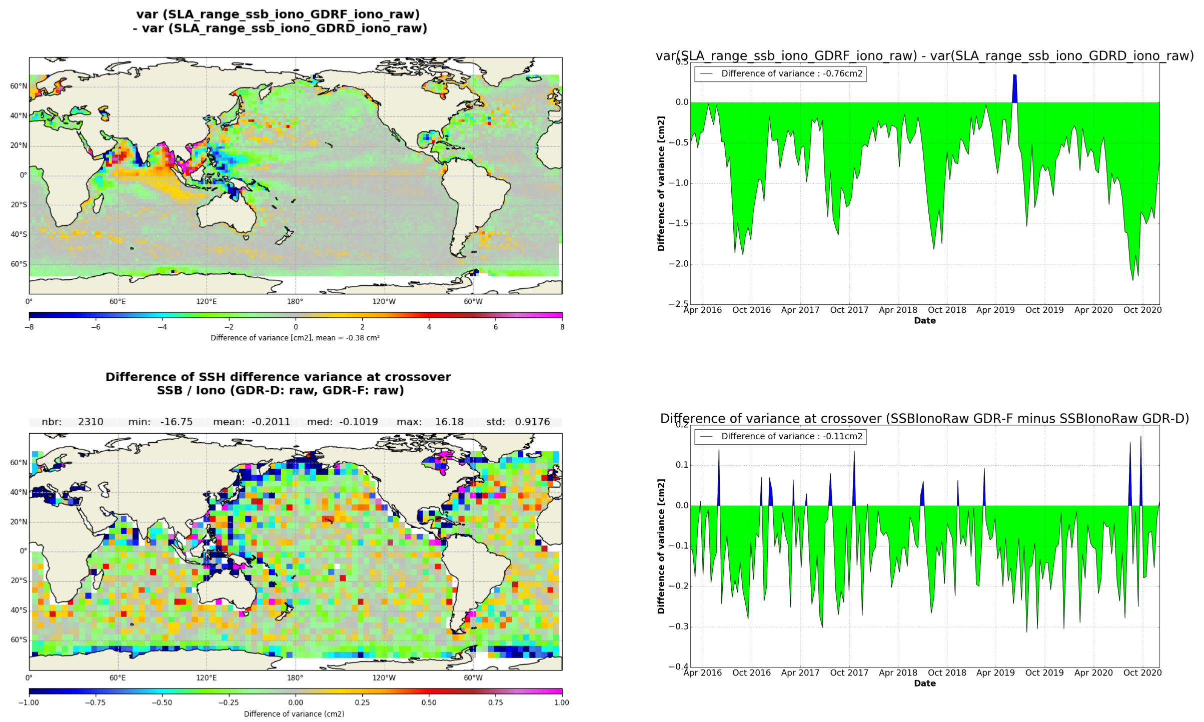

*Figure 37 – Difference of GDR-F and GDR-D SLA variance using non filtered ionospheric correction in both cases **(top left)**. Cyclic monitoring (without Caspian sea) **(top right)**. Variance difference at crossovers **(bottom)***

An iterative filtering method was applied to the ionospheric correction in the production of Jason-3 GDR-F altimetry products. The process is applied to the non filtered solution computed from the formula:

$$Iono = \delta f[(Range_{KU} + SSB_{KU}) - (Range_C + SSB_C)] \tag{4}$$

with :

$$\delta f = (FrequencyC_{band})^2/((FrequencyKU_{band})^2 - (FrequencyC_{band})^2) \tag{5}$$

for Jason-3, frequency is 5.3 GHz for C-band and 13.575 GHz for Ku-band.

The iterative filtering scheme was developed to achieve two main goals:

- Base the correction on as many dual-band ionospheric observations as possible
- Improve the correction where altimetric observations are discontinuous or isolated.

Selection of the ionospheric observations used for the correction is independent from the quality of sea level observations. This maximizes the number of observations selected, but at the same time increases the number of potential outliers.
The iterative filtering applies a median and a Lanczos filter in sequence, in order to progressively reduce the number of outliers in the ionospheric observations used to compute the final filtered correction.
Since the filtered correction has long spatial correlation scales, a spline interpolation is used to fill gaps in the interpolated correction up to few hundreds kilometers.
An overview of the main results is presented in "Filtering ionospheric correction from altimetry dual-frequencies solution" report [10]. This report give editing results for Jason-3 GDR-F. More points are edited near coast and along the border of the Antarctic sea ice and less points are edited on open sea with iterative filtered corrections (part 4.2, figure 19 of [10]).
Adding this filtering solution to the ionospheric correction used during sea surface height computation leads to a variance reduction of the along-track SLA by 4.1cm^2 (figure 38). In addition to this improvement, a variance reduction at crossovers is visible as shown on figure 14 and figure 13, and here at bottom of figure 38. There is no significant impact on mean of ssh differences at crossovers (not shown here).

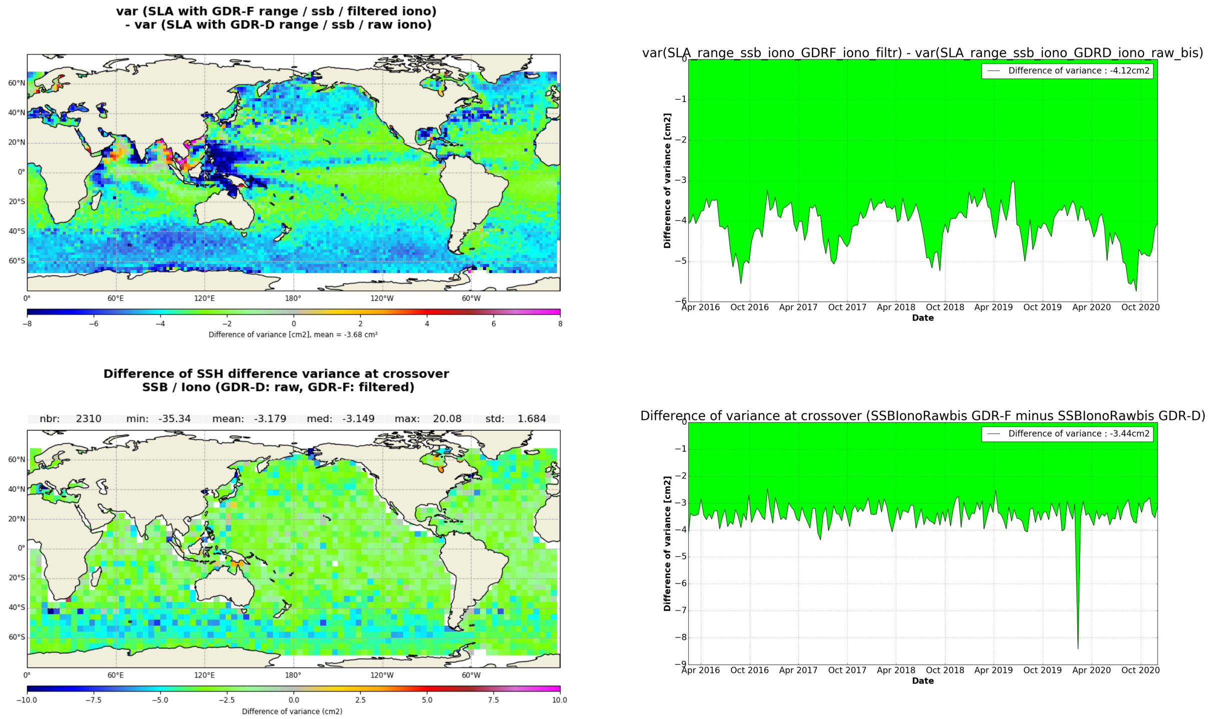

Figure 38 – Difference of GDR-F and GDR-D SLA variance using filtered ionospheric correction in case of GDR-F and non filtered solution in case of GDR-D ***(left)****. Cyclic monitoring (without Caspian sea)* ***(right)****. Variance difference at crossovers* ***(bottom)****, note that a seection is done on $|latitude| < 50$, bathymetryi-1000m and on shallow waters on the difference at crossover monitoring (bottom right).*

Finally, note that a 3D sea state bias solution, including an additional input parameter from MFWAM mean wave period is now available into GDR-F. A dedicated study is done to analyse the impact of this new solution at the end of this report.

5.5. Others corrections involved into SSH computation

5.5.1. Global tide models

The latest global tide versions of the GOT and FES models (GOT4.10 or FES2014b [18]) are available instead of GOT4.8 or FES2004. Daily mean of old minus new GOT or FES models shows slight differences of few milimeters, with a reduction of 60 days signal in case of GOT (see top part of figure 39). The reference ssha used the FES model in GDR-F instead of GOT in GDR-D, which has an impact on 120 days signal of the mean difference of SSH at crossovers and on Hudson Bay (see bottom part of figure 39).

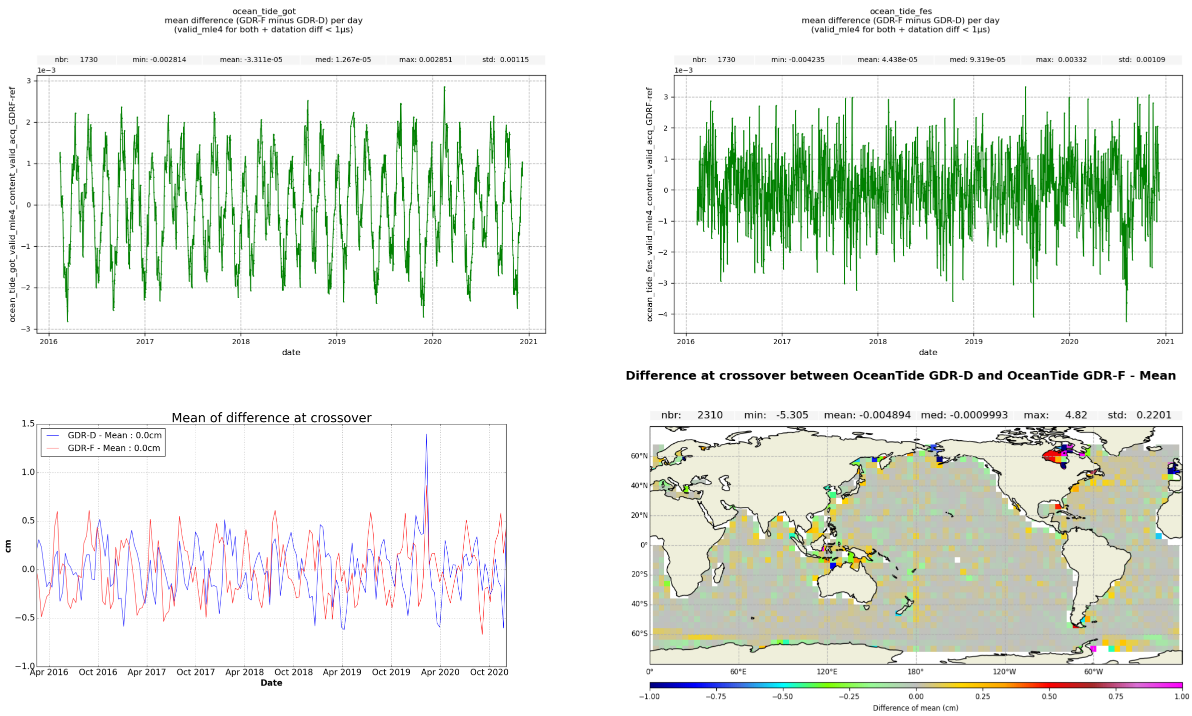

*Figure 39 – Daily monitoring of GDR-F minus GDR-D GOT or FES ocean tide mean difference **(top)**. Mean difference of SSH at crossover between global tide models FES2014b and GOT4.8 **(bottom)***

These solutions improve the coherence between ascending and descending passes as the global variance reduction of SSH crossover difference when using FES2014b instead of GOT4.8 has a value of about 0.48 cm^2 and variance of along-track SLA is lower using FES2014b than with GOT4.8 by $2cm^2$ (see figure 40).

Global Mean Sea Level is equivalent with both solutions (GOT4.10 and FES2014, not shown here). Regional differences between SLA using FES2014 or GOT4.10 is not significant.

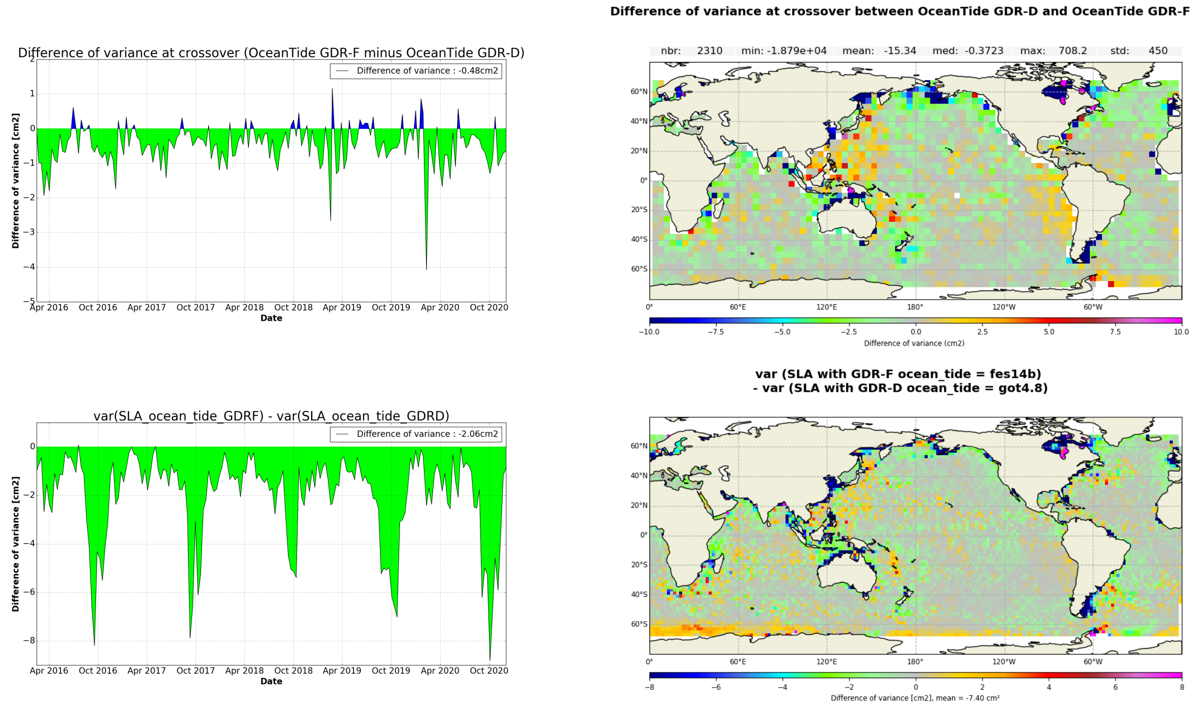

Figure 40 – Difference of SSH differences at crossovers and along-track SLA variance (without Caspian sea) between global tide models FES2014b and GOT4.8

Non equilibrium long period ocean tide height

The long period non equilibrium part of global ocean tide model correction is deduced from FES14B 6 dynamic waves in GDR-F whereas it was from 4 waves from FES2004 model in GDR-D (see [1]). Note that this part of the correction is not included into ocean_tide_fes variable but it is now used into GDR-F ssha variable computation (GDR-D ssha used ocean_tide_got solution, without this dynamic part). The GDR-F minus GDR-D difference of this correction is lower that 1 mm on daily averaging (figure 41).

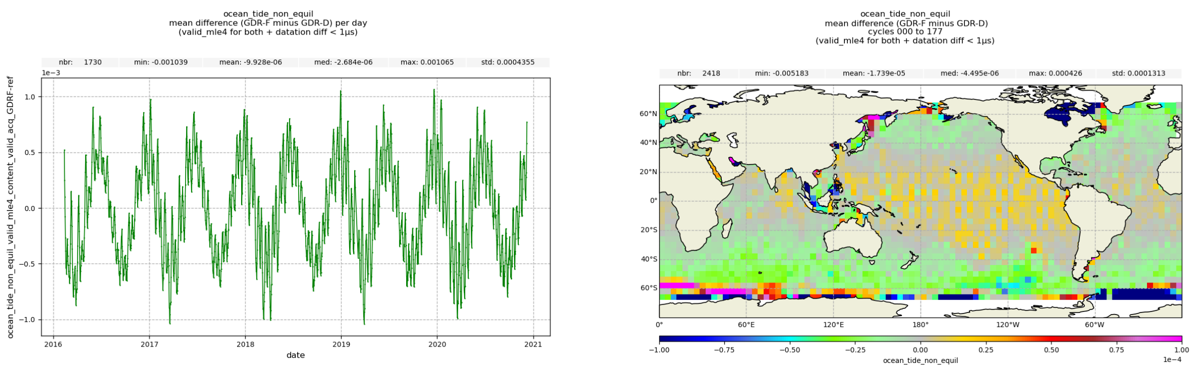

Figure 41 – ocean_tide_non_equil GDR-F minus GDR-D difference (selection on SLA_MLE4 valid points only).

5.5.2. Internal tide

Following the scientific community recommandations, the new correction related to internal tides is now available into GDR-F (Zaron Hret8.1 model for M2, K1, O1 and S2 waves). *[More information about internal tide correction in [20]].*

To take into account internal tide correction improves SSHA performance indicators on along-track Sea Level Anomaly and error at crossover. Over Jason-3 period, there is no significant impact on SSH difference at crossover points or on Global Mean Sea Level trend estimation taking into account internal tides or not (not shown here). Variance of SSH differences at crossovers are compared using different solutions as a key performance indicator. In our case, this difference is lower by around 0.5 cm^2, with significant geographically correlated patterns where internal tides areas are defined (figure 42). In the same way, a reduction is visible in case of global along-track SLA variance (>0.2cm^2), with geographical patterns (figure 43).

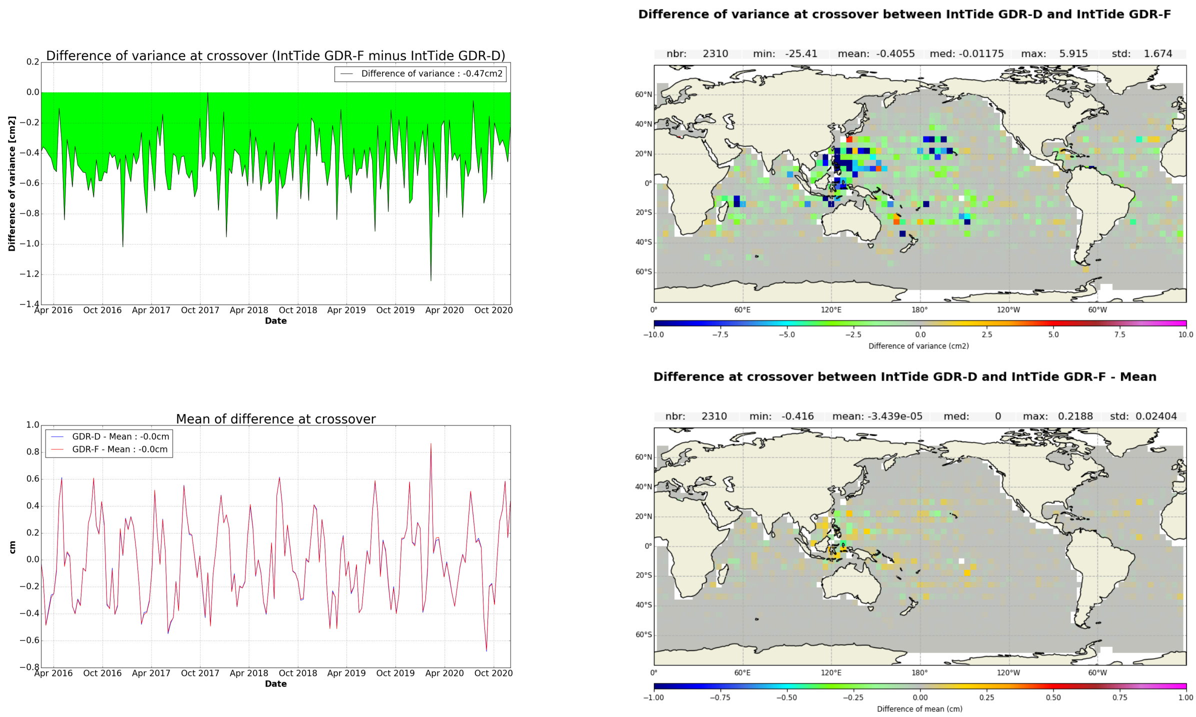

Figure 42 – Variance and mean difference of SSH at crossover between GDR-F without internal tide and GDR-F with internal tide

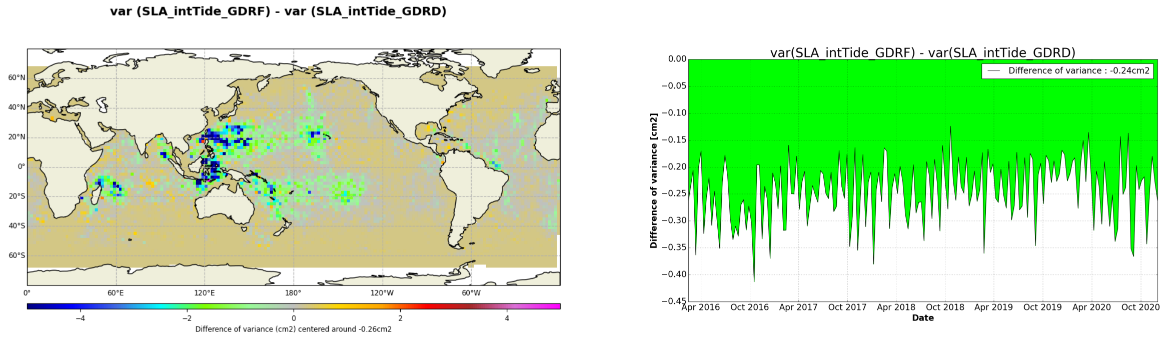

Figure 43 – Difference of SLA variance (without Caspian sea) between GDR-F without internal tide and GDR-F with internal tide

5.5.3. Pole tide correction

The pole tide altimeter correction is used to correct the response of the solid earth and oceans to the polar motion. The Wahr (1985) model has been used for all missions since TOPEX and another model is now available (Desai 2015). Legeais et al. [in 2015] showed the last model has a significant positive impact on the regional mean sea level trends and the comparison with independent in-situ data (Argo profiles) has demonstrated that the use of this model reduces the amplitude of the annual signal of the global mean sea level. A new recommendation for Mean Pole Location equation was done in 2017: this model for the linear mean pole is recommended based on a linear fit to the IERS C01 time series spanning 1900 to 2015: in milliarcsec, Xp = 55.0+1.677*dt and Yp = 320.5+3.460*dt where dt=(t-t0), t0=2000.0 and assuming a year=365.25 days. The new mean pole location equation **has a significant impact on the regional mean sea level trends** thanks to the remove of the long term mean pole drift in pole tide computation (see part 8.2 in [4]).

There is no significant impact on performances at crossover. A small reduction of along-track SLA variance (-0.08cm^2) is visible in average over the whole mission period.

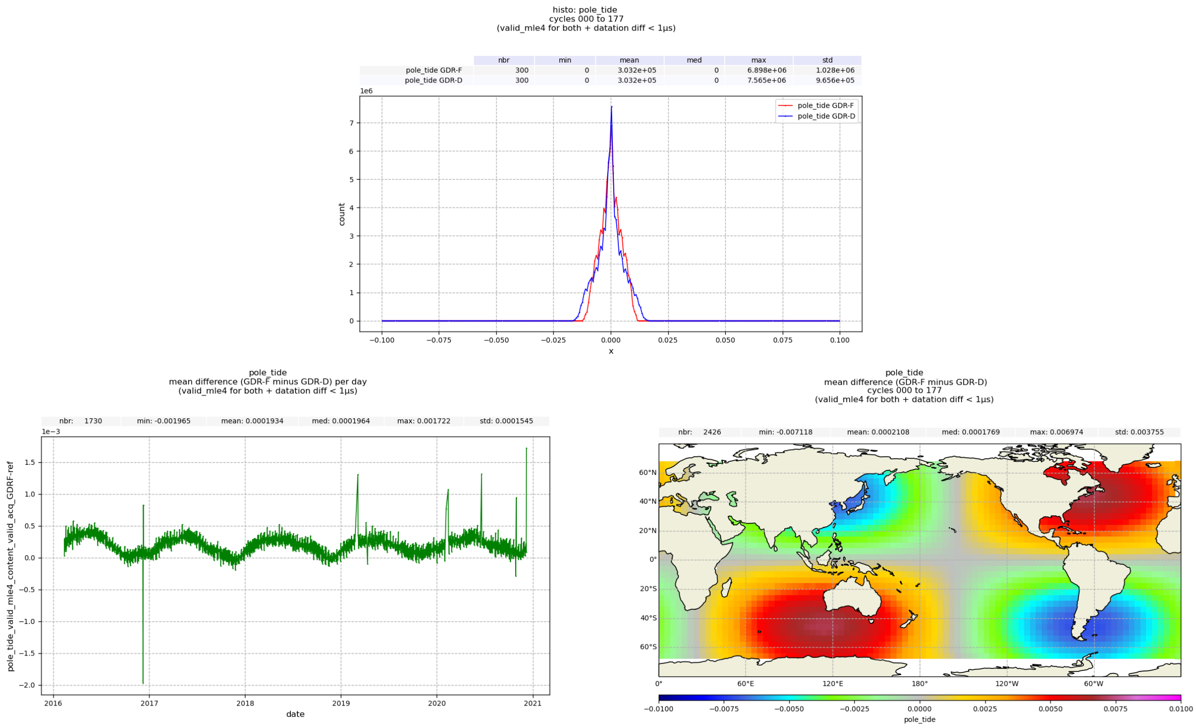

*Figure 44 – GDR-F and GDR-D histograms of pole_tide over the whole mission period **(top)**. GDR-F munis GDR-D pole_tide difference **(bottom)** (selection on SLA_MLE4 valid points only).*

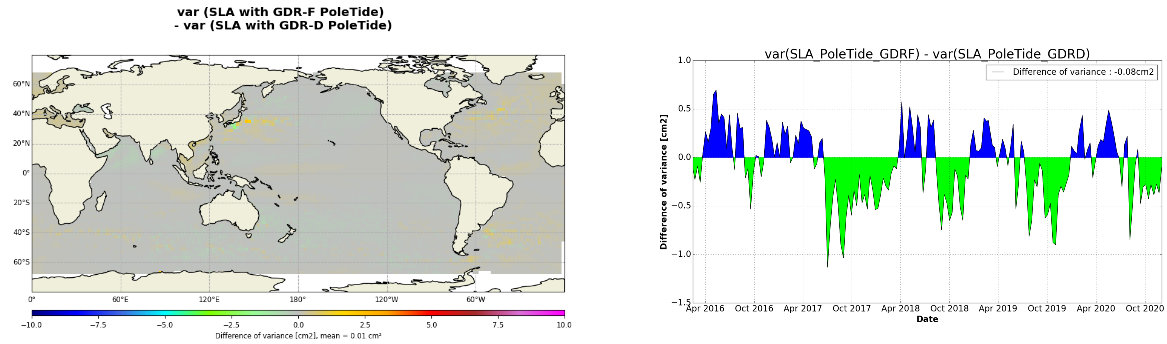

Figure 45 – Difference of SLA variance (without Caspian sea) between GDR-F without pole tide models Wahr (1985) and Desai (2015)

5.5.4. Mean Sea Surface

GDR-D L2 products included one MSS solution (CNES/CLS 11, referenced over 7 years) whereas two solutions (CNES/CLS 2015 and DTU 2018) are available into GDR-F. The change of the reference period from 7 year to 20 years leads to a global bias of 2.4 cm between the two CNES/CLS solutions due to the global mean sea level rise over the 13 years [15]. This change have positive impact on variance of SLA along-track (-5.65cm^2) (see figure 46).

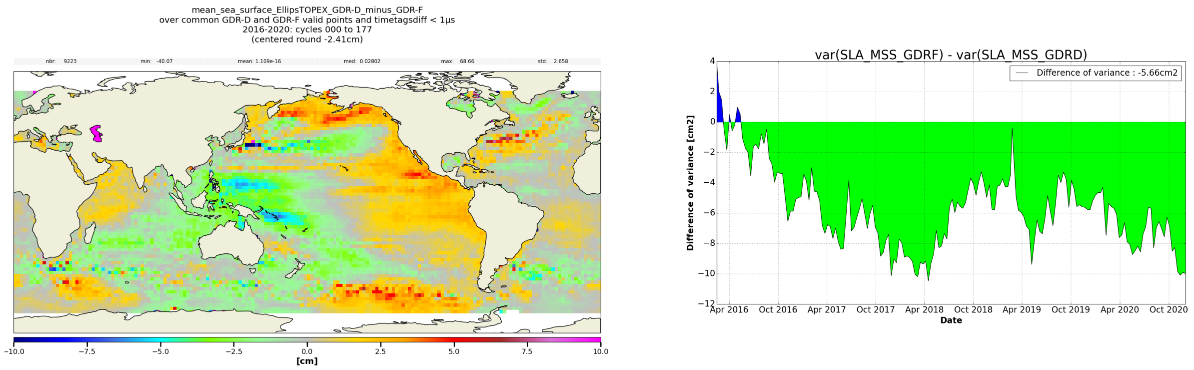

*Figure 46 – GDR-F minus GDR-D MSS difference **(left)**. Difference of SLA variance (without Caspian sea) between MSS CNES/CLS11 and MSS CNES/CLS15 **(right)***

5.6. Other ancillary data

5.6.1. Mean Dynamic Topography

Mean Dynamic Topography move from CNES/CLS-2009 for GDR-D to CNES/CLS-2018 for GDR-F. The latest version is +2.8 cm higher in average. Geographically correlated patterns of the difference can reach near 40 cm locally (see figure 47).

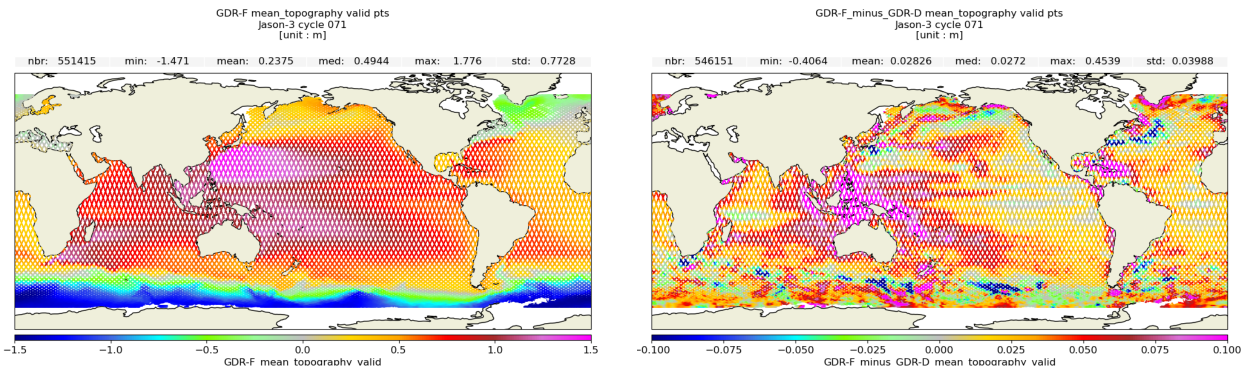

*Figure 47 – mean_topography over 1 cycle (selection on SLA_MLE4 valid points only): GDR-F **(left)** and GDR-F minus GDR-D difference **(right)**.*

5.6.2. Geoid

Geoid variable has been updated from EGM96 to EGM2008. Difference between both solutions is about 29 cm in average over ocean (figure 48). Note that the change in reference ellipsoid (70 cm on global averaging) has been applied to mean sea surface before computing this analysis.

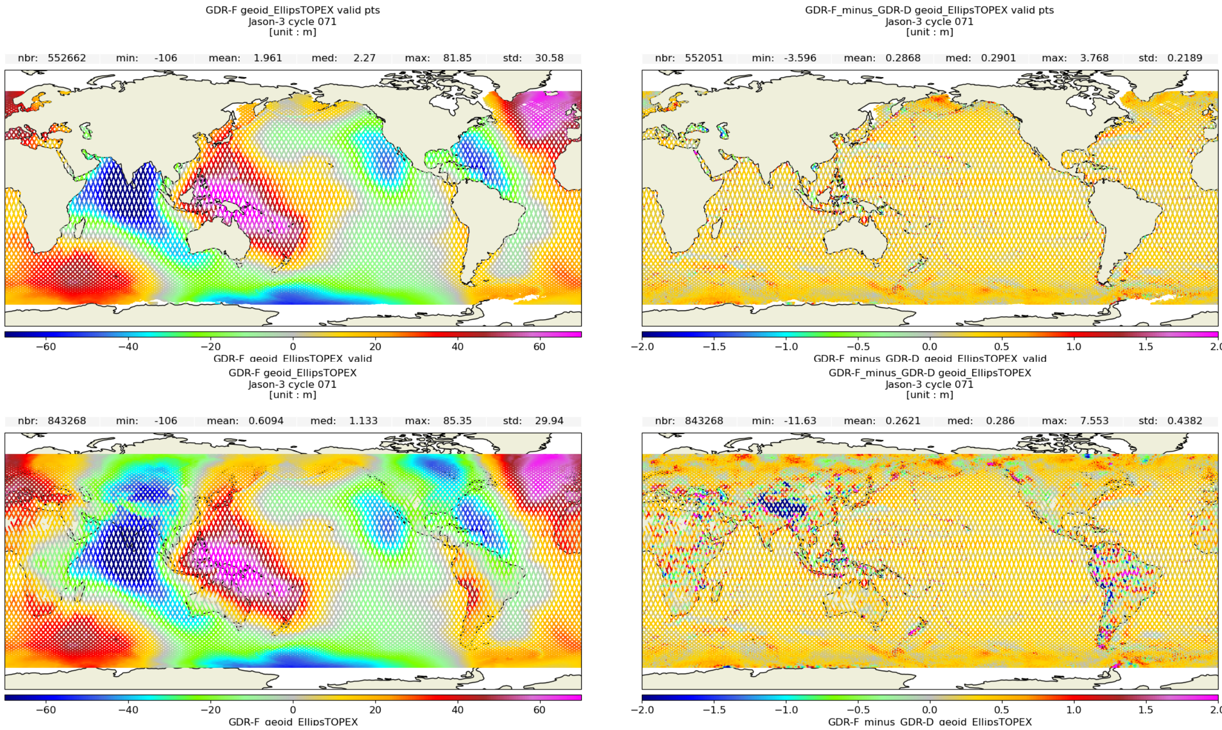

Figure 48 – geoid over 1 cycle (selection on SLA_MLE4 valid points only ***(top)*** *or all along-track global monitoring* ***(bottom)****): GDR-F* ***(left)*** *and GDR-F minus GDR-D difference* ***(right)****.*

5.6.3. Bathymetry

Bathymetry (variable depth_or_elevation in GDR-F) solution moved from DTM2000 to ACE2 model. There is a difference of -5m in average between both solutions with important geographical differences (figure 49).

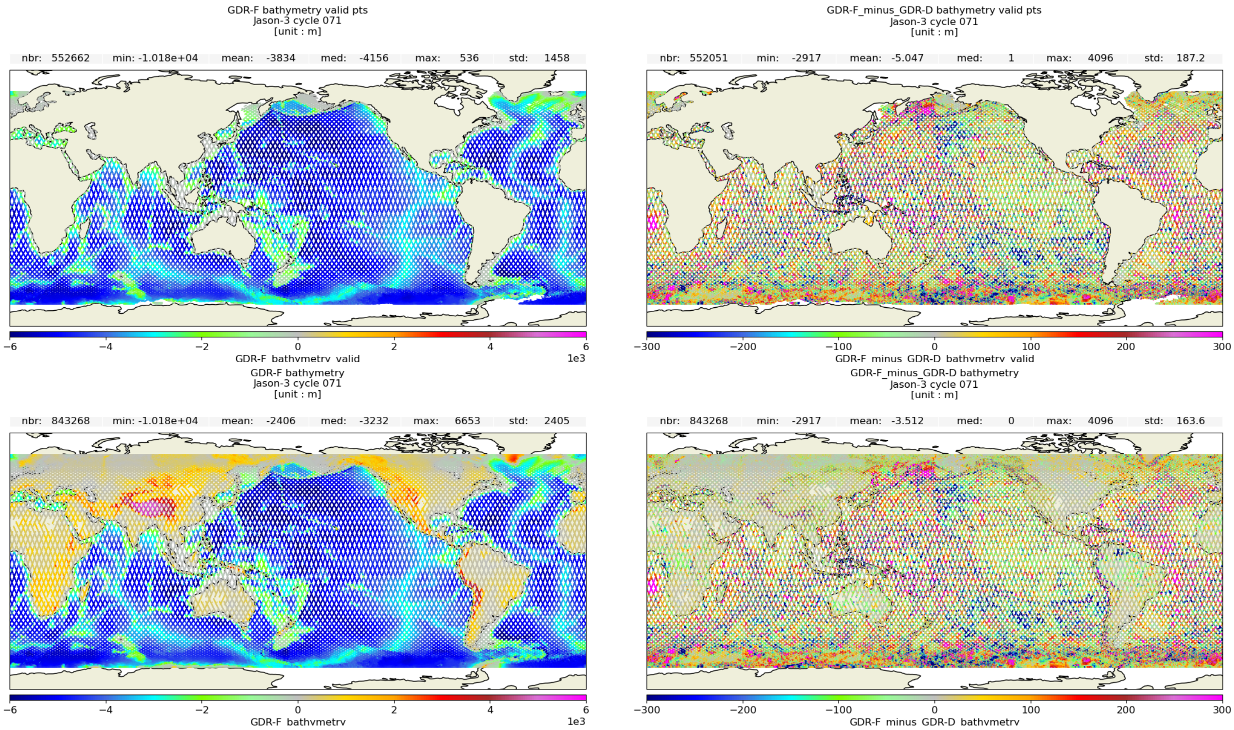

*Figure 49 – bathymetry over 1 cycle (selection on SLA_MLE4 valid points only **(top)** or all along-track global monitoring **(bottom)**): GDR-F **(left)** and GDR-F minus GDR-D difference **(right)**.*

5.6.4. Surface type

Surface classification evolution is described in part “Data coverage”, see table 3 and figure 4.

5.6.5. Rain flag

GDR-D binary flag (0: no rain, 1: rain) is replaced by a 6-states flag in GDR-F.

	Previous classification (GDR-D)	New classification (GDR-F)
0	no rain	no rain
1	rain	rain
2	-	high rain probability from altimeter
3	-	high probability of no rain from altimeter
4	-	ambiguous situation possibility of ice
5	-	evaluation not possible

Table 9 – Previous (GDR-D) and new (GDR-F) rain flag values

Over land, rain flag was set to 1 (corresponding to *rain*) in GDR-D whereas it is flagged to 5 (corresponding to *evaluation_not_possible*) in GDR-F as seen on figure 50.

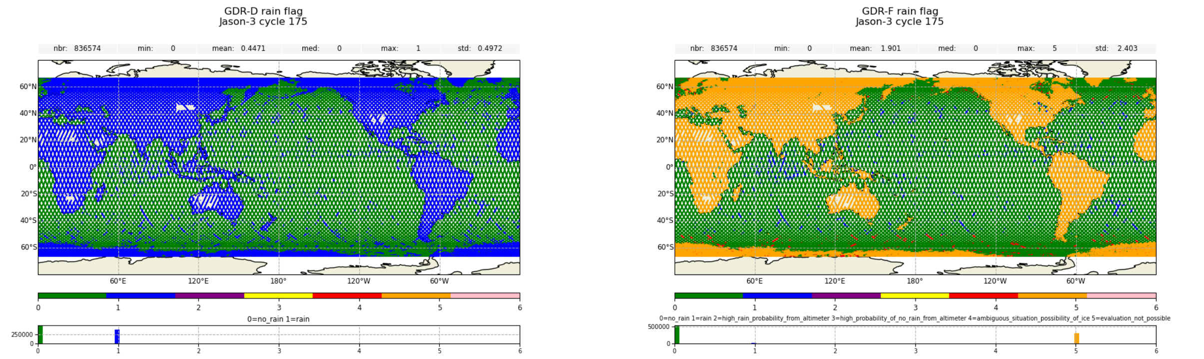

*Figure 50 – Global rain flag for GDR-D (**left**) and GDR-F (**right**) over cycle 175.*

Over latitude higher than 50°, each flagged measurement out of land is set to 4 (corresponding to *ambiguous situation possibility of ice*) for GDR-F solution (in red on right part of figure 51).

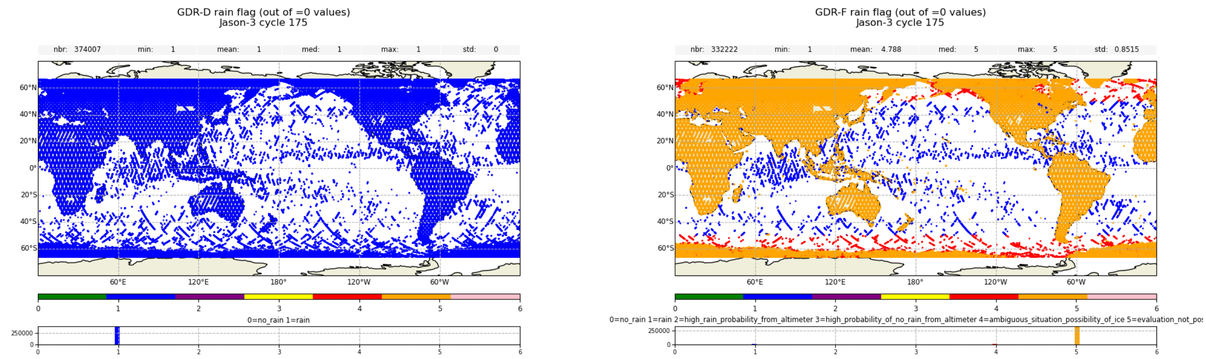

*Figure 51 – Rain flag activated for GDR-D (**left**) and GDR-F (**right**) over cycle 175.*

Finally, all flagged as rain measurements on GDR-D data are set to *no rain* in GDR-F (green points on figure52), or GDR-F flag :

- is set to 5 over land,
- seems to be 0 (*no_rain*) near coasts,
- is sometimes set to 4 for latitude higher than 50°,

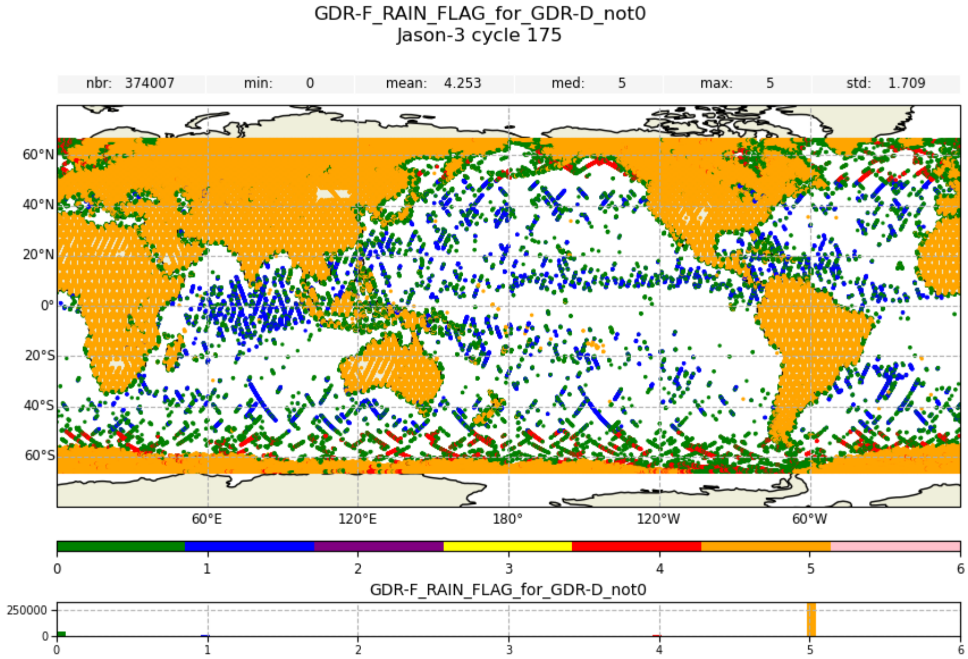

Figure 52 – Rain flag for GDR-F for activated flag in GDR-D.

6. Global and Regional Mean Sea Level long term monitoring

The global mean sea level is one of the most important indicators of climate change as it incorporates the reactions from several different components of the climate system. First, the analysis of the global surface height biases are detailed in this chapter. Then, the changes concerning the MSL trends are presented.

6.1. Sea Level Anomalies along-track analysis

6.1.1. Difference between Jason-3 GDR-F and GDR-D

A global bias of about -3 mm is visible in average for SSHA GDR-F minus GDR-D (see left of figure 53), each component contribution is detailed in table 10.

SLA parameter	GDR-D	GDR-F	Mean difference for GDR-F and GDR-D valid points
Dynamical atmospheric correction Dry tropospheric correction Solid earth tide	No change from GDR-D to GDR-F		0 mm
Internal tide	Not available	HRET8.1 (Zaron2019)	0 mm (in average)
Pole tide	WAHR85 with MPL TOPEXlegacy	DESAI2015 with MPL2017	(GDR-D minus GDR-F) = -0.2 mm
Ocean tide	GOT4.8	FES14b	(GDR-D minus GDR-F) = -0.1 mm
Wet tropospheric correction	Radiometer	Radiometer (new coefficients)	(GDR-D minus GDR-F) = +6.4 mm
Ionospheric correction	Dual-frequency	Dual-frequency	(GDR-D minus GDR-F) = -3.7 mm
Sea state bias	Non-parametric	Non-parametric	ku: (GDR-D minus GDR-F) = +18.3 mm
Range	Ku: MLE4	Ku: MLE4	ku: 0 mm
Orbit	POE-E until cycle 94, POE-F cycle 95 onwards	POE-F	0 mm
Mean sea surface	CNES/CLS11	CNES/CLS15	(GDR-D minus GDR-F) = -24.1 mm

Table 10 – Contributions in sea surface height anomaly global bias

Regional patterns of several centimeters are visible on the difference between GDR-F and GDR-D sea level anomaly. These are mainly due to the change of mean sea surface from CNES/CLS11 (reference : 7 years) to CNES/CLS15 (reference : 20 years), as shown on figure 53 (see also part 5.5.4.). The change in the period of reference directly contain the global bias of +2.4cm due to mean sea level rise (as explained in [15] and [16])

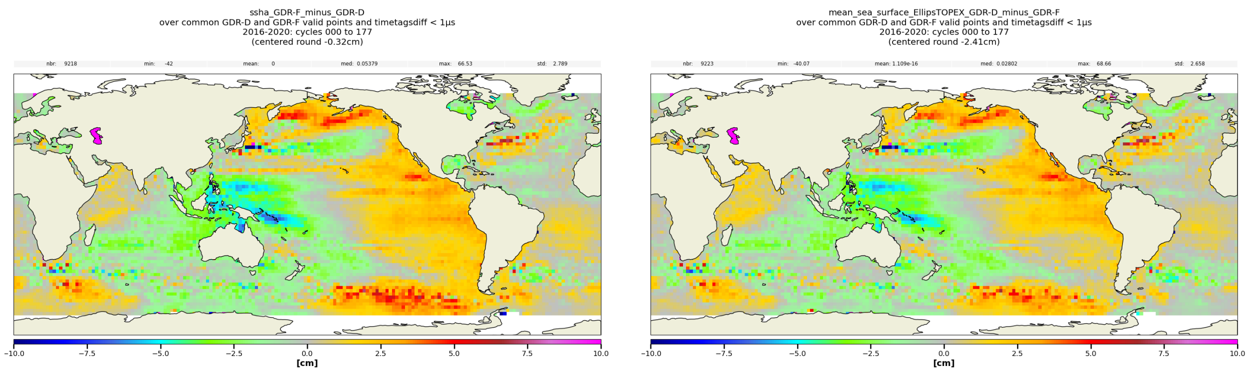

Figure 53 – GDR-F minus GDR-D : Sea surface height anomaly (left) and mean sea surface (right) over common valid points

The regional contribution of orbit-range is lower than 1cm (top left of figure 54). Once the patterns due to MSS are explained, the regional residual differences are mainly due to corrections applied to the range measurement (top right of figure 54). The involved corrections are SSB and pole tide (bottom figure 54).

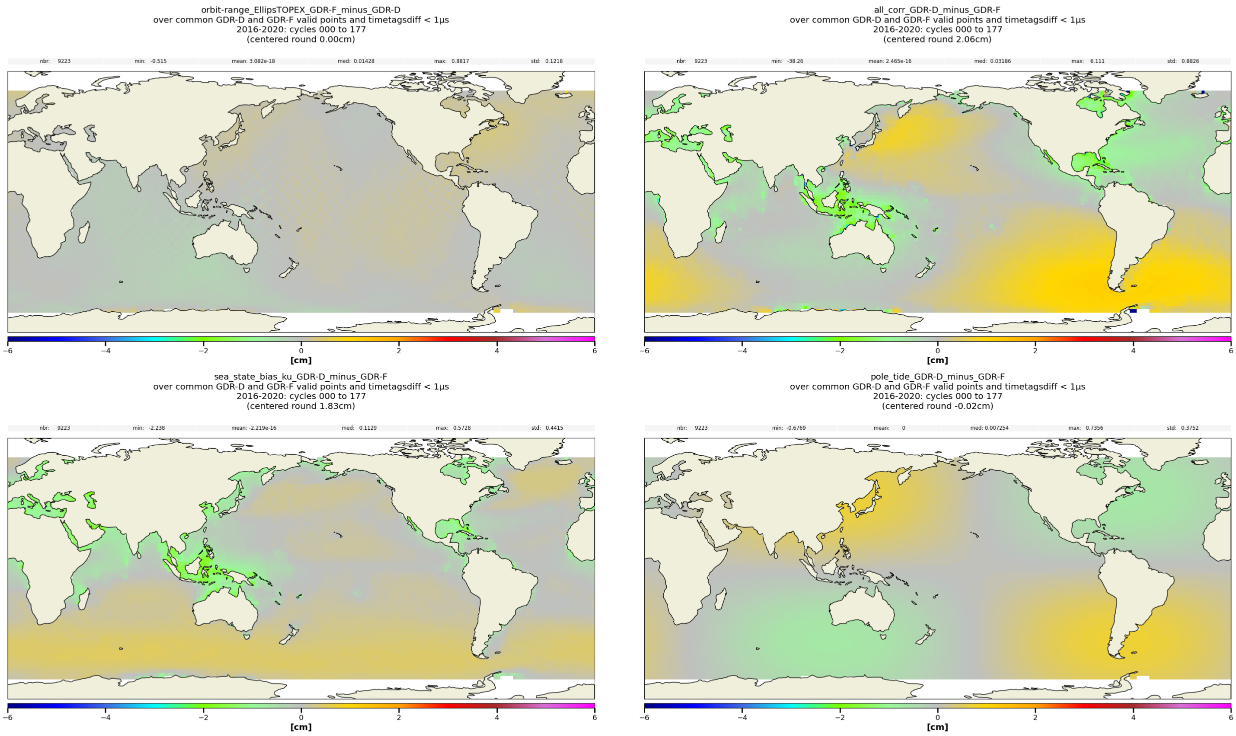

*Figure 54 – GDR-F minus GDR-D : orbit minus range difference (**top left**) and GDR-D minus GDR-F : sum of range corrections differences (**top right**), sea state bias (**bottom left**) and pole tide (**bottom right**) contributions.*

The global bias is quite stable along the time (in green on figure 55). The average difference between GDR-D and GDR-F is slightly higher than when computing on spatial boxes averaging (-4.3 mm instead of -3.2 mm presented before): on this figure SLA is monitoring on along-track cyclic averaging, without taking into account the Caspian sea. The periodogram of the SLA difference indicates 2 major peak :

- near 60 day signal, linked to the use of the FES14B solution for ocean tide correction (see part 4.1.2.).
- at annual signal.

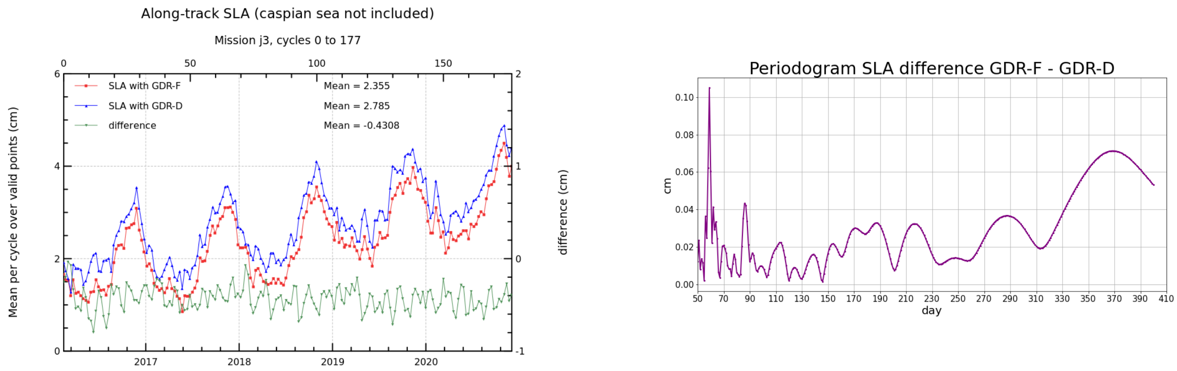

Figure 55 – Cyclic mean of along-track SLA, without Caspian sea. Periodogram of SLA difference (GDR-F - GDR-D)

6.1.2. Difference between Jason-3 and Jason-2

The Sea Level Anomalies (SLA) are computed along track with the SSH calculated as defined in previous sections 4.1.1. (for Jason-3) and 2.3. (for Jason-2) minus the CNES/CLS15 version of mean sea surface for both missions. In order to take advantage of the Jason-3/Jason-2 tandem flight (cycle 1 to 23), we performed direct SLA comparisons between both missions during this period. Colocated Jason-2 minus Jason-3 $orbit - range - MSS$ and SLA differences averaged over the period of tandem phase (cycle 001 to 023) are shown on figure 56, before (top) and after (bottom) reprocessing.
The global bias between Jason-3 and Jason-2 $orbit - range - MSS$ is identical round 2.23 to 2.25 cm. The bias between their corrected SLA is reduced from 2.99cm to 2.56cm. As both satellites measure the same oceanic features only 1'20" apart, only a weak hemispheric bias is visible. Nevertheless, these patterns are slightly different between GDR-D (top) and GDR-F (bottom).
Considering GDR-F maps only, patterns are different taking into account all range corrections compared to $orbit - range - MSS$ but their amplitude are still under 1cm (from bottom left to bottom right of figure 56): these changes in difference are mainly due to ssb as the two solutions are not computed from the same ssb tables for these comparisons (whereas it was the case in GDR-D).

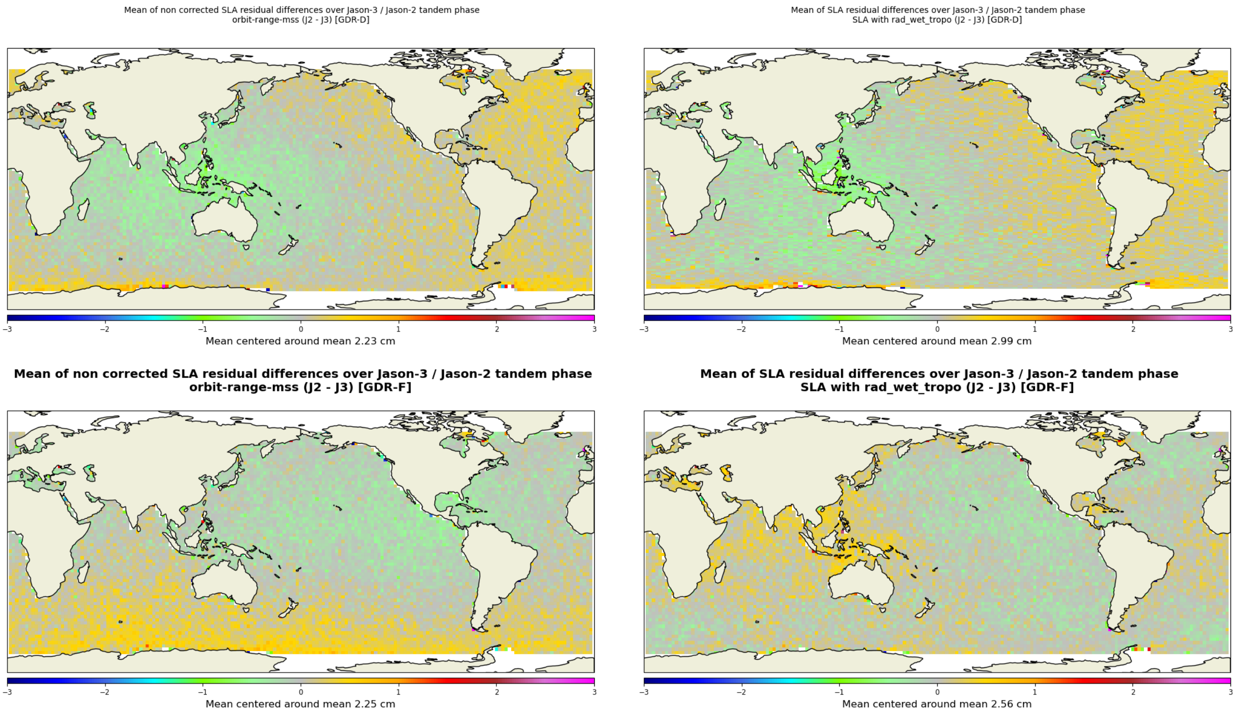

*Figure 56 – Mean per cycle of SLA without correction (**left**) and SLA (**right**) of residuals (= interpolated over theorical ground track) SLA along-track. For $GDR-D$ comparisons (**top**) or $GDR-F/GDR-F_{l}ike$ (**bottom**)*

Since Jason-2 has moved to its new interleaved orbit, maps of direct Jason-2 minus Jason-3 SLA measurements are no longer available, but differences of gridded SLA for Jason-2 and Jason-3 can be made. This difference is quite noisy for one cycle, especially as both satellites are shifted in time and sea state changes especially in regions of high ocean variability. Therefore figure 57 shows an average over SLA grid differences from Jason-3 cycles 025 to 058. High variability regions as Gulf Stream and Antarctic circumpolar current are visible. Geographically correlated patterns are slightly reduced from GDR-D to GDR-F.

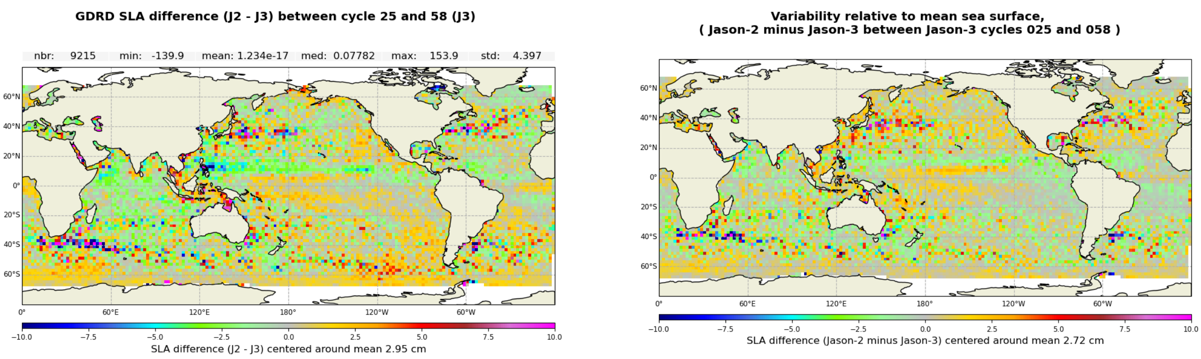

Figure 57 – SLA difference (Jason3 - Jason2) between cycle 25 to 58

6.2. Reprocessing impact on Global Mean Sea Level trends

Cyclic mean of along-track Sea Level Anomaly is monitored, including a remove of annual and semi-annual signals. It highlights no trend difference (figure 58). GMSL analysis are done as described in aviso web site [11].

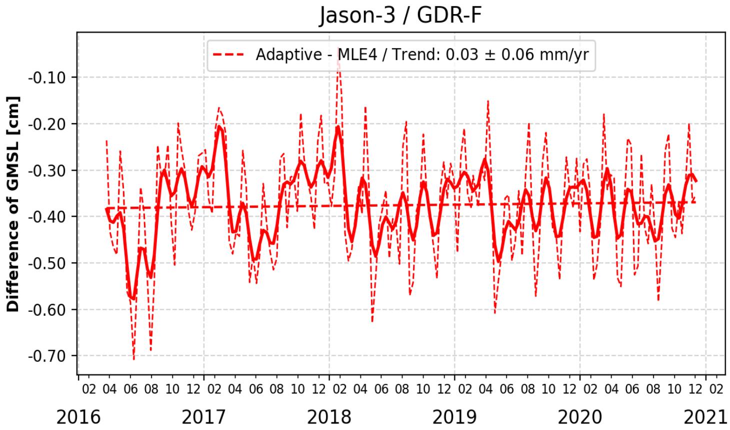

Figure 58 – GMSL difference GDR-F - GDR-D of reference SLAs

7. Analysis of the new retracker solution : the adaptive retracker

Jason-3 GDR-F product contain a new retracking solution called "Adaptive retracking" in addition to the historical MLE3 and MLE4. The objective of this part is to provide an estimation of the Jason 3 adaptive retracker available in GDR-F product quality by comparison with historical Jason 3 MLE4 retracker in terms of sea level anomaly (SLA) evaluation and crossover performance. Adaptive retracking have 4 major evolutions :

- A parameter correlated to the mean square slope (describing the sea surface roughness) of the reflective surface has been introduced in the mathematical formulation of the backscattered energy
- The Adaptive algorithm directly accounts for the real in-flight Point Target Response of the instrument, by numerically convolving its discretized values to the analytical model of the backscattered energy. It makes the 1Hz Look Up Table correction unnecessary. All drifts or instabilities of the PTR are thus "natively" accounted for (without any approximation) in the Adaptive solution making this solution an excellent reference for evaluating and confirming the quality of the current GMSL estimation.
- A true Maximum Likelihood Estimation method (using the exact likelihood function) is used that accounts for the statistics of the speckle noise corrupting the radar echoes
- The algorithm adapts the width of the window on which the fitting procedure is performed in order to reject spurious reflections coming from off nadir directions, in particular when the satellite is approaching the coastlines

Benefits of adaptive retracking solution for Jason and CFOSAT are described in many documents :

- technical note on the benefits for SLA, waves, wind (Jason3) [12],
- annex part of the CalVal at 1Hz activities annual report (using Jason-3 GDR-F preliminary 1 year of data) [3],
- OSTST presentation of adaptive benefits for GMSL (Jason3) [13],
- benefits for retracking altimeter nadir echoes (CFOSAT) [14].

7.1. Waveforms classification

A waveform classification has been done in order to adapt the retracking process to their shape (see figure 59). The list of classes defined for the Jason-3 waveform classification is detailed in table 11. The method to defined this classification is detailed in "Jason-3 Products Handbook" [1]. The main class selected by classification neural network trained on shape features of the waveforms is available in the variable "wvf_main_class" of the GDR 1Hz product.

Waveform classification value	Waveform classification meaning
0	No wave
1	Brownian echoes, mainly found in open ocean

Waveform classification value	Waveform classification meaning
2	Peaky echoes, mainly encountered over narrow rivers, small lakes (smaller than the altimeter footprint) and water leads in sea ice regions
3	Several peaks, corresponds to multiple reflection in the footprint, encountered over land or heterogeneous areas
4	Strong peak with a very low trailing edge, corresponds to high reflective surfaces, often encountered on sea ice, most of the time over First Year Ice (FYI)
5	Brownian shape with a peak on the trailing edge, mainly found in coastal areas where the altimeter is close to the coast and a “bright point” is present in the footprint (but not at nadir)
6	Brownian shape with a peak on the leading edge or Brownian shape with a sharp trailing edge. Can be encountered over sea ice.
7	Brownian shape with a flat or increasing trailing edge. Can be found in rain cells or over land ice (it can also be a sign of a platform mispointing even if Jason-3 have good pointing performances).
8	Peaky echo shifted at the end of the analysis window, mainly found on hydrology and land
9	Trash echoes
10	Brownian shape with a high thermal noise level mainly found on land, land ice and sometimes on very heavy rain event
11	Double leading edge, can be encountered over land
12	Shifted Brownian, can be found over land ice and hydrology (big lake with a non-optimal tracker command)
13	Brownian shape with a noisy leading edge
15	Linear rise, can be found over land
18	Linear decrease, can be found over land

Table 11 – Waveform classification definition

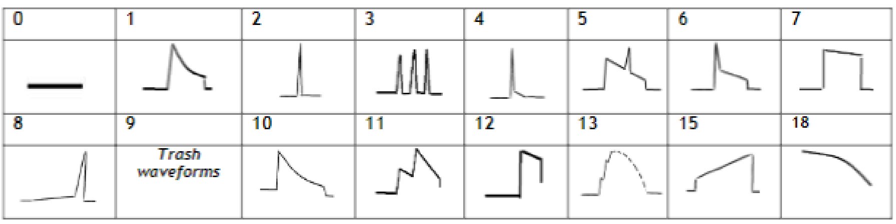

Figure 59 – Waveform classification

7.2. Point to point validation process (editing)

The following results are obtained using the same validation point procedure for MLE4 and adaptive outputs. Detailed on this procedure are available in part 3.2 of [3]. Note in particular that the same thresholds are used with both retrackers outputs, as described in handbook. As in case of MLE4 editing process over ocean, note that there is no data rejected during the last step (the last step consists in removing an entire pass if SSH-MSS mean and standard deviation have higher values than thresholds.)
Adaptive data are globally more valid than MLE4 data (figure 60), with +0.34% of additional valid data over ocean in average. The differences are mainly located in low swh and rain areas (figure 61).

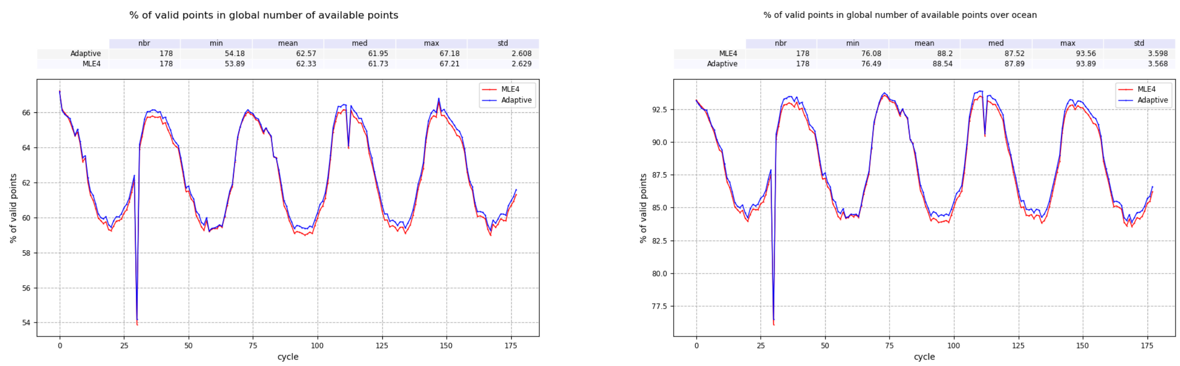

Figure 60 – Pourcentage of valid point for GDR-F MLE4 and GDR-F Adaptive

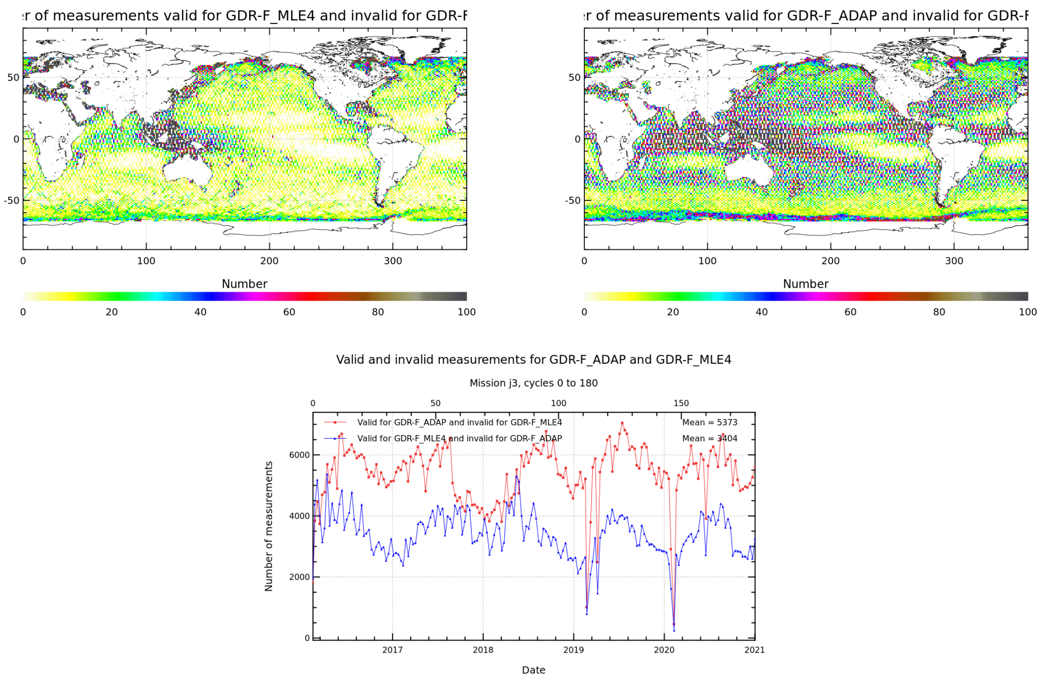

Figure 61 – Number of measurements that are valid for GDR-F MLE4 and invalid for GDR-F Adaptive (top left, and bottom blue). Number of measurements that are invalid for GDR-F MLE4 and valid for GDR-F Adaptive (top right and bottom red)

Parameter	Threshold: min	Threshold: max	GDR-F MLE4	GDR-F Adaptive
swh	0	11m	0.64 %	0.57 % ↘
square off nadir angle	-0.2 deg^2	0.64deg^2	0.65 %	Same as MLE4
sea surface height (orbit - range)	-130 m	100 m	0.82 %	1.14 % ↗
range : number of 20Hz meas.	10	20	1.10 %	1.91 % ↗
range : std of 20Hz meas.	0	0.2 m	1.40 %	1.53 % ↗
sigma0	7 dB	30 dB	0.63 %	0.62 % ↘
sigma0 : number of 20Hz meas.	10	20	1.09 %	1.88 % ↗
sigma0 : std of 20Hz meas.	**0**	**1 dB**	**2.13 %**	**1.02 %** ↘
wind speed from altimeter	0	30 m/s	1.08 %	1.00 % ↘
sea state bias	-0.5 m	0	0.58 %	0.47 % ↘
ionospheric correction (filtered)	-0.4 m	0.4 m	0.90 %	1.61 % ↗
ionospheric correction (raw data)	-0.4 m	0.4 m	1.05 %	1.29 % ↗
radiom. wet tropospheric corr.	-0.5 m	-0.001 m	0.15 %	Same as MLE4
sea level anomaly	-2 m	+2 m	1.45 %	1.84 % ↗
sea level anomaly (iono raw)	-2 m	+2 m	0.96 %	1.34 % ↗
ocean tide (FES)	-5 m	5 m	<0.01 %	Same as MLE4
ocean tide (GOT)	-5 m	5 m	<0.01 %	Same as MLE4
cyclic mean number of edited points by thresholds (GDR-F: filtered iono)			17856	15786
percentage of rejected points by thresholds wrt non ice (ocean + caspian sea)			3.30 %	2.98% ↘

Table 12 – Thresholds editing rates MLE4 vs Adaptive, from 2016 to 2020 (cycles 001 to 177)

7.3. Focus on altimeter parameters

The metric presented here qualify the adaptive retracking using 1Hz data. The rms of the 20 elementary measurements used to compute the 1Hz range is higher for MLE4 solution than with adaptive (left part of figure 62). This reduction is coherent with SLA spectrum shown on figure 68. The difference in range evaluation between the two solutions is linked to the SWH estimations (see right part of figure 62), these differences are included into ssb corrections.

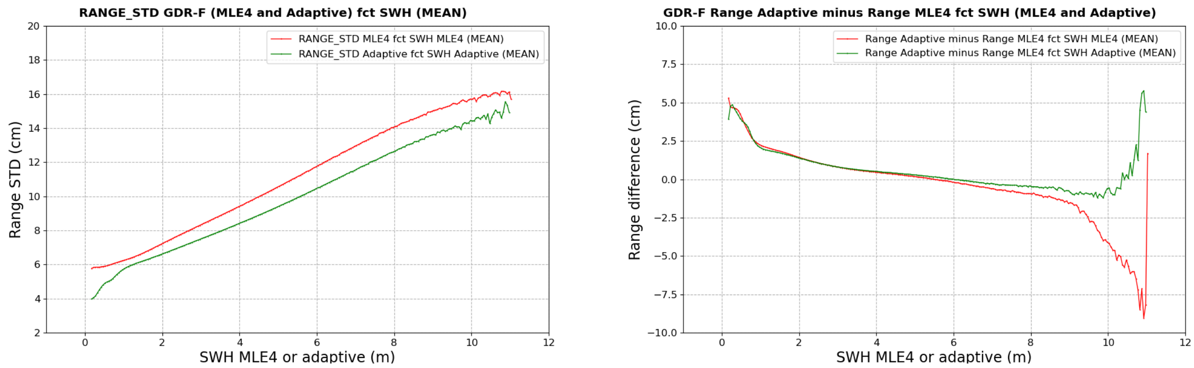

Figure 62 – Standard deviation of range fonction of SWH for ***MLE4*** *and* ***Adaptive***

A reduction of about 60% of the SWH noise level is observed with the adaptive solution, mainly thanks to the use of an exact MLE criterion in the estimation procedure (see figure 63 and [12])

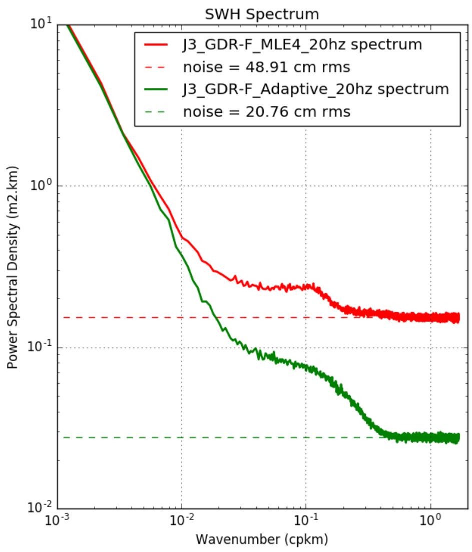

Figure 63 – SWH spectrum 20hz for cycle 174

Over the common valid points datasets, adaptive and mle4 swh are different by about 3.6 cm in average (top left of figure 64).

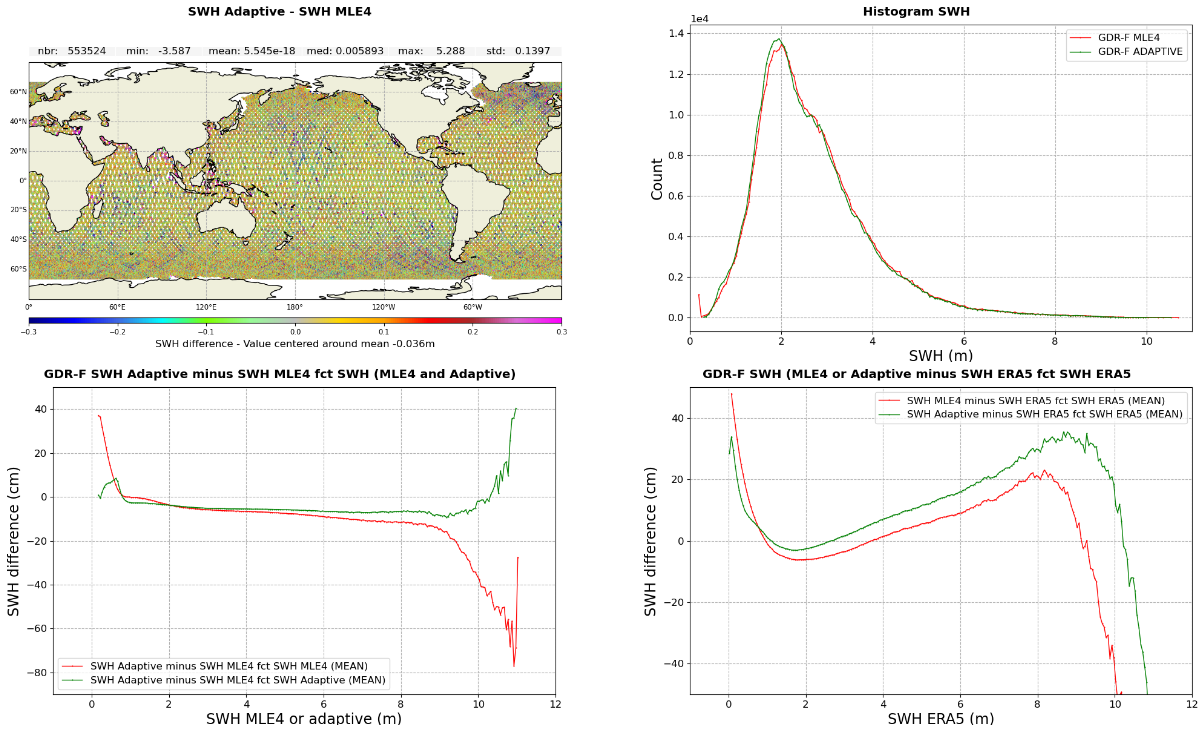

*Figure 64 – Histogram (**top left**) of SWH for GDR-F MLE4 and GDR-F Adaptive retracking and adaptive minus mle4 swh difference (**top right**) over cycle 073. swh differences wrt altimeter or era5 model over the whole period (**bottom**)*

7.4. Performances

7.4.1. Performances at crossovers

SSH crossover differences are the main tool to estimate the whole altimetry system performances. They allow to analyze the SSH consistency between ascending and descending passes: it should not be significantly different from zero. More importantly, special care is given to the geographical homogeneity of the mean difference at crossovers. However in order to reduce the impact of oceanic variability, we select crossovers with a maximum time lag of 10 days. Mean and standard deviation of SSH crossover differences are computed from the valid dataset to perform maps or a cycle by cycle monitoring over all the altimeter period. In order to monitor the performances over stable surfaces, additional editing is applied to remove shallow waters (bathymetry above -1000m), areas of high ocean variability (variability above 20 cm rms) and high latitudes ($> |50|deg$). SSH performances are then always estimated with equivalent conditions.
The performed comparisons between SSH with MLE4 and adaptive outputs show no global neither regional impact on mean of SSH difference at crossovers (figure 65). Global variance of SSH difference at crossovers is reduced by 0.52cm^2 in average with adaptive retracker compared to MLE4 (left of figure 66). Geographic reduction (right of figure 66, in blue) of variance of SSH difference at crossovers shows no geographically correlated pattern. *Note that only points that are valid with both solutions are used to compute this analysis.*

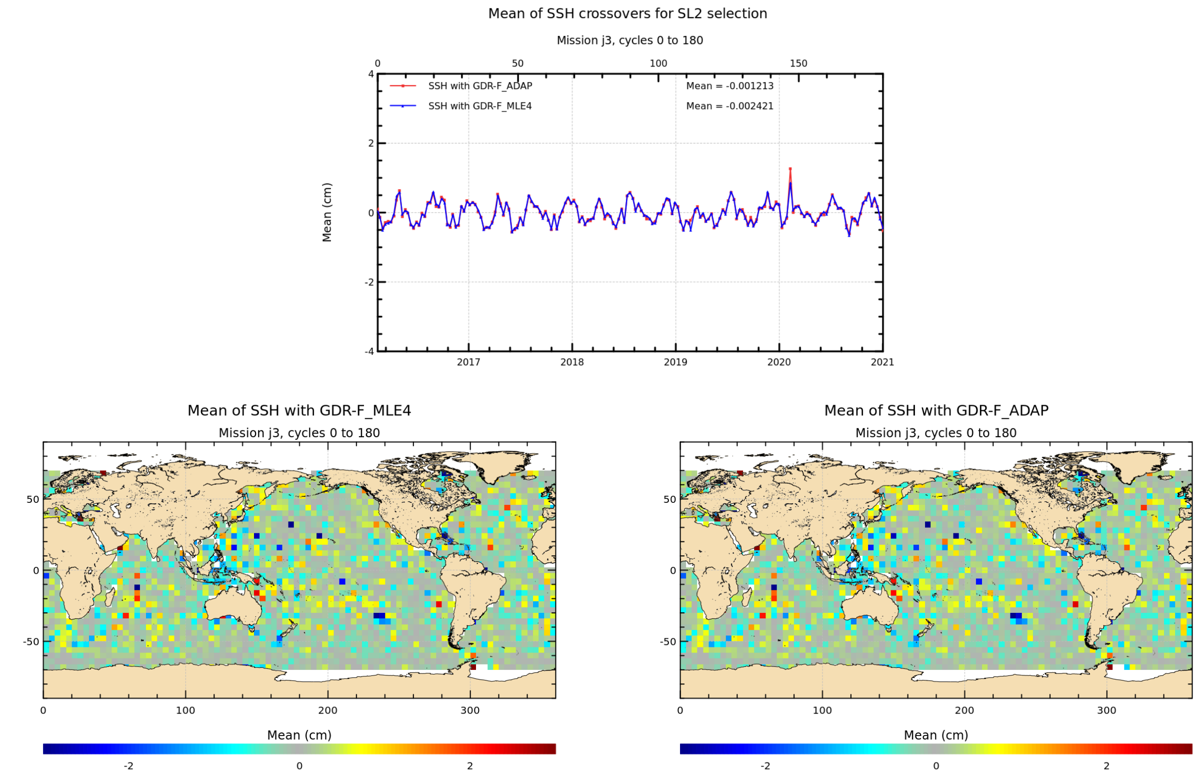

*Figure 65 – Mean of SSH difference at crossover points (selection on common valid points, $|latitude| < 50$, oceanic variability < 20cm and bathymetry < -1000m): cyclic monitoring (**top**), and map averaging (**bottom**) for GDR-D (**left**) or GDR-F (**right**).*

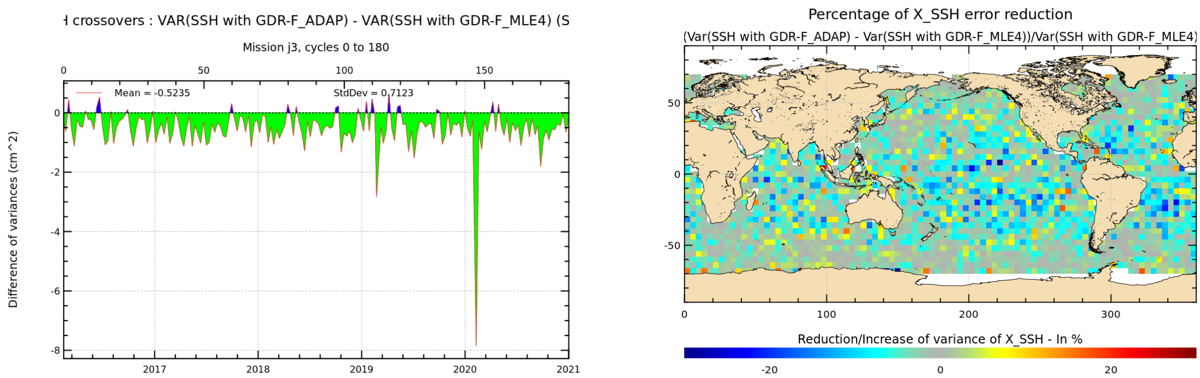

Figure 66 – Difference of SSH at crossover points : Variance difference (left) (selection on common valid points, $|latitude| < 50$, oceanic variability < 20cm and bathymetry < -1000m), pourcentage of error reduction (right)

7.4.2. Performances of along-track SLA

The Sea Level Anomalies (SLA) are computed along track from the substraction of the mean sea surface to the SSH: SLA = SSH − MSS. SLA analysis is a complementary indicator to estimate the altimetry system performances. It allows to study the evolution of SLA mean (detection of jump, abnormal trend or geographical correlated biases), and in particular the evolution of the SLA variance highlighting the long-term stability of the altimetry system performances .

Figure 67 present along-track SLA variance difference between GDR-F adaptive and GDR-F MLE4. Variance is lower for GDR-F adaptive than GDR-F MLE-4 by -0.18cm^2, mainly due to better estimations over rain areas. The behavior is quite different near coasts (in the last 10km), due to expected differences in retrackers performances in the last 3km that impact 1Hz data until 10km (top right of figure 67).

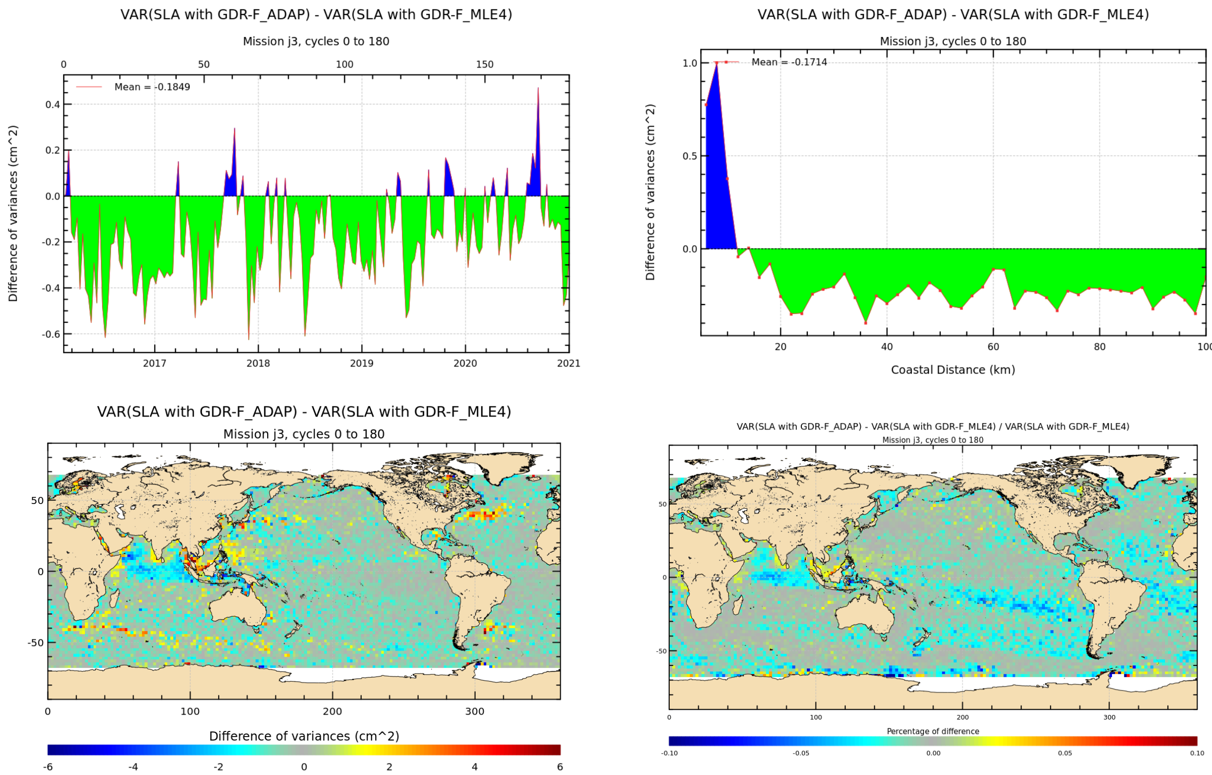

*Figure 67 – Along track SLA variance difference between GDR-F adaptive and GDR-F MLE4 (caspian sea not included). Cyclic monitoring (**top left**), in function of distance to coast (**top right**). Map of absolute difference of variance (**bottom left**) and percentage relative to MLE4 level of variance (**bottom right**)*

At a spectral point of view (computed over 1 cycle of 20Hz data), the reduction of noise level is 9.3%. This performance improvement is important when considering the objective to observe smaller and smaller scale of oceanic signals (figure 68).

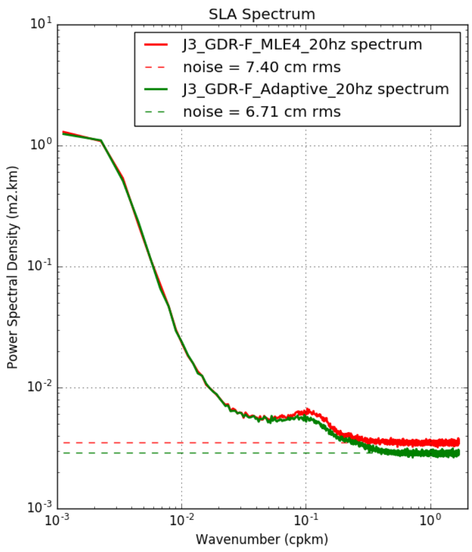

Figure 68 – SLA spectrum 20hz for cycle 174

7.5. SLA and GMSL

Caution: Note that it is recommanded not to use the adaptive data until cycle 003 as mispointing (see 5.4.1.) is not taken into account during GDR-F adaptive processing.
There is a global bias of -2,5 cm from MLE4 SLA to adaptive SLA , with small geographically correlated to SWH patterns (right of figure 69). This bias is partly due to range differences (48%), ssb differences (42%), and with a lesser impact to ionospheric correction (10%), regional biaises of these contributions in differences are shown on figure 70.

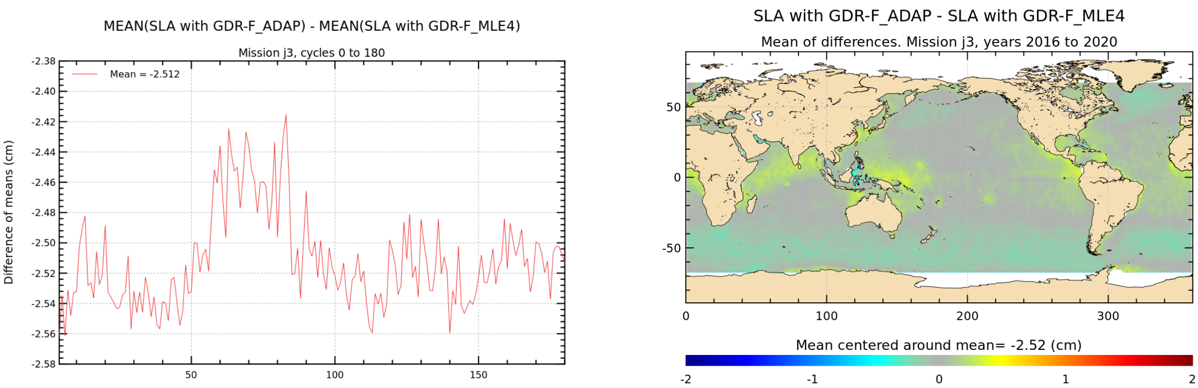

Figure 69 – Difference of cyclic mean of Sea Level Anomaly (GDR-F adaptive - GDR-F MLE4)

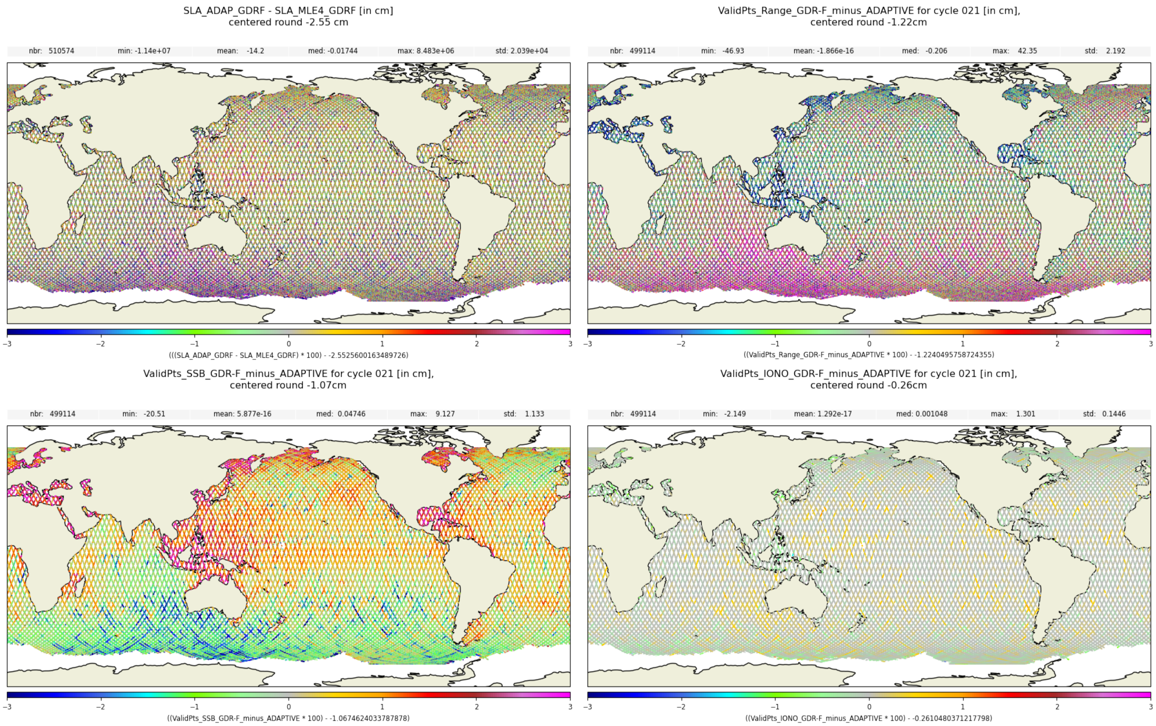

Figure 70 – SLA, range, ssb and ionospheric correction differences between adaptive and MLE4 over one cycle

The difference of SLA means (Adaptive – MLE4) shows a very good consistency between the two solutions but jumps (from about -2.52cm to -2.46cm) can be observed after the instrument reset (upload of the DEM at cycle 057 and BDR update at cycle 085 on left part of figure 69). This may be due to a difference in the echo centering between these cycles 57 and 85 (see part 8.2 in [5]). It also can indicate that potential changes in the PTR have occurred and that these changes may not have been accounted for in the internal path delay (see also [12] for more details). We recall that the LUT (only applied during MLE4 processing) have been computed only once at the beginning of the mission and never updated since then .

The trend differences over the near 5 years of data are not significant (figure 71, GMSL analysis done as described in aviso web site [11].).

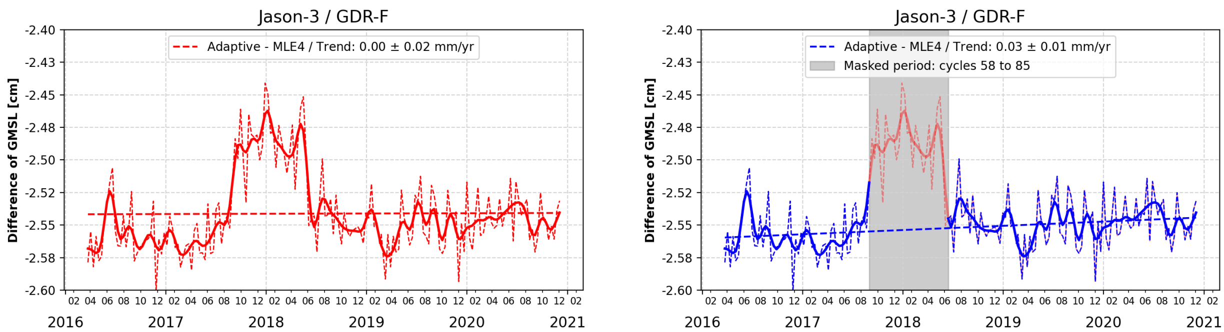

*Figure 71 – GMSL difference GDR-F adaptive - mle4 SLAs over the whole period **(left)** or excluding cycles 057 to 085 **(right)***

7.6. Conclusions

There is a global bias of -2,28cm from MLE4 SLA to adaptive SLA. SLA MLE4 data are globally more rejected than SLA Adaptive data (using recommended in handbook procedure). Taking into account valid in both datasets points, performances are better with adaptive solution than with MLE4:

- variance of SSH difference at crossovers is reduced by -0,52cm^2
- variance of along-track SLA is reduced by -0,18cm^2 (except for coastal) distance $<$ 10km.

8. Analysis of the new sea state bias solution : add of mean wave period information

Jason-3 GDR-F includes new alternative solutions for sea state bias correction. These solutions use an additional parameter as input: the mean wave period (available into GDR product as *mean_wave_period_t02*). These new sea state bias corrections (*sea_state_bias_3d_mp2* and *sea_state_bias_adaptive_3d_mp2*) were fitted on one year of preliminary Jason-3 GDR-F data (and will be named in this analysis *ssb_3d* in opposition the the reference *ssb* described in part 5.4.5.). For more details on *ssb_3d*, see [21].
This part studies the differences and impact on system performances between the reference ssb and this new solution for MLE4 and adaptive sea level anomalies.

8.1. Mean wave period and direction

MFWAM is a forcasting model of sea state (wind sea and swell). Mean wave direction gives average direction (degrees) of sea surface wave where they come from. Mean wave period gives the average periodicity (seconds) of sea surface wave, and so help to better consider the sea surface conditions.

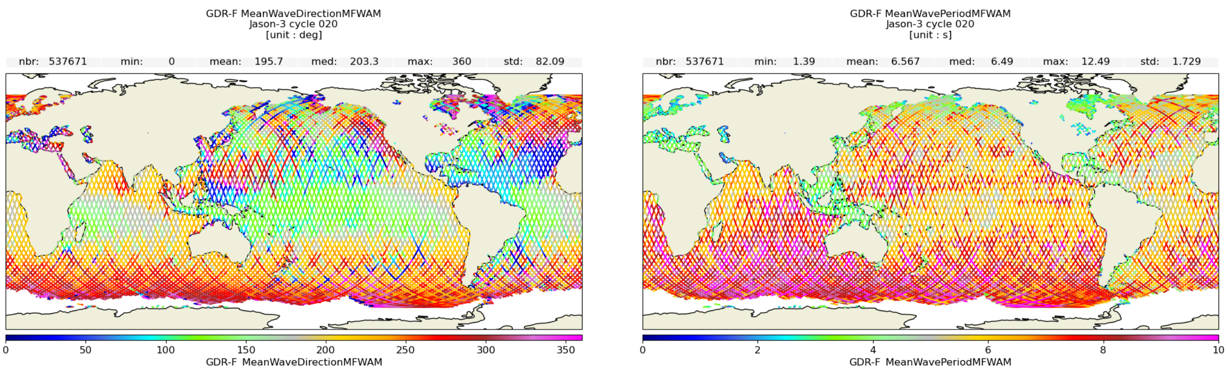

*Figure 72 – Mean wave direction **left** and period **right** for one Jason-3 GDR-F cycle*

8.2. Results on MLE4 retracking

The same editing procedure is applied to Sea Level Anomaly replacing the reference sea state bias with the new solution. All points that are valid (meaning within thresholds) for ssb all also valid using ssb_3d (red curve at left of figure 73). On contrary, 4537 points per cycle are valid with but invalid with ssb_3d in average (blue curve), mainly at high latitudes (see figure 73), this is directly linked to the mean wave period unavailabiliy at high latitudes.

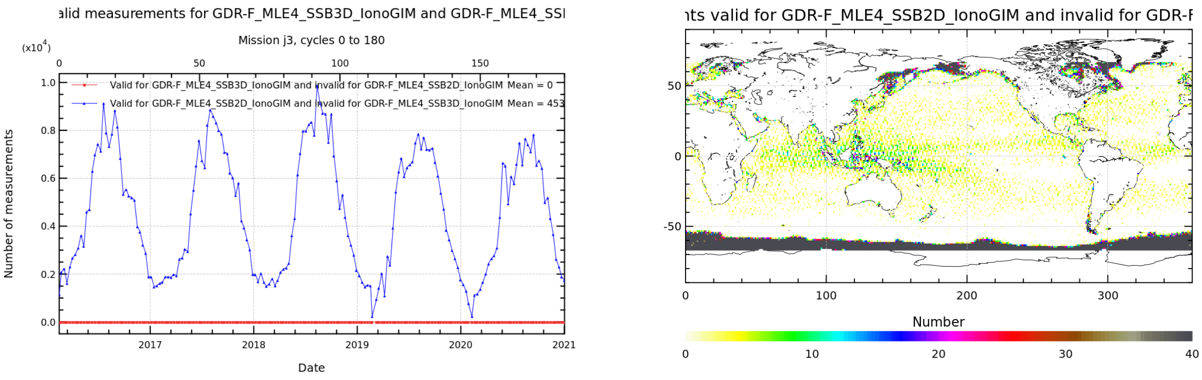

Figure 73 – Difference of editing point between SSB and SSB 3D (MLE4 retracking)

No significant impact is observed on mean difference of SSH at crossover between both solutions (figure 74). A variance reduction of about 0.96 cm^2 is measured with the 3d solution compared to the reference (figure 75).

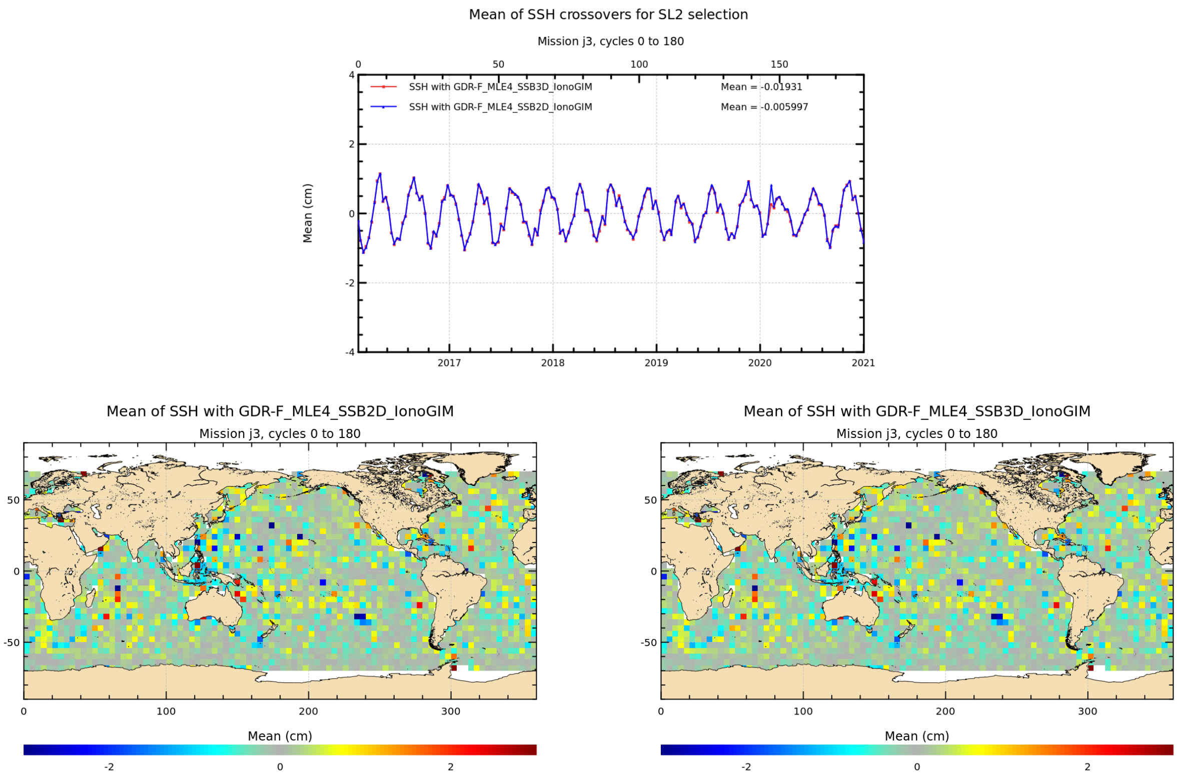

Figure 74 – SSH difference at crossover for ssb_3d and ssb (with iono GIM). Note that figures are computed over a common valid points dataset.

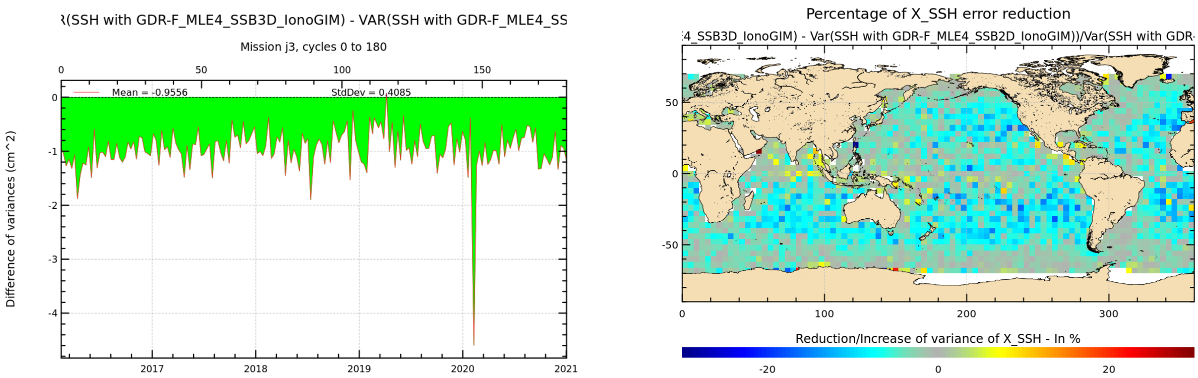

Figure 75 – SSH at crossover for ssb_3d and ssb (with iono GIM): difference of variance (ssb_3d - ssb) and pourcentage of error-reduction (ssb_3d - ssb). Note that figures are computed over a common valid points dataset.

Performances on along-track SLA are improved with a reduction of variance of -1.2cm^2 in average, depending on seasonal signal (figure 77).

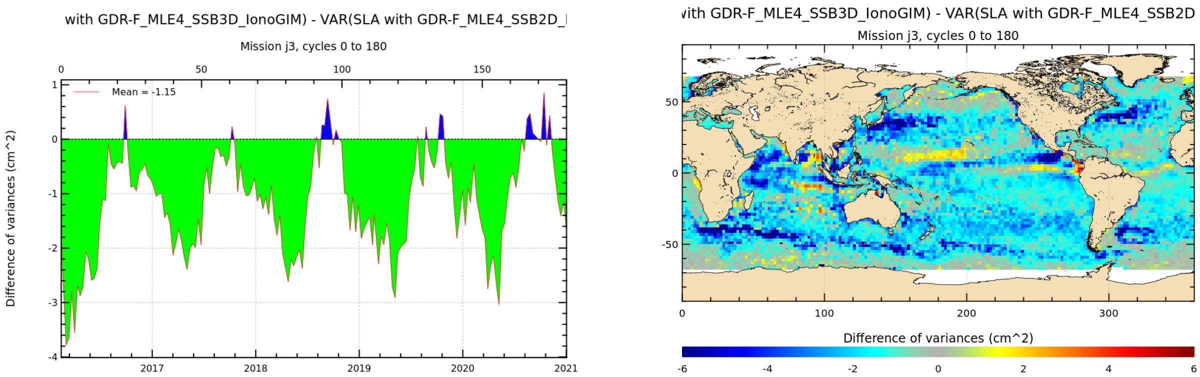

*Figure 76 – SLA for ssb_3d and ssb (with iono GIM). Difference of variance (SSB_3D - SSB_2D) on cycllic monitoring **(left)** or geobox averaging **(right)** .*

Long term monitoring of cyclic sea level anomaly differences highlight a difference of behaviour from the beginning of 2017 to mid-2018 (figure 77). It results in a difference of GMSL trend of -0.34 mm/yr over the whole period, but from mid-2018 to end of 2020, there is no difference in GMSL trend using ssb or ssb_3d. Further investigations are needed in order to better understand how the mean wave period behaves and impacts the GMSL trend over these first 2 years of the mission.

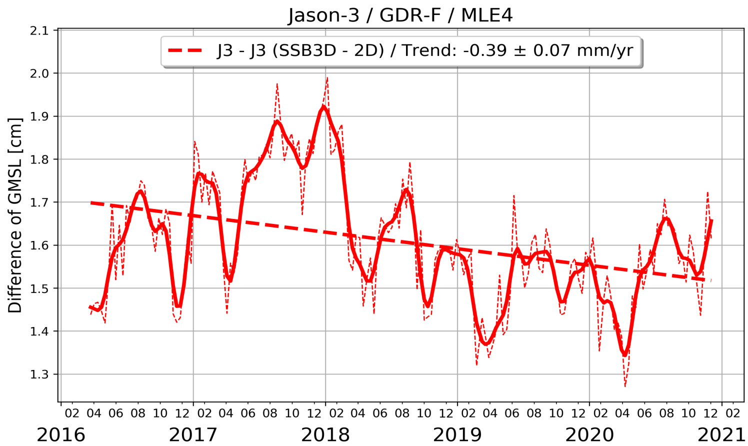

Figure 77 – GMSL difference GDR-F mle4 SLA with ssb - SLA with ssb_3d

8.3. Results on adaptive retracking

Results are quite equivalent with the adaptive solutions. The related figures are available below (from figure 78 to figure 82).

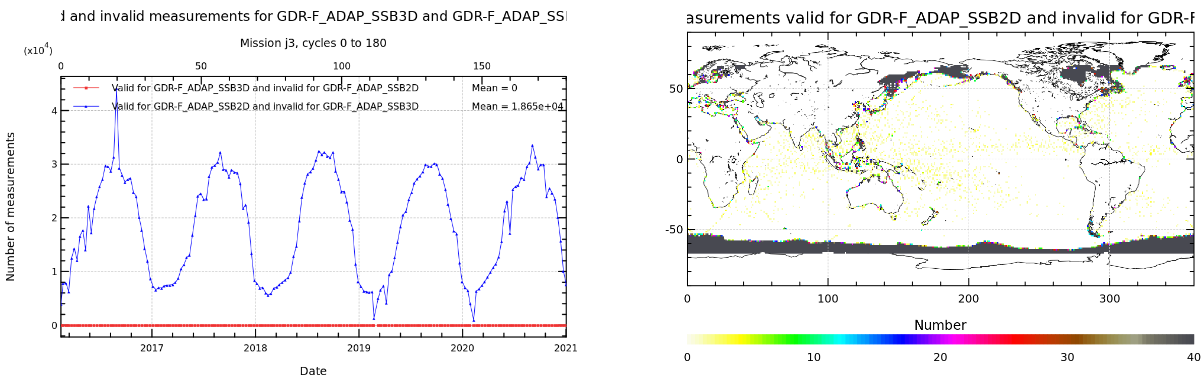

Figure 78 – Difference of editing point between SSB and SSB 3D (adaptive retracking)

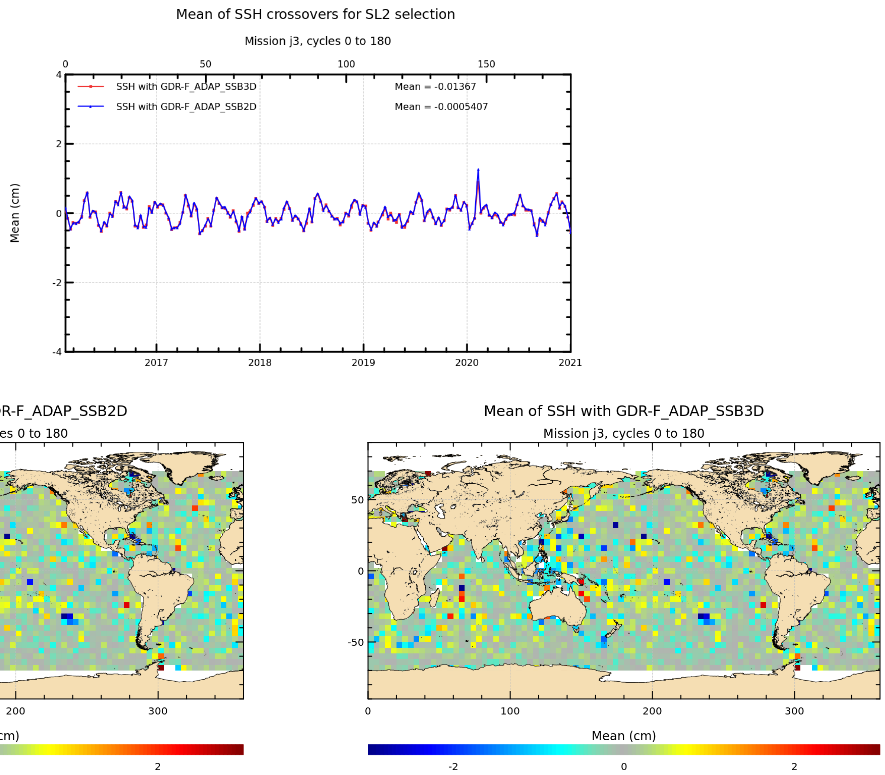

Figure 79 – SSH (adaptive retracking) difference at crossover for ssb_3d and ssb (with iono GIM). Note that figures are computed over a common valid points dataset.

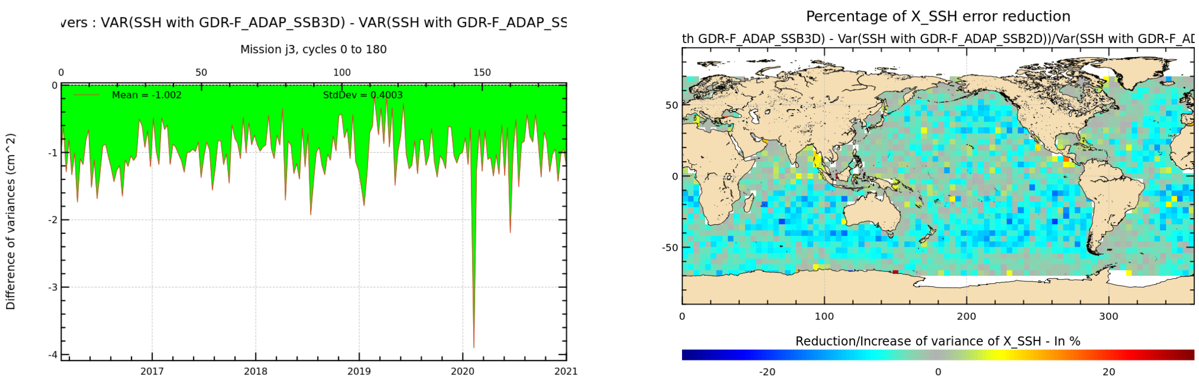

Figure 80 – SSH (adaptive retracking) difference at crossover for ssb_3d and ssb (with iono GIM): difference of variance (ssb_3d - ssb) and pourcentage of error-reduction (ssb_3d - ssb). Note that figures are computed over a common valid points dataset.

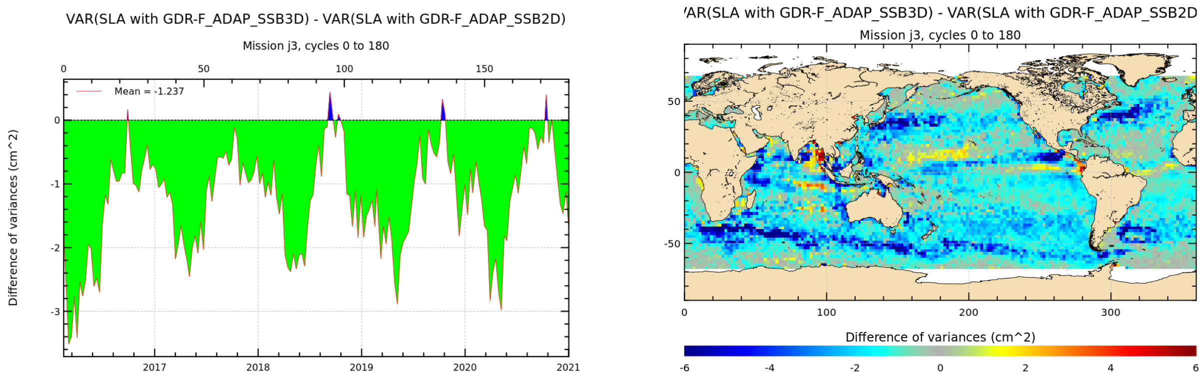

*Figure 81 – SLA for ssb_3d and ssb. Difference of variance (SSB_3D - SSB_2D) on cycllic monitoring (**left**) or geobox averaging (**right**)*

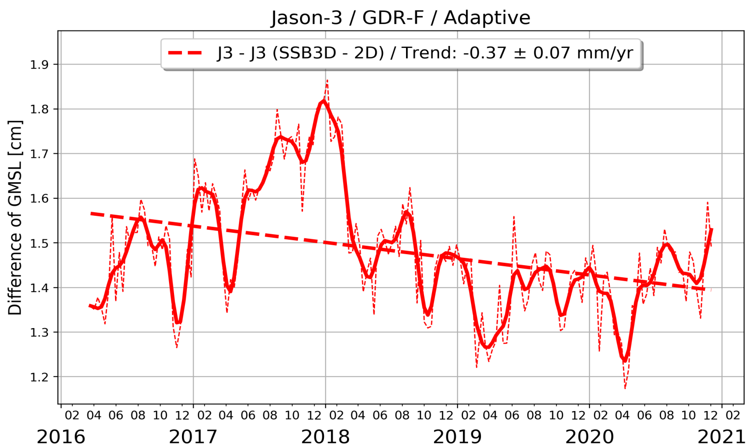

Figure 82 – GMSL difference GDR-F adaptive SLA with ssb - SLA with ssb_3d

9. Conclusion

An overview of the impact of the GDR-F version of Jason-3 altimeter system over ocean has been presented in this report. Comparisons have been done with previous version data (GDR-D). Comparison with Jason-2 data during the tandem flight phase (between February 12 2016 to October 2 2016), taking advantage that both satellite were only 80 seconds apart on the same ground track, have also been presented.

The reprocessing of the Jason-3 altimetric mission allows several modifications that improve the sea surface height estimations quality:

- Due to a change in surface classification, more points are identified over ocean.
- Thanks to a new filtered solution for ionospheric correction, measurements are more valid over open ocean on GDR-F dataset than on GDR-D dataset but there are more rejected data in GDR-F near ice and coasts.
- At crossovers, geographically correlated patterns are slightly reduced for mean of SSH differences, global variance decreases everywhere between 5 and 25 %. The main contributor to this variance reduction is the filtering version of the ionospheric correction. Note that GDR-F significantly reduced 60 days signal for pseudo datation bias observed in GDR-D, probably linked to the use of the FES14B solution for oceantide correction.
- In terms of along-track performance of Sea Level Anomaly, the variance is also reduced with GDR-F (-15.47 cm^2 using the filtering version of ionospheric correction).

Note the following evolutions:

- The GDR-F and the GDR-D data contain the Precise Orbit Ephemeris standard F (POE-F). Before cycle 85, GDR-D used the Precise Orbit Ephemeris standard E (POE-E). Variance of SSH differences at crossovers reduction (-0.2cm^2) using POE-F SSH computation compared to SSH POE-E indicates an improvement.
- Using the latest global tide model FES2014b instead of GOT4.8 allows to reduce variance at crossovers by -0.48 cm^2, and along-track SLA variance by -2 cm^2.
- Internal tide is a new correction available in GDR-F compared to GDR-D: it contributes to an improvement of -0.47cm^2 for variance reduction at crossovers
- The computation of a dedicated sea state bias (fitted on Jason-3 data whereas instead of a solution fitted on Jason-2 that was available in GDR-D), and the updated associated ionospheric correction contribute to an improvement of -0.11cm^2 for variance reduction at crossovers, and -0.76 cm^2 for along-track SLA variance
- The filtered solution for ionospheric correction allows to reduce SSH difference at crossover variance and along-track SLA variance by about 3 cm^2
- Pole tide correction was modified between GDR-D (Wahr 1985) and GDR-F (Desai 2015): it contribute to gain of variance for SLA along-track can be observed (-8mm^2).
- GDR-D L2 products included one MSS solution (CNES/CLS 11, referenced over 7 years) whereas two solutions in GDR-F (CNES/CLS 2015 and DTU 2018) : This change have positive impact on variance of SLA along-track (- 5.65cm^2).

The analysis of the data from Adaptive retracking confirm the benefits of this solution against MLE4 retracking.
Finally, a new solution of of SSB (including the mean wave period information) was compared to actual version and leads to quite good results. Nevertheless, further investigations are needed in order to better understand the impact of this solution on Global Mean Sea Level trends.

10. References

References

[1] Jason-3 handbook available at https://www.aviso.altimetry.fr/fileadmin/documents/data/tools/hdbk_j3.pdf

[2] Jason-3 annual report https://www.aviso.altimetry.fr/en/data/calval/systematic-calval/annual-reports/jason-3.html

[3] Roinard H. Jason-3 validation and cross calibration activities (Annual report 2020). https://www.aviso.altimetry.fr/fileadmin/documents/calval/validation_report/J3/SALP-RP-MA-EA-23473-CLS_Jason-3_AnnualReport2020_v1-1.pdf

[4] Roinard H. Jason-3 validation and cross calibration activities (Annual report 2019). https://www.aviso.altimetry.fr/fileadmin/documents/calval/validation_report/J3/SALP-RP-MA-EA-23399-CLS_Jason-3_AnnualReport2019_v1-1.pdf

[5] Roinard H. Jason-3 validation and cross calibration activities (Annual report 2018). https://www.aviso.altimetry.fr/fileadmin/documents/calval/validation_report/J3/SALP-RP-MA-EA-23248-CLS_Jason-3_AnnualReport2018_v1-1.pdf

[6] Roinard H. Jason-2 validation and cross calibration activities (Annual report 2014). https://www.aviso.altimetry.fr/fileadmin/documents/calval/validation_report/j2/annual_report_jason2_2014.pdf

[7] Roinard H. Jason-3 mission performance towards GDR-F https://ostst.aviso.altimetry.fr/fileadmin/user_upload/2019/CVL_09_Jason-3_mission_performance_towards_GDR-F.pdf

[8] Bignalet-Cazalet F.Jason-3 GDR-F standard : ready for operational switch https://meetings.aviso.altimetry.fr/fileadmin/user_upload/tx_ausyclsseminar/files/CVL_J3_GDRF_ready_v02_ostst2020_02.pdf

[9] Boy, François and Jean-Damien Desjonqueres. 2010. Note technique datation de l'instant de reflexion des échos altimètres pour POSEIDON2 et POSEIDON3. Reference: TP3-JPOS3-NT-1616-CNES

[10] Nencioli Francesco, Roinard Hélène, Bignalet-Cazalet Francois. 2021. Filtering ionospheric correction from altimetry dual-frequencies solution. DOI 10.24400/527896/a02-2021.001. https://www.aviso.altimetry.fr/fileadmin/documents/data/tools/NT-Nencioli_FilteredIonosphericCorrection.pdf

[11] Mean sea level rise and the Greenhouse effect https://www.aviso.altimetry.fr/en/applications/ocean/mean-sea-level-greenhouse-effect.html

[12] Thibaut P. Benefits of the "Adaptive retracking solution" for the Jason-3 GDR-F reprocessing campaign https://www.aviso.altimetry.fr/fileadmin/documents/data/tools/NT-Thibaut_AdaptiveRetrackingForJason3GDRF.pdf

[13] Thibaut et al. OSTST 2020. Benefits of the Adaptive retracker for improving Jason-3 GMSL estimations

[14] Benefits of the Adaptive Algorithm for Retracking Altimeter Nadir Echoes: Results From Simulations and CFOSAT/SWIM Observations. IEEE Transactions on Geoscience and Remote Sensing. 2021 — journal-article. DOI: 10.1109/TGRS.2021.3064236

[15] DUACS/Aviso team : 'A new version of SSALTO/Duacs products available in april 2014' https://www.aviso.altimetry.fr/fileadmin/documents/data/duacs/Duacs2014.pdf

[16] Pujol et al. OSTST2013. A 20-YEAR REFERENCE PERIOD FOR SSALTO/DUACS PRODUCTSSSALTO/DUACSPRODUCT https://www.aviso.altimetry.fr/fileadmin/documents/OSTST/2013/oral/pujol_ChgtRef.pdf

[17] Présentation du modèle de vagues MFWAM. https://donneespubliques.meteofrance.fr/client/document/20160705_doc_mfwam_210.pdf

[18] Lyard F. H. and all. FES2014 global ocean tide atlas: design and performance https://os.copernicus.org/articles/17/615/2021/os-17-615-2021.html

[19] https://www.aviso.altimetry.fr/fileadmin/documents/data/tools/hdbk_L2P_all_missions_except_S3.pdf

[20] Loren Carrere, Brian K. Arbic, Brian Dushaw, Gary Egbert, Svetlana Erofeeva, Florent Lyard, Richard D. Ray, Clément Ubelmann, Edward Zaron, Zhongxiang Zhao, Jay F. Shriver, Maarten Cornelis Buijsman, and Nicolas Picot. Accuracy assessment of global internal-tide modelsusing satellite altimetry. Ocean Sci., 17, 147–180, 2021 https://doi.org/10.5194/os-17-147-2021 https://os.copernicus.org/articles/17/147/2021/os-17-147-2021.pdf

[21] Tran N., D. Vandemark, E.D. Zaron, P. Thibaut, G. Dibarboure, and N. Picot (2019): "Assessing the effects of sea-state related errors on the precision of high-rate Jason-3 altimeter sea level data", Advances in Space Research / special issue " 25 Years of Progress in Radar Altimetry", Volume 68, Issue 2, Pages 963-977, https://doi.org/10.1016/j.asr.2019.11.034, 2021